Universidade Federal de Santa Catarina

Centro Tecnológico (CTC)

Programa de Pós-Graduação em Engenharia Mecânica

A Computational Model for the Mechanical Behavior of the Achilles Tendon

por Otávio Teixeira Pinto

Florianópolis, SC

2024

Otávio Teixeira Pinto

A Computational Model for the Mechanical Behavior of the Achilles Tendon

Tese submetida ao Programa de Pós-Graduação em Engenharia Mecânica da Universidade Federal de Santa Catarina para a obtenção do título de doutor em Engenharia Mecânica na área de Análise e Projeto Mecânico.

Supervisor: Prof. Eduardo Alberto Fancello, Dr.

Florianópolis, SC

2024

Otávio Teixeira Pinto

A Computational Model for the Mechanical Behavior of the Achilles Tendon

O presente trabalho em nível de Doutorado foi avaliado e aprovado, em 28 de fevereiro de 2024, pela banca examinadora composta pelos seguintes membros:

Prof. Rogério José Marczak, Dr. Eng.
Universidade Federal do Rio Grande do Sul - UFRGS

Prof. Estevam Barbosa de Las Casas, PhD
Universidade Federal de Minas Gerais - UFMG

Prof. Carlos Rodrigo de Mello Roesler, Dr. Eng.
Universidade Federal de Santa Catarina - UFSC

Mario Kuhn Adames, Me.
Hospital Regional de São José - HRSJ

Certificamos que esta é a **versão original e final** do trabalho de conclusão que foi julgado adequado para obtenção do título de Doutor em Engenharia Mecânica.

_____
Prof. Henrique Simas, Dr. Eng.
Coordenação do Programa de
Pós-Graduação

_____
Prof. Eduardo Alberto Fancello, Dr.
Orientador

Florianópolis, SC
2024

Esta obra é dedicada àqueles cujas circunstâncias os fizeram desistir.

Acknowledgements

Em primeiro lugar, gostaria de agradecer às instituições públicas de ensino brasileiras que, através de seus diversos trabalhadores, contribuíram para a minha formação e para a de milhões de outros. Dentre vários, agradeço especialmente ao professor Francis Henrique Ramos França por me mostrar que engenharia é uma arte, aos professores, Jun Sérgio Ono Fonseca e Ignácio Iturrioz por me mostrarem que engenharia é divertida, e ao professor Carlos Rodrigo de Mello Roesler por me convencer que empreender na universidade pode ser algo bom. Em particular, eu agradeço à dedicação e amor pela arte demonstrado pelo professor Eduardo Alberto Fancello que vem me orientando e me inspirando pelos últimos 12 anos.

Agradeço aos colegas e amigos do Laboratório de Engenharia Biomecânica, onde trabalhei antes e no início deste doutorado, e que inspiraram o início deste trabalho. Em particular, agradeço a Arthur Paiva Grimaldi Santos, Leonardo Corrêa Piedade e Luciano Fontes e Silva. Agradeço também aos diversos colegas e amigos do Grupo de Análise e Projeto Mecânico que me receberam de volta e escutaram minhas tagarelices quase que diárias. Em especial, agradeço ao companheirismo fraterno dos meus amigos Bruno Klahr e José Luiz Thiesen e aos vários amigos das noites de jogos de RPG.

Agradeço aos meus muitos familiares, cujas derrotas e vitórias compartilhamos juntos e esta tese é mais uma. Em especial, agradeço aos meus pais, Elisabete e Joaquim, pelo apoio e pela inspiração que me fizeram chegar onde estou. Ao meu irmão, Henrique, por nossa relação eternamente infantil e ambiciosa. E a minha esposa, Carolina, pela parceria na luta que travamos em busca de nossos sonhos. Amo vocês.

"O Brasil é feito por nós. Está na hora de desatar esses nós."

(Barão de Itararé)

Resumo

Proteínas como o colágeno dos tendões e outras estruturas do corpo tendem a formar ligações cruzadas com moléculas adjacentes como resultado do envelhecimento. Sabe-se que estas novas ligações químicas aumentam a transferência de força lateral entre as moléculas de colágeno e, consequentemente, aumentam as tensões cisalhantes presentes em tecidos com formados por fibras alinhadas, como o tendão de Aquiles. Nesse trabalho é proposto um modelo de elementos finitos do tendão de Aquiles para comparar três níveis de severidade da lesão em dois modelos diferentes de tendões de Aquiles (jovem e idoso). Os níveis baixo e alto de severidade da lesão não mostram qualquer diferença entre o caso idoso e o caso jovem, mas o nível médio de gravidade mostra que o módulo de cisalhamento mais baixo do caso jovem protege o tendão, resultando num campo de tensões mais homogéneo, enquanto o caso idoso mostra um aumento da concentração de tensões perto do local da lesão. Além disso, o modelo é também utilizado para simular a técnica de reparo Achillon. Esta simulação foi concebida para testar a hipótese de que, após o último nó ser executado, a força nos dois primeiros nós diminuiria significativamente. Os resultados mostraram alguma perda de tensão da sutura durante a sequência de aperto dos nós da técnica Achillon.

Palavras chave: Modelo computacional do tendão de Aquiles, Envelhecimento, Tendinopatia, Deslizamento, Achillon.

Abstract

Proteins such as the collagen of tendons and other structures of the body tend to form cross-links with their neighbors as a result of aging. These new chemical bonds are known to increase the lateral force transfer between collagen molecules and, as a consequence, increase the shear stresses present in tissues with a high degree of fiber organization such as the Achilles tendon. A finite element model of the Achilles tendon is proposed to compare three levels of lesion severity on two different Achilles tendon models (young and elderly). The low and high levels of lesion severity show no difference between the elderly and the young case, but the medium level of severity shows that the lower shear modulus of the young case protects the tendon by resulting in a more homogeneous stress field, whereas the elderly case shows an increase in the stress concentration near the lesion site. In addition, the model is also used to simulate the Achillon tendon repair technique. This simulation was designed to test the hypothesis that after the last knot is tied, the force in the first two knots would decrease significantly. The results showed some loss of suture tension during the knot tying procedure of the Achillon repair technique.

Keywords: Achilles tendon computational model, Aging, Tendinopathy, Sliding, Achillon.

Resumo Expandido

Introdução

Proteínas como o colágeno dos tendões e outras estruturas do corpo tendem a formar ligações cruzadas com moléculas adjacentes como resultado do envelhecimento. Sabe-se que essas novas ligações químicas aumentam a transferência de força lateral entre as moléculas de colágeno e, consequentemente, aumentam as tensões cisalhantes presentes em tecidos formados por fibras alinhadas, como o tendão de Aquiles. Esse tipo de comportamento pode ser simulado com modelos de material existentes, específicos para tecidos moles, dentro de softwares comerciais de elementos finitos. Contudo, para investigar o comportamento do tendão de Aquiles, é necessário levar em conta também aspectos geométricos do tendão e de sua estrutura interna, formada por três subtendões orientados helicoidalmente de maneira similar a uma corda.

Objetivos

O objetivo deste trabalho é criar, desenvolver e validar um modelo computacional do tendão de Aquiles e demonstrar potenciais capacidades desse modelo em aplicações clínicas. Para isso, foram realizados quatro estudos diferentes. O primeiro estudo foca na validação do comportamento homogeneizado do tendão sob tração. O segundo estudo concentra-se na validação das não homogeneidades do campo de deformação do tendão quando submetido a diferentes casos de carga. O terceiro consiste na proposição de uma estratégia para modelar tendinopatias e tem como objetivo comparar o nível de severidade de uma dada tendinopatia em tendões idosos e jovens, a fim de testar a hipótese de que mudanças no módulo de cisalhamento têm uma relação causal com a diminuição na carga de ruptura do tendão de Aquiles. O quarto estudo visa demonstrar a habilidade do modelo em simular técnicas de reparo do tendão de Aquiles.

Metodologia

Nesse trabalho é proposto um modelo de elementos finitos do tendão de Aquiles. A geometria do tendão foi idealizada como um conjunto de seções elípticas paralelas e concêntricas. Todas as elipses possuem a mesma orientação de seus eixos principais, porém, internamente, elas são subdivididas em quatro regiões: uma para o subtendão do músculo gastrocnêmio lateral, uma para o subtendão do músculo gastrocnêmio medial, uma para o subtendão do músculo sóleo e uma para a interface entre essas três estruturas. Adotou-se um modelo de material hiperelástico transversalmente isotrópico para os subtendões e um modelo hiperelástico isotrópico para a interface. Uma função escalar foi utilizada para controlar a modificação local de propriedades mecânicas do modelo. Essa função escalar foi utilizada para a inclusão de lesões e a consideração da transição entre o material tendinoso e o tecido muscular. Na simulação da técnica de reparo de Achillon, adicionou-se no modelo

a geometria da sutura e um conjunto de elementos elásticos lineares visando modelar a rigidez passiva dos músculos e o procedimento de aperto dos nós da sutura.

Resultados e Discussão

O primeiro e o segundo estudo visavam a comparação do modelo com resultados experimentais. O modelo foi capaz de reproduzir o comportamento observado nos experimentos; no entanto, ainda é cedo para afirmar que o processo de validação foi finalizado. No segundo estudo, os níveis baixo e alto de severidade da lesão não mostram qualquer diferença entre o caso idoso e o caso jovem. Entretanto, o nível médio de gravidade mostra que o módulo de cisalhamento mais baixo do caso jovem protege o tendão, resultando num campo de tensões mais homogêneo, enquanto o caso idoso mostra um aumento da concentração de tensões perto do local da lesão. No quarto estudo, os resultados mostraram alguma perda de tensão da sutura durante a sequência de aperto dos nós da técnica Achillon (de 25 N para 16,5 N).

Considerações Finais

De maneira geral, o trabalho apresenta um modelo do tendão de Aquiles com uma nova estratégia para modelar o deslizamento entre os subtendões, a geometria do tendão e de seus subtendões, além de representar lesões no tendão. Essas capacidades do modelo foram utilizadas para testar a hipótese de que mudanças no módulo de cisalhamento têm uma relação causal com a diminuição na carga de ruptura do tendão de Aquiles. Essa hipótese foi confirmada, mostrando que as modificações das propriedades de deslizamento nos tendões idosos podem ser a causa da correlação entre idade e queda na resistência mecânica do tendão de Aquiles. Adicionalmente, no quarto estudo, foi demonstrada a capacidade do modelo de simular técnicas de sutura.

Palavras chave: Modelo computacional do tendão de Aquiles, Envelhecimento, Tendinopatia, Deslizamento, Achillon.

List of figures

List of Tables

List of abbreviations and acronyms

AGEs   Advanced Glycation end Products

APR   Anterior Posterior Radius

FEM   Finite Element Method

HGO   Holzapfel-Gasser-Ogden

MLR   Medial Lateral Radius

MRI   Magnetic Resonance Imaging

MTJ   Myotendinous Junction

PSO   Particle Swarm Optimization

RP   Reference Point

TSMTU   Triceps Surae Muscle-Tendon Unit

USP   United States Pharmacopeia

Contents

1 Introduction

The Achilles tendon is one of the most important components of human locomotion (Yin et al., 2021a). It is the main plantar flexor of the ankle joint, being also affected by the movement of the knee joint because some of the muscles attached to it originate from the femur bone. From a distance, the Achilles tendon is a fairly simple structure. A long, thin, rope-like, dense regular connective tissue. It is considered an energy-storing tendon since it present less hysteresis and more elongation at physiological loads than positional tendons (Thorpe et al., 2013). However, on closer inspection, the picture changes considerably as a number of complex interactions, still to be fully understood, appear. The details of the mesostructure of the Achilles tendon influence the global behavior of the tendon in such a way that it is important that computational mechanical models of the Achilles tendon take them into account.

In the following pages, the main aspects of the mesostructures of the Achilles tendon are examined and a computational model is proposed. The proposed model aims to be complex enough to represent the heterogeneities in the strain field of the tendon and as simple as possible in order to facilitate the interpretation of the results. At the end of the text a glossary with some of the medical terms used in this text can be found (Appendix A).

Interest in the mechanics of the Achilles tendon and its pathologies has increased in recent years. There are three main explanations for this increase. 1) The incidence of Achilles tendon pathologies has increased with the increase in recreational sports and in the overweight population, 2) The capabilities of computational mechanics are perceptibly approaching the point where it could be used in the real world as a tool to evaluate the tendon behaviour, 3) Imaging techniques have improved to the point where it is possible to measure the strain field and visualise subtendon separation *in vivo*.

1.1 Motivation of the study

The incidence of Achilles tendon rupture in the United States in 2016 was 2.5 per 100,000 person-year (Lemme et al., 2018). Extrapolating this number to the world, we can estimate a total of incidence of more than 200,000 Achilles tendon ruptures per year. Among athletes the incidence of Achilles tendinopathy (not ruptures) is much higher, during a period of only 20.4 weeks a group of runners had an incidence of 4.2% of some Achilles tendinopathy (Chen et al., 2023). And a cumulative incidence of Achilles tendinopathy before the age of 45 of 31.2% for middle and long distance runners (Kujala, Sarna & Kaprio, 2005). The incidence of Achilles tendon rupture is increasing as more people engage in

recreational and competitive sports activities (Park et al., 2019). Due to the importance of the Achilles tendon for human locomotion, any rupture, tendinopathy or pain in it can affect our ability to stand, walk, run or jump. This can affect lifestyle, autonomy, work and even end the careers of some professions such as manual workers, porters, soldiers, dancers and athletes.

A computational model of the Achilles tendon could be a useful tool for the medical community (Knaus & Blemker, 2021). Simulating the kinematics of the tendon under a given load could help the professionals to understand with greater precision the limits of the performance envelope of a specific Achilles tendon in its current state. This precision could be used to assess the risk of certain movements. In particular, The need for clarifications regarding the inhomogeneities in the Achilles tendon strain field has been mentioned several times in the literature (Screen et al., 2005; Roux et al., 2016; Shim et al., 2018; Karathanasopoulos & Hadjidoukas, 2019; Winnicki et al., 2020; Knaus & Blemker, 2021).

There is a consensus that the intensity and volume of stimulation are critical parameters in Achilles tendon healing. Tendon healing is similar to bone healing, where too little mechanical stimulation can lead to no healing or even tissue absorption, and excessive mechanical stimulation can lead to an aggravation of the tendinopathy (Schulze-Tanzil et al., 2022). Due to this fact, physical therapists have to propose exercise protocols within these limits. In addition, even though the proposition of evidence based protocols is already difficult, the proper use of such protocols by physical therapists is still a challenge (Zadro, O'Keeffe & Maher, 2019; Wallis et al., 2021).

In this context, a functional Achilles tendon model could be an asset to the physical therapist's toolbox by adding to it an additional source of evidence. It should be able to be modified to represent the specific tendon being treated in its current state and in different scenarios, and it should be able to produce results with sufficient accuracy. These criteria are necessary to meet the requirements of most health authorities for health products, i.e. safety and performance. The current state of the art in Finite Element Method (FEM) and constitutive modeling of soft tissues already provides a good basis for the yet to happen construction of a high performance model. The current main limitation to the commercial use of FEM for tendon simulation is safety, i.e. the reliability of the results of a given model. To achieve safety, an Achilles tendon model must undergo extensive validation.

1.2   Finite Element Method

The finite element method is widely used for modeling complex solid structures in engineering. It is based on continuum mechanics, where the solid body is simplified as a continuum, i.e. the microstructure of the material and phenomena such as atomic interactions are simplified as continuum fields. This allows the use of differential equations

as a tool to describe the behavior of the solid. However, the complexity of the geometry and material typically found in models of soft tissues such as tendons does not allow the possibility of solving such equations analytically. Hence the need for a numerical strategy.

Rather than solving the differential equations for the entire solid body, the finite element method starts by dividing the body into small parts called elements and proposing a very simple set of possible solutions for each element. In addition to representing the solid body as a series of elements, it is necessary to define the boundary conditions and the material models.

1.3 Soft tissues material modeling particularities

The modeling of soft tissues using FEM presents a number of additional difficulties when compared to the most commonly modeled materials in mechanical engineering. Soft tissues are typically subjected to larger strains than the acceptable for small strain theory. As a result, the use of small-strain formulations is not appropriate. Most soft tissues do not respond equally to loads acting in different directions, they usually have one or more directions in which they have some kind of reinforcement, hence the material models used to describe soft tissues must be sensitive to the direction of the load.

When tested under simple elongation, soft tissues exhibit a highly non-linear load-elongation curve represented in the literature as an S-shaped curve (Fig.1). The S-shaped curve is divided into three regions. Region I is called the "toe" region, where the perceived stiffness of the material progressively increases until it stabilizes. Region II is called the linear region, and the region III is where the material begins to lose stiffness (Fung, 1993). Some works model the region III using damage formulations (Pinto, 2014; Vassoler, Stainier & Fancello, 2016), but the definition of damage in biological tissues is not trivial and can be seen as a time-dependent, non-monotonically increasing internal variable, since biological tissues have self-healing capabilities.

1.4 Computational models of the Achilles tendon

The finite element method (FEM) has already been used to model the Achilles tendon. Yin et al. (2021b) used a series of photographs of dissected Achilles tendons to create a model that takes into account the actual geometry of the tendon and its subtendons. They used several photographs of the cross section of dissected human Achilles tendons as a reference. Similarly, Obrezkov, Finni & Matikainen (2022) based their geometry on a single image of the tendon cross sections, taking into account the actual geometry of the tendon and its subtendons. Diniz et al. (2023b) also based their geometry on images, but in their case they used MRI images of live subjects. However, the subtendon twisting was

Figure 1 – The S-shape describe the stress-strain behavior of soft tissues under simple elongation. The curve is divided in the "toe" region (I), the linear region (II) and the non-linear region (III)
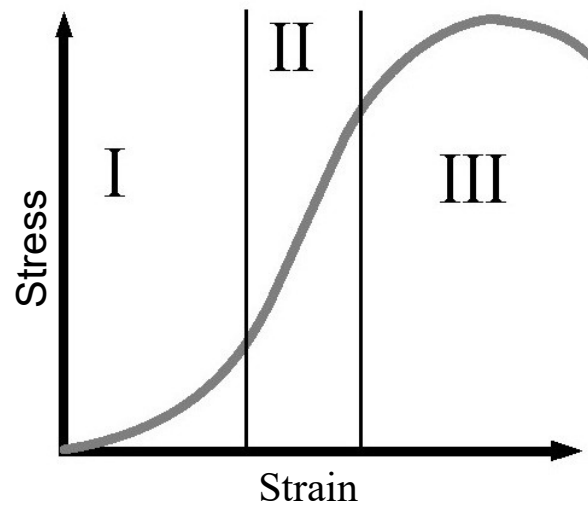
Source: Adapted from Pinto (2014)

not obtained from the images, but added afterwards by proposing two different levels of twisting based on the findings of Edama et al. (2015). Finally, Shim et al. (2014), Shim et al. (2018) and Shim et al. (2019) also based their geometry on medical images (Ultrasound) and included subtendon twisting.

With the exception of one (Obrezkov, Finni & Matikainen, 2022), all of these works included in their geometries the general external silhouette of the Achilles tendon with its misalignments and even some of its topography.

1.5 Objective and scope of the dissertation

This dissertation uses the finite element method with finite strain theory to investigate the particularities of the behavior of the Achilles tendon under different conditions. It includes the definition of a simplified geometry for the Achilles tendon where its internal structure is represented. It proposes an interface region as a novel mechanism of shear transmission between the internal substructures of the tendon and includes in the model a transition region to represent a smooth transition from pure tendon material to muscle material. Local fiber orientation is represented and the functionally graded material strategy is used to represent both the tendon-muscle transition and the presence of tendinopathies.

The objective of this work is to create, develop and validate the computational model and to demonstrate the potential capabilities of the model for clinical applications. The first study focuses on validating the homogenized behavior of the model under simple tension. The second study focuses on validating the inhomogeneities of the strain field of

the tendon under different load cases. The third study consists on the proposition of a strategy for modeling tendinopathy and it is used to compare the perceived severity of a given tendinopathy in elderly and young subjects in order to test the hypothesis that changes in shear modulus have a causal relationship with the decrease in perceived tensile rupture stress of the Achilles tendon. The fourth study aims to demonstrate the ability of the model to simulate tendon repair techniques.

1.6 Scientific contributions

Taking into consideration the propositions made in this work and their comparison with the current literature on the use of computational models to represent the Achilles tendon, the main scientific contributions of this dissertation are listed below.

- The proposition of a computational model of the Achilles tendon with a particular strategy of geometry simplification.

- The inclusion in the model of a representation of the interface separating the subtendons of the Achilles tendon rather than the use of contact formulation strategies.

- The proposition of the representation of a transition between pure tendon material and muscle material using the functionally graded material strategy

- The proposition of a representation of tendinopathies using the functionally graded material strategy.

- A validation of the inhomogeneities of the tendon strain fields when under different loading scenarios.

- An investigation of the perceived severity of a lesion when comparing elderly and young subjects.

- The simulation of a tendon repair technique.

2 The Achilles tendon (Biology)

The Achilles tendon is one of the most popularly known structures of the body. It is named after the epic hero from the poem Iliad from Homer, but its claim to fame is not exclusive due to its cultural relevance. The Achilles tendon is the strongest tendon in the human body and have an important role in human locomotion (Yin et al., 2021a).

2.1 Tendons

Tendons, ligaments, fascia and aponeuroses have as their main functional component a type of tissue called Dense Regular Connective Tissue. This type of tissue is composed primarily of fibers (Dense Connective), and these fibers are oriented in one main direction (Regular). In this type of tissue, the main function of the fibers is to transmit force, the main function of the cells is to maintain the fibers, and the main function of the extracellular matrix is to provide a pathway for the nutrients to the cells and a healthy environment for the fibers and cells (Junqueira & Carneiro, 2013). These are the characteristics of a tissue focused on its mechanical function. All the parts work towards the goal of having a strong material, with very little compromise. From an evolutionary point of view, this combination can be seen as maximizing strength in the trade-off between strength and other functionalities.

Tendons and ligaments can be separated from other dense connective tissues, such as aponeuroses and fascia, by a mechanistic classification. The former are generally structures that behave much like a rope would, i.e. as an approximately one-dimensional structural element. Aponeuroses and fascia, on the other hand, are more like membranes and behave as two-dimensional structural elements. In the first case, the fibers are mostly arranged in the direction of the rope. In the second, the fibers are arranged in multiple layers, with the fibers in each layer oriented at approximately 90 degrees to the fibers in the next layer (Junqueira & Carneiro, 2013). Similar to some man-made composite structures.

Ligaments, tendons, aponeuroses, and fascia also differ in function. Tendons and aponeuroses connect muscles to other structures. Tendons are used when a small area of attachment is needed, and aponeuroses are used when a larger area of attachment is needed. Some structures have a mixture of the two, in which case the muscle attaches with an aponeurosis-like structure that becomes progressively thinner until it has a more tendon-like shape and then attaches to the bone (for more details see pennate muscles (Azizi, Brainerd & Roberts, 2008) and (Martini et al., 2024) section 11-1). Ligaments connect bone to bone and play an important role in joint stabilization. Fascia acts as

a boundary for structures such as organs and muscles, providing additional protection and limiting the effect that one structure can have on its neighbors. In muscles, fascia is particularly strong and is called deep fascia.

Tendons transmit large forces as they facilitate movement and provide stability (Screen et al., 2015). Two main types of cells populate the tissue; the elongated and highly specialized fibroblasts, found within the fascicles, which specialize in synthesizing a collagen-rich matrix, and a population of more rounded cells in the interfascicular matrix, as well as another type of cell located in the peritenon sheet (Screen et al., 2015). The three groups of cells have slightly different functions. In tendon repair, it is sometimes desirable to maximize the function of one group and deactivate the other.

Tendons can then be divided into two main groups according to their mechanical behavior, positional tendons and energy storing tendons. The first group undergo lower levels of strain at physiological loads ($\approx 2 - 3\%$) and are more associated with precise movements. The latter undergo higher levels of strain at physiological loads ($\approx 10\%$), are more prone to injury, are more elastic, and exhibit less hysteresis. Two examples of energy storing tendons are the human flexor tendons and the Achilles tendon. They work in a spring-like fashion, storing energy during movement, contributing to the energy efficiency of some gestures, and absorbing impact.

The difference in behavior between energy storing tendons and positional tendons can be attributed to two major compositional differences. The first one is the higher presence of proteoglycans in energy storing tendons, which indicates greater osmotic gradients and thus a greater tendency to swell by absorbing surrounding water. They also have differences in crosslinking characteristics and in the geometrical arrangement of their fascicles, more specifically, energy storing tendons appear to have helically arranged fascicles (Thorpe et al., 2013; Screen et al., 2015).

Like any mechanical structure, tendons can fail under load. Such failures can cause varying degrees of damage, ranging from mild inflammation to complete rupture. Tendinopathies (tendon disorders) are likely related to overuse. In other words, although tendinopathies can result from a single impact or single overload, it is more likely that the tendon was not healthy before this abrupt event, given the high resistance of healthy tendons. The etiology of tendinopathies is still unclear and could be matrix driven or cell driven. However, Screen et al. (2015) suggests that the mechanical environment is of great importance, be it matrix perturbations due to mechanical overuse, a cellular response to altered loading conditions, or both. The literature seems to indicate that an unhealthy mechanical environment over time is the primary cause of tendinopathies. However, defining what constitutes an unhealthy mechanical environment is not a trivial task.

2.2 The triceps surae muscle-tendon unit (TSMTU)

The Achilles tendon is the distal portion of the triceps surae muscle-tendon unit (TSMTU) (Fig. 2). Its distal extremity inserts into the posterior portion of the calcaneus, forming a contact region (enthesis) that is not perpendicular to the tendon fibers. Its proximal end is indirectly connected to the three heads of the triceps surae by three aponeurosis (one for each head of the triceps surae (Edama et al., 2015)).

Figure 2 – Visualization of the origin and insertion of the TSMTU and its main parts. Image shows a view of the sagittal plane of the left leg (straight) and a the right leg (bent).
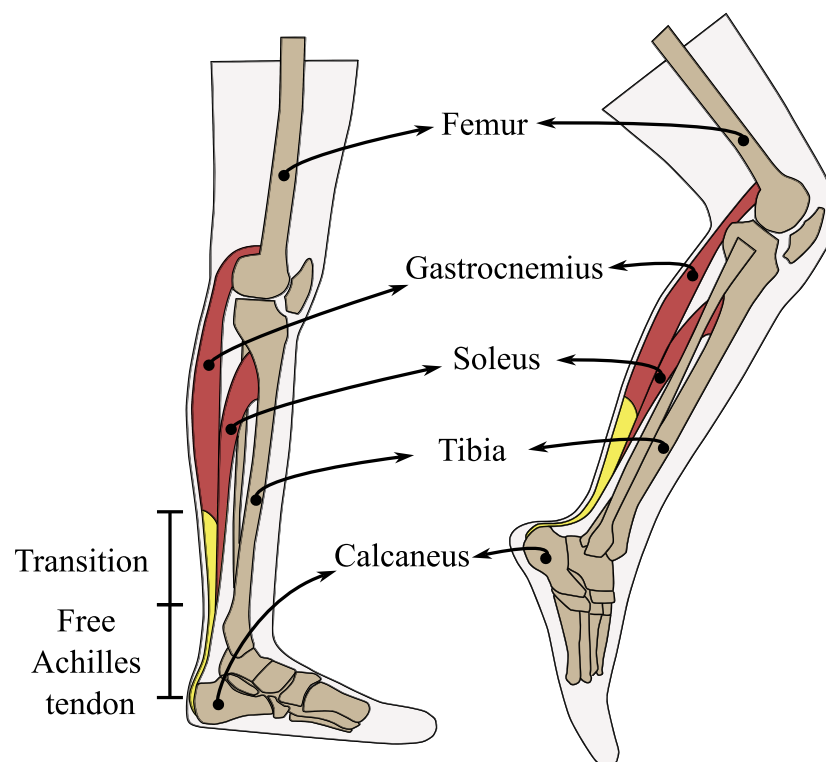
The triceps surae is composed of three muscles, the lateral gastrocnemius muscle, the medial gastrocnemius muscle and the soleus muscle (Fig. 2). The soleus muscle originates from the proximal and posterior portions of the tibia and fibula (*i.e.*, distal to the knee joint). The lateral and medial gastrocnemius originate from the lateral and medial condyles of the femur, respectively (*i.e.*, proximal to the knee joint) (Winnicki et al., 2020). The gastrocnemius muscles cross three joints from their origin to their insertion: the knee joint, the talocrural joint, and the subtalar joint. The soleus muscle crosses only the last two (Fig. 2) (Gils, Steed & Page, 1996). As the knee joint changes its position, the relative lengths of these muscles also change, affecting the load distribution in the Achilles tendon.

As the TSMTU becomes more distal, it begins to become thinner and gradually transfers its load to a set of three aponeurosis. At the soleus muscle-tendon junction

(MTJ), this load transfer effectively ends because, by definition, there are no muscle fibers distal to this point. The region of the TSMTU from the soleus MTJ to the end of the TSMTU (*i.e.*, its insertion into the calcaneus bone) is called the free Achilles tendon (Fig. 2). In most cases, the free Achilles tendon is a modestly long structure with a length of 2.54 to 7.62 cm (Pichler et al., 2007).

The main movement of the knee joint is the flexion and extension, which shortens or lengthens the gastrocnemius muscle. The main movement of the talocural joint is the plantarflexion and dorsiflexion of the ankle, which shortens or lengthens the entire TSMTU. The primary motion of the subtalar joint is the inversion and eversion of the ankle, which produces a rotation in the distal portion of the Achilles tendon about a sagittal axis passing through the center of rotation of the joint. The position of the femur, tibia, fibula, talus, and calcaneus bones determines the position of the TSMTU extremities in space at any given time (Figure 2). In addition, each of these joints has other secondary movements with a smaller range of motion, and the joint structures are covered with cartilaginous tissue that can change shape allowing small displacements and rotations in multiple axes. To keep these structures stable, a complex set of antagonist muscles, secondary muscle-tendon units, and ligaments are distributed along the distal portion of the leg. However, the large loads associated with the heel movements cause the auxiliary structures to deform. The result is that the multiple degrees of freedom of the knee, talocural, and subtalar joints can affect or be affected by the TSMTU, even though some of them are partially constrained (Lersch et al., 2012) . To simplify this scenario, it is useful to consider only the simple elongation of the tendon. However, plantarflexion-dorsiflexion and the inversion-eversion of the ankle are movements with a large range of motion and subject the Achilles tendon to significant bending (Lersch et al., 2012).

2.3　The Achilles tendon anatomy/morphology

Internally the Achilles tendon fibers are segregated to the point that they can be separated by dissection (Edama et al., 2016). Such separated regions are known to twist along the AT axis in a rope-like fashion. The twist occurs as a right-hand thread in the left leg and as a left-hand thread in the right leg. The degree of twisting can vary between subjects and between the legs of the same subject (Edama et al., 2016; Benjamin et al., 2007; Pekala et al., 2017).

As the three aponeurosis cross the muscle-tendon junction, their shape becomes gradually thicker and less broad transitioning from the shape of an aponeurosis to that of a tendon. It is then more appropriate to call each of then a subtendon. The subtendons and aponeurosis are an uninterrupted structure, however the strains in the tendon can be much higher than in the aponeurosis (Finni & Lichtwark, 2016). Each subtendon is

attached to a different muscle of the triceps surae and may experience loads or elongations that are different from the other two subtendons. This is especially true when we compare a subtendon of the gastrocnemius muscles to the subtendon of the soleus muscle. However, because they are twisted and the lateral force transfer is not negligible (non-negligible shear stresses), a non-negligible influence of a given subtendon on its neighbors is observed. This lateral force transfer tends to be less present in young subjects and more present in elderly subjects, and such correlation with age is associated with the well-known adhesion phenomenon caused by the accumulation of advanced glycation end products (AGEs) (Yin et al., 2021a; Pekala et al., 2017; Handsfield et al., 2017).

Sliding occurs at the interface between the subtendons. This interface is usually represented as a contact interaction in finite element models of the Achilles tendon (Yin et al., 2021a; Shim et al., 2018). Despite its small thickness, the interface was used as a guide in dissections aimed at separating the subtendons (Prosenz et al., 2018), and its thickness was seen on magnetic resonance imaging (Szaro et al., 2020). However, to our knowledge, its mean thickness has not been reported.

2.3.1 Subtendon twist particularities

The amount of subtendon twist in the Achilles tendon is known to vary considerably between subjects or even between the legs of a given subject (Edama et al., 2015; Edama et al., 2016; Benjamin et al., 2007; Szaro et al., 2009; Gils, Steed & Page, 1996; Schepsis, Jones & Haas, 2002). However, the measurements of subtendon twisting *in vivo* are not common, even though the visualization of the interface with imaging techniques is already possible (Szaro et al., 2020). This makes the study of the effect of subtendon twisting on performance a difficult task. Evidence suggests that the presence of subtendon twisting is not a phenotypic plasticity to the load environment, since subtendon twisting with adult-like characteristics has been observed in fetuses as early as the second trimester of gestation (Szaro, Witkowski & Ciszek, 2021; Edama et al., 2021). In addition, recent observations showed no correlation between the amount of twisting and either sex or side (Szaro et al., 2020).

Some authors classify the amount of twisting into three categories (Edama et al., 2015; Pekala et al., 2017): Type I represents the least amount of twist, where the calcaneal insertions follow approximately the same pattern of the muscle origins (i.e. close to zero degrees of twist); Type II represents moderate twist, where the soleus subtendon inserts mainly into the medial region of the calcaneus and the anterior portion of the Achilles tendon is shared by soleus and lateral gastrocnemius subtendon fibers (i.e. close to 90 degrees of twist); Type III represents extreme twisting, where the subtendon fibers of the lateral gastrocnemius dominate the anterior portion of the Achilles tendon with the soleus subtendon fibers getting almost completely posterior (i.e. almost 180 degrees).

Different studies have used slightly different definitions for types I, II, and III and different measurement techniques, but their results show a pattern of about 50% of prevalence for Type I, about 45% of prevalence for Type II and about 5% prevalence for Type III when the measurements are taken proximal to the insertion (Edama et al., 2015; Pekala et al., 2017). When the measurements are taken at the bone insertion, the values change significantly in favor of more rotation, as expected (Edama et al., 2016; Edama et al., 2021).

2.3.2   Bone insertion particularities

The Achilles tendon is inserted in the most posterior region of the foot, the calcaneal tuberosity (Pekala et al., 2017; Schepsis, Jones & Haas, 2002). The insertion geometry is crescent shaped when seen in the transverse plane (Lohrer et al., 2008) and near elliptical when seen in the frontal plane in (Edama et al., 2016). The insertion area is close to parallel to the tendon line of force and it is considerably larger than the cross-sectional area of the tendon itself. Its width and length can vary between individuals (Mahan et al., 2020; Pekala et al., 2017). Reported values are as follows: width = 34.72 ($\pm$ 3.20) mm, length = 45.70 ($\pm$ 5.58) mm, area = 1246.85 ($\pm$ 201.53) mm2 (Pekala et al., 2017).

The calcaneal tuberosity can be divided into three facets: superior, middle and inferior. Most of the Achilles tendon inserts into the middle facet, with some fascicles inserting into the uppermost part of the inferior facet (Edama et al., 2016; Ballal, Walker & Molloy, 2014). The exact position of the insertion may vary among subjects. Reported observations are: 55% of the Achilles tendons insert at the superior one-third of the calcaneal tuberosity, 40% at the middle one-third and 5% at the inferior one-third (Edama et al., 2016). There is a superior region of the superior facet that does not receive insertions from the Achilles tendon, but it plays an important role because it can rub against the Achilles tendon during use (posterior ankle impingement), causing local inflammation or even calcification in the region. Among others causes, the use of poorly fitting shoes can start this process leading to conditions such as the Haglund's syndrome (Vaishya et al., 2016).

2.4   Tendon composition

The Achilles tendon, like other tendons, has three main components: water, collagen and proteoglycans. However, many other constituents can be found in the tissue and affect its mechanical properties, its metabolism or both. Two of these are of interest of this work, elastin and lubricin.

Water is the main constituent of tendons making more than 60% of its weight (Hannafin & Arnoczky, 1994). Water plays an important role in the tissue mechanics due

to its large presence. It can be a source of internal pressure due to osmotic effects and can permeate in the tissue in response to loads (Lai, Hou & Mow, 1991). Water is also the most abundant chemical actor, playing a fundamental role in the metabolism of the tissue, and acting as a media for the transport of other molecules (Yao & Gu, 2007).

Collagen accounts for 60-85% of the dry weight of tendon (Kjær, 2004). Collagen fibers can be highly oriented and are responsible for the anisotropic behavior observed in tendons (Lynch, 2003). More specifically, collagen type I is specialized in resisting tension loads (Junqueira & Carneiro, 2013) and it is the main constituent of tendons (Gelse, Poschl & Aigner, 2003). As tendons approach an insertion or pulley, other proteins such as type II and type III collagen are more present, making it more cartilage-like in these regions (Winnicki et al., 2020).

Proteoglycans are molecules of great importance to the mechanical behavior of cartilage and intervertebral discs due to its ability to "attract" water to the inside of the tissue, even when the pressure gradient indicates otherwise (Lai, Hou & Mow, 1991). However, their role in tendons is not fully understood. They play a role in increasing the water content of the tendon, and a case could be made that this would have an effect on tendon stiffness and/or ultimate stress, but the observations do not support this conclusion (Thorpe et al., 2013). However, it is likely that these proteins play a role in the time-dependent mechanical behavior of tendons. Since proteoglycan content lowers with age, and injury in tendons increase with age, one can argue that the proteoglycan content affect the sliding of fascicles (Thorpe et al., 2013). The efficiency of healing and maintenance mechanisms can also be affected by the lack of water in the environment.

Elastin is a protein with elastic behavior. When cyclically stretched, elastin exhibits a very low hysteresis when compared to other biological soft materials (Fung, 1993). It can be observed by immunohistochemistry and it is found to be localized longitudinally around groups of cells and transversely between collagen fascicles (Grant et al., 2013). The properties of elastin suggest that it plays a role in mechanotransduction (Grant et al., 2013). Given its highly elastic behavior and its small presence in most tendons, it can be argued that elastin helps the material to eventually "remember" its original shape. The ligamentum nuchae (ligament that pulls the head from behind the neck) of ungulates (large hoofed animals such as pigs, horses, and elephants) is almost pure elastin (Fung, 1993); this allows such animals to hold their massive heads up for long periods of time without expending much energy, even though their necks are horizontal most of the time.

Lubricin is a liquid substance present in the interfascicular regions of tendons (Thorpe et al., 2012b; Sun et al., 2015; Kohrs et al., 2011) and in the surface of cartilage (Jay & Waller, 2014) that acts as a lubricant. Its effect on tendon mechanics can be seen in the decline of tendon performance with age, since one of the major differences between a young tendon and an elderly one is the sliding ability of the fascicle. Low lubricin levels

are associated with less effective load distribution, making the tendon more prone to injury (Sun et al., 2015; Funakoshi et al., 2008; Thorpe et al., 2012a).

Thousands of other molecules are present in the tendon's tissue and the study of each one and its effect on tendon behavior is quite overwhelming. For now, the above five groups have been selected as sufficient for the goals of this work. However, it is important to remember that even molecules at very low concentrations have the potential to cause major changes in a tissue. The biochemical aspects of a tissue should never be underestimated, and the choice of the above five groups is due more to a lack of specific knowledge of the effects of each of the other substances than to a proper simplification process.

Cells and blood vessels have the important task of managing this complex array of molecules and keep the tendon healthy. Among the cells, the tenocytes and tenoblasts (tendon cells) constitute 95% of the cells in the tendon (Winnicki et al., 2020) and are the main collagen synthesizers of the tendon (Junqueira & Carneiro, 2013). Synovial cells, chondrocytes, vascular cells and macrophages can also be found in the tendon (Winnicki et al., 2020; Junqueira & Carneiro, 2013).

2.5   Nutrition, exercise, and metabolism

Nutrition is known to aid in muscle growth and recovery, but its effects on tendon healing are not yet clear. However, it is known that protein intake associated with physical activity has a positive effect on tendon development and recovery (Tomlinson et al., 2018). The muscle-tendon unit has also been shown to be positively affected by amino acid and vitamin intake in animal models (Tack, Shorthouse & Kass, 2018). Advanced glycation end products (AGEs) appear as the villains having a negative effect in animal models (Grasa et al., 2013). The results are not different from those expected for these molecules, and it seems that a diet that benefits muscle tissue also benefits tendons. However, some authors call for caution:

> "Much more research and clinical attention is needed to develop better treatment strategies for torn or damaged tendons. Most of the research on tendons and nutrition have dealt with animal or cell culture studies which may or may not be representative of the effects of nutrition and tendon health in humans.[...]" (Curtis, 2016).

Exercise is known to stimulate tendon's protein synthesis (Screen et al., 2005), but rest periods are also important. Strict immobilization has been shown to reduce both resistance and stiffness, and aging can reduce size and resistance, increasing the risk of rupture (Singh et al., 2015). Rapid tendon recovery is of particular interest to athletes, since each day of recovery is one less day of training. Studies such as Baar (2018) focus on this population.

The mechanism of tendon response to mechanical stimulus is sometimes explained

in purely mechanical terms. Similar to bone, tendons respond to mechanical stimulus with adaptation, but unlike bone, tendons are usually under inhomogeneous strain due to their internal mesostructure combined with a highly ortotropic microstructure. These localized strains are sensed at the cellular level. The matrix is then changed in response, so the same external load may be perceived differently at the cellular level over time (Screen et al., 2005).

Tendons are also affected by purely chemical phenomena. Genetics and protein expression can alter the behavior of tendons, as is the case with the Ehler Danlos Syndrome and Osteogenesis Imperfecta (Ribbans & Collins, 2013), both genetic disorders related to the genes associated with collagen synthesis. Tendon is not only collagen, other molecules are known to play a big role in its behavior, especially since their concentration can change much faster than the concentration of collagen(Screen et al., 2015). In addition, the circadian clock and hormonal changes are known to be factors (Screen et al., 2015).

The Achilles tendon is surrounded by the paratenon, which is a tissue richly vascularized by a series of transverse vincula (flexible attachments to the surrounding tissue) (Schepsis, Jones & Haas, 2002). Some of these blood vessels reach the tendon directly, and some reach it indirectly by feeding the paratenon and reaching the tendon by difusion (Schepsis, Jones & Haas, 2002). The tendon also receives blood from its muscle-tendon junction and through its insertion (Schepsis, Jones & Haas, 2002). Vascularization is considered a key factor in rupture etiology and healing (Winnicki et al., 2020). Tendinopathies can be followed by a local increase in blood flow due to neovascularization and inflammation (Cook et al., 2004; Punchard, Whelan & Adcock, 2004), which can be detected and measured by ultrasound imaging (Winnicki et al., 2020).

2.6 Tendinopathy and rupture of the Achilles tendon.

The main disorders affecting the Achilles tendon can be divided into two major groups, ruptures and tendinopathies, and both can then be subdivided into insertional and non-insertional (Peek, Malagelada & Clark, 2016). Although both insertional and non-insertional tendinopathies are common, ruptures are usually non-insertional, more specifically, they tend to occur in the least vascularized region and with the smallest cross-sectional area of the Achilles tendon, $\approx 5\,\text{cm}$ proximal to the insertion (Peek, Malagelada & Clark, 2016; Park et al., 2019).

2.6.1 Tendinopathy

The term tendinopathy is used to describe a number of disorders of the Achilles tendon usually associated with pain. Tendinopathy can be defined as a failure of the healing response of the tendon (Aicale, Tarantino & Maffulli, 2019; Giuseppe Longo, Ronga & Maffulli, 2009). Its definition is more general than tendinitis and tendinosis, although both can be present in a case of tendinopathy. Tendinitis is used to describe an inflammatory process that is not always important for the pathology (Aicale, Tarantino & Maffulli, 2019), while tendinosis is used to describe a series of histological changes that deviate from the "normal" tissue which include a change in the mechanical properties due to a loss of the normal collagenous architecture (Aicale,

Tarantino & Maffulli, 2019; Xu & Murrell, 2008; Khan K.M. et al., 1999; Alfredson, Öhberg & Forsgren, 2003). Such histological changes do not necessarily result in a pathology (i.e. they may not be a problem requiring the attention of a physician) (Docking, Ooi & Connell, 2015). Because of that, the literature prefers the term tendinopathy (Aicale, Tarantino & Maffulli, 2019), since it describes a problem in the tendon that requires attention and not a specific phenomenon.

So it is a viable hypothesis that a tendinosis could result in tendinopathies with different perceived severities depending on the tendon where the tendinosis occur. This work explores this hypothesis as it will be shown in the next sections.

Insertional tendinopathy of the Achilles tendon includes the presence of tears in the tendon tissue, with a higher incidence of tears in the subtendons of the lateral gastrocnemius (Mahan et al., 2020). The etiology of the preference of this pathology for the lateral gastrocnemius subtendon is still not clear, but it is hypothesized that it is related to a poorer blood supply of this subtendon when compared to the other two (Mahan et al., 2020).

Calcific tendinopathy and insertional calcific tendinopathy are localized calcium deposits in the substance of the tendon. Such deposits are known to cause stiffening of the material and, as a consequence, changes in the strain field of the tendon material in the vicinity of the deposits (Oliva, Via & Maffulli, 2012). The body's response includes surrounding the deposits with cartilage-like material (Oliva, Via & Maffulli, 2012), a likely adaptation for the compressive stresses that typically are present around a stiff inclusion in soft materials under tension.

Ultrasound can be used to identify the presence of tendinosis and its geometry. Not all tendinosis is tendinopathy, but most tendinopathies present some type of tendinosis (Docking, Ooi & Connell, 2015). When the tendinosis is significant, it alters the sound transmission properties of the tissue, resulting in abnormal echogenic regions (Docking, Ooi & Connell, 2015). The regions of different echo properties can be identified and measured and the severity of the tendinosis can also be assessed by measuring the characteristics of the abnormal echo region (Docking, Ooi & Connell, 2015; Azzoni & Cabitza, 2004; Öhberg, Lorentzon & Alfredson, 2001). Calcifications can also be identified by Ultrasound (Azzoni & Cabitza, 2004). The shape of the tendinosis can vary from multiple small affected regions to single large ellipsoidal regions affecting almost the entire tendon cross section (Harris & Peduto, 2006).

For tendinopathy, the range of possible treatments varies widely. There are three main categories of treatment: Conservative, minimally invasive and open surgery. When the severity of the tendinopathy is too extreme open surgery may be the only option (Giuseppe Longo, Ronga & Maffulli, 2009). If surgery is necessary, but the case allows for minimally invasive techniques such as minimally invasive stripping, then they are preferred over open surgery due to the high possibility of wound complications of open surgery (Giuseppe Longo, Ronga & Maffulli, 2009). Conservative treatment can consist of different procedures that can be as simple as rest and modification of activity or more aggressive and complex such as platelet-rich plasma injection (Riley, 2008).

2.6.2 Rupture

Rupture cases are treated differently. Ruptures are classified by some authors as partial or complete (Miller & Shemory, 2017). The main diagnostic tool for identifying Achilles tendon ruptures is a series of simple tests performed by the professional with little to no equipment in the clinic (Peek, Malagelada & Clark, 2016). When in doubt or in need of more detailed information, the professional may request medical images such as ultrasound, magnetic resonance imaging (MRI) or even X-rays. Ultrasound is preferred because it has a dynamic nature, and it is generally more available and cheaper than MRI (Peek, Malagelada & Clark, 2016).

The treatment of ruptures can be conservative or surgical, conservative techniques are labeled as leading to re-rupture while surgery is associated with other complications such as unwanted adhesion and infection (Rebeccato et al., 2001). In the literature there are works defending conservative over surgery (Chutkan, 2013; Willits et al., 2010) and works defending surgery over conservative (Buddecke, 2021; Schepsis, Jones & Haas, 2002). However, the consensus seems to be that the best approach can vary depending on the case (Ochen et al., 2019; Khan, 2005; Peek, Malagelada & Clark, 2016; Uquillas et al., 2015; Nunley, 2009). The tendency is to use conservative treatment in patients with general contraindication for surgery or low level of expectations in terms of Achilles tendon function and use surgery in cases of athletes or active persons (Schepsis, Jones & Haas, 2002). Patients in between these two groups would be evaluated on a case-by-case basis.

Percutanous surgical procedures appear as an intermediate option. Three examples are: the Achillon, PARS and triple shoelace techniques (Ismail et al., 2008; Clanton et al., 2015; Adames et al., 2023; Daleffe et al., 2023). The first two are widely known and used by the community and the third is a technique that aims to produce a stronger repair by: 1) Making the anchoring distal to the ruptured region, hence avoiding to anchor suture in the injured tissue. 2) Passing the suture inside the tendon and through the rupture ends, hence avoiding bayoneting (Heitman et al., 2011). 3) The technique, arguably, improves the chances of using early rehabilitation strategies. The Achillon technique is of particular interest in this work.

2.6.3 The Achillon technique

The Achillon technique is considered a percutaneous technique since it is performed with minimal opening. By causing less damage to the tissue surrounding the tendon during surgery, the risk of inflammation is reduced, however, the surgeon will be working with limited visualization and limited access to the tendon.

The technique starts by making a small vertical incision close to the rupture site. The skin is then retracted using Gillis type hook retractors. A secondary incision of similar size and position is then made in the paratenon which is held in place by temporary small sutures. At this point, the opening is large enough for the insertion of the ACHILLON® special device.

The special device is a fork-shaped clamp that is partially inserted into the incision and clamps the Achilles tendon stump between its two central branches. Once the device is properly

positioned, the surgeon uses a series of holes in the sides of the two outer branches of the device as templates to insert three different strands of suture into the tendon. The suture is passed through the holes in the four branches of the device, twice through the skin and paratenon, and through the Achilles tendon stump. Once the suture is properly placed, the device is gently pulled back, allowing all the 6 sections of suture (two for each strand) to exit through the initial incision. The same procedure is then repeated on the other stump, and the resulting 12 sections of suture are tied in pairs, forming a total of six knots. More details on the technique can be found in Heitman et al. (2011) and Ismail et al. (2008). A number of useful images can be found in Assal (2024).

2.6.4   Rehabilitation

After the surgery, rehabilitation plays an important role in the final outcome of the operative treatment (Schepsis, Jones & Haas, 2002). In the flexor tendon literature, the principle of early mobilization is well established as it promotes the proper healing mechanisms. The literature began to refer to two main mechanisms of healing for flexor tendons, the intrinsic and the extrinsic. The latter is related to unwanted adhesions of the tendon to the surrounding tissues, especially when associated with immobilization. And the literature refers to the intrinsic mechanism as the one to pursue. One way of doing so is by mobilising the healing tendon as soon as possible. This is true for the flexor tendons of the hand (Roberts, 2011; Schöffl, Heid & Küpper, 2012; Klifto, Bookman & Paksima, 2019; Singh et al., 2015). Similarly, early mobilization is sometimes advocaded in the Achilles tendon literature (Screen et al., 2005; Khan, 2005). This principle is very important for flexor tendon repair as adhesions are a major problem for them (especially in the no man's land region, zone II). However, when repairing the Achilles tendon, percutaneous techniques produce less adhesion than open techniques (Buddecke, 2021), and early mobilization seems to be less important for preventing complications and more important for athletes or persons who want to return to activity as soon as possible.

3 The Achilles tendon (Mechanics)

One of the most interesting facts about the tendon is its ability to withstand up to 12 times the weight of the body while running (Winnicki et al., 2020), reaching up to 110 MPa average stress (Winnicki et al., 2020), close to the yield strength of some aluminum alloys. However, the Achilles tendon is also one of the most commonly injured tendons (Śmigielski, 2008). Many of the injuries to the Achilles tendon have some relation with the practice of sports such as football, track and field and basketball (Śmigielski, 2008). Other animals are more specialized in running and jumping than humans, and it is argued that one of the reasons the Achilles tendon suffers from so many injuries is the asymmetrical loading caused by its special anatomical structure (Śmigielski, 2008).

The Achilles tendon is not a single homogeneous unit. It is an assembly of three subunits. Each may have different loading conditions resulting in non-uniform strain fields as can be seen in (Laura Chernak Slane & Thelen, 2014; Franz et al., 2015; Lersch et al., 2012). The presence of lubricin (Sun et al., 2015) and the sliding observed in the interfascicular matrix (Thorpe et al., 2015) point to the importance of the sliding mechanism. That is, it is not something that happens by chance, but rather the result of evolutionary adaptation. Sliding is a desirable trait.

The need for a sliding mechanism can be explained by two main facts. The first and most obvious is that the ankle joint has a range of motion that can be greater than 30 degrees (Hageman & Blanke, 1986; Csapo et al., 2010). This rotation is transmitted to the Achilles tendon by the calcaneal tuberosity and, if no sliding were possible, it would result in big shear stresses. The second and less obvious is that the two muscles of the Achilles tendon interact differently with the leg's kinetic chain. The soleus behaves almost as a uniarticular muscle, and the gastrocnemius as a biarticular muscle, making their relative motion a function of the position of the knee joint. In actions such as vertical jumping, these two muscles may be activated at slightly different instants of the gait in order to achieve maximum power output (Farris et al., 2015), resulting in different loads in different subtendons of the Achilles tendon at a given time.

The macroscopic behavior of the Achilles tendon seen as a homogeneous unit has been studied by some authors and it is a useful point of view because it provides insight into the behavior that results from the sum of the various factors involved. However, viewing the Achilles tendon as a unity is limiting. When investigating the mechanical behavior of the Achilles tendon, it is important to remember that it is a tendon made up of three subtendons from different muscles that are twisted, and that the subtendons and fascicles have the ability to slide with respect to each other. These phenomena will be discussed in the following few sections.

3.1   Uniaxial Behavior

Works such as Stenroth et al. (2012) simplify the Achilles tendon and choose to consider it as a homogeneous unit. Such simplifications make it easier to model factors such as the resulting longitudinal tangent modulus and the effect of age on the overall behavior of the tendon. When tested as a unit, the tendon exhibits a longitudinal tangent modulus close to 1 GPa (Stenroth et al., 2012; Arya & Kulig, 2010). It behaves close to an ideal rope, but shows some resistance to flexion in the sagittal (Harkness-Armstrong et al., 2020) and frontal (Lersch et al., 2012) planes.

Tendons such as the Achilles tendon and the flexor tendons in general are classified with respect to their function as energy storing tendons. Other tendons such as the anterior tibialis are classified as positional tendons (Thorpe et al., 2013). As the name suggests, positional tendons are more rigid and act less as a spring in the mechanical system and more as a simple rigid connection with little to contribute other than transferring the force from the muscle to a particular point in the body. Energy storing tendons, on the other hand, are more influential components of their mechanical environment. They act as springs, absorbing large amounts of energy and releasing it quickly (Thorpe et al., 2013). By doing so, they improve the movement efficiency. These properties may be achieved by means of helically oriented fascicles (Thorpe et al., 2013).

Both extremities of the Achilles tendon are considerably wider than its central cross section (Edama et al., 2015; Shim et al., 2018). The resulting geometry is close to a three-dimensional dog bone tensile specimen with an ellipsoidal cross section. At first glance, this geometry may seem to be simply the result of the body's adaptation to the Saint-Venant principle, but the tendon is highly anisotropic and undergoes large deformations, which can lead to kinematics that differ from a normal dog bone specimen (Carniel et al., 2019).

In addition to the tendon fibers following a spiral-like orientation, each fascicle may have mechanical properties that differ from those of its neighbors (Komolafe & Doehring, 2010). In Komolafe & Doehring (2010) the Achilles tendon fascicles and the whole tendon were tested uniaxially. Stress-strain curves were shown and a failure pattern was investigated. The stress-strain curves of the tendon showed significantly less stiffness than the single fascicle curves, leading to the conclusion that the fascicles are not equally loaded when the tendon is pulled.

The loads in the Achilles tendon can vary greatly depending on the gesture being made. As a general rule, slow and controlled movements impose lower loads than dynamic movements. During maximal voluntary isometric contraction loads can reach up to 2 kN (Olszewski, Dick & Wakeling, 2015) or even 3 kN (value calculated using the torque of 105 Nm measured by Nuri et al. (2018) and the moment arm of 35 mm measured by Olszewski, Dick & Wakeling (2015)). During dynamic movements peak values start at 2 kN for less intensive exercises such as walking, hopping, squat jumping, and countermovement jumping (Schepsis, Jones & Haas, 2002). But can go up to 6 to 8 times body weight (Schepsis, Jones & Haas, 2002) or even 9 kN (≈ 12 times body weight) in more intensive exercises such as running (Winnicki et al., 2020). These results show that the Achilles tendon can receive loads that can triple the maximum load that the TSMTU is capable of producing. During such movements, the entire TSMTU acts more like

a spring and less like a motor.

Dynamic movements can result in stresses of 110 MPa (Winnicki et al., 2020; Maganaris, Narici & Maffulli, 2008), which is in the same order of magnitude as the ultimate stress measured for the Achilles tendon (Maganaris, Narici & Almekinders L. C. Maffulli, 2004). This partially explains the high injury rate among athletes, but the direct comparison of these two numbers can be misleading. It is important to take into account that the experimental conditions of ultimate stress measurements are usually of comparatively lower strain rates than the loads measured during exercises such as running (Louis-Ugbo, Leeson & Hutton, 2004). It is also important to consider that ultimate stress measurements are usually made using fixtures that are known to influence the strain field (Carniel et al., 2019). In addition, the strains in tendons are known to be non homogeneous (Lersch et al., 2012; Franz et al., 2015; Farris et al., 2015; Śmigielski, 2008), so the local stress could be higher in both experiments. However, the values are too close to be representative of the situation. With ultimate stresses so close to those expected for a common repetitive activity such as running, it would be reasonable to expect much higher rates of tendinopathy before the age of 45 than the reported 31.2% for middle and long distance runners (Kujala, Sarna & Kaprio, 2005). Because of that, the interpretation of such numbers must be made with caution.

3.2   Shear Behavior (sliding)

The lateral interactions between fascicles are perceived as weak when observing energy storing tendons. This lack of lateral force transmission is usually described as sliding and has been hypothesized as a possible underlying mechanism for partial Achilles tendon injury (Śmigielski, 2008). The reported shear modulus of tendon fascicles is $\approx$ 5 kPa (Purslow, 2009), many orders of magnitude lower than the reported longitudinal tangent modulus ($\approx$ 1 GPa (Stenroth et al., 2012; Arya & Kulig, 2010)), making some authors describe it as negligible and conclude that fascicles act as independent structures (Haraldsson et al., 2008). However, the full picture may not be so simple. Experiments with fascicles usually focus on a single fascicle pair (Haraldsson et al., 2008; Thorpe et al., 2012a) or a small fraction of the tendon (Haraldsson et al., 2008). The first type of experiment, although insightful, fails to represent the effect of the multiple neighbors of a given fascicle. The second may lead one to assume that the lateral force transmission of the fascicles is of little or no importance, but the combination of the three-dimensional geometry of the fascicles (Edama et al., 2015) and the large non linearity of the stress-strain curve shown in Purslow (2009) points to the other direction.

The existence of sliding is perceived more as an energy-storing tendon characteristic. Comparing the whole tendon behaviour with its fascicles, Thorpe et al. (2012b) observed that the fascicles failed at lower strains and stresses than their tendon. Then Thorpe et al. (2012b) tested a pair of fascicles axially, fixing then in a manner that fascicle A was being pulled by one side of the machine and fascicle B by the other. By using this strategy, the force transmission from one loading grip to the other through a single fascicle was impossible. All the force needed to be laterally transmitted to get from one grip to the other. When the protocol above was

executed, larger strains were observed and the authors concluded that the sliding is sufficient to account for the differences in failure strain between fascicles and whole tendons. They also concluded that the sliding between fascicles prior to fascicle extension may protect the fascicles from damage. This particular observation may lead the reader to conclude that sliding may be the culprit for the differences in failure strains and stresses between fascicles and whole tendons. But the authors of Thorpe et al. (2012b) specifically chose the word "damage", which clearly indicates that the explanation for the stress differences was not found in Thorpe et al. (2012b).

The sliding ability of energy-storing tendons is a well-known phenomenon. It is one of the major differences between energy storing tendons and positional tendons (Thorpe et al., 2015). Sliding is mostly an interfacial phenomenon, localized in the interfascicular matrix. The main actor of this phenomenon is the protein lubricin (Kohrs et al., 2011; Thorpe et al., 2016; Funakoshi et al., 2008). This protein is more abundant in energy-storing tendons, especially in the interfascicular regions. Proteoglycans and elastin are also found more abundant in the interfascicular matrix of energy-storing tendons and may help to explain the overall behavior of the tendon.

The sliding capabilities of tendons are known to prevent tendinopathies, and the lowering in sliding capabilities of tendons is shown to be related to age in a horse model (Thorpe et al., 2012a). The relationship between lowering in sliding capabilities and tendinopathies is also shown in human Achilles tendons (Sun et al., 2015).

In conclusion, sliding is a phenomenon present in energy-storing tendons such as the Achilles tendon. It may be related to the capability of such tendons to withstand greater strains than positional tendons. However, its relationship to the other characteristics of energy-storing tendons is less evident. The lack of lateral force transmission cannot be used by itself to explain why fascicles fail at lower stresses than the tendon they belong to. The existence of sliding equates to the existence of a dissipation mechanism, what is not desirable when one thinks on an efficient energy-storing spring. None or almost no lateral force transmission indicates highly heterogeneous stress fields, which in itself makes the whole tendon as resistant to damage as its weakest fascicle in a given loading condition. Sliding alone is insufficient, and one or more additional phenomena are needed to answer the questions above. A good first step is to consider the spiral-like three-dimensional geometry of energy-storing tendon fascicles.

3.3   Strains in the Achilles tendon

Since the Achilles tendon is composed of multiple fibers running longitudinally, traditional uniaxial tensile test results could be influenced by the test technique (Carniel et al., 2019). To properly investigate the strains in the Achilles tendon, the experimental strategy should be performed *in vivo*, such as in Franz et al. (2015), or try to mimic the fixture conditions as close to the *in vivo* as possible, as in Lersch et al. (2012). The ultrasound techniques are particularly interesting because they are able to measure the displacement of tendons in real time *in vivo* under controlled conditions such as in an isokinetic dynamometer (Kay & Blazevich, 2009;

Olszewski, Dick & Wakeling, 2015) or in more realistic conditions through the use of portable devices fixed in the heel of the subject (Franz et al., 2015).

Measurements using 2D ultrasound elastography speckle tracking have shown that the fibers of the superficial and deep regions of the free Achilles tendon undergo significantly different longitudinal displacements and elongations during walking (Franz et al., 2015). During walking, the peak strains of the Achilles tendon fibers can reach values of 13% for the superficial fibers and 10% for the deep fibers (Franz et al., 2015). Measurements taken in the transition region, i.e. between the soleus and gastrocnemius muscle-tendon junctions, showed lower values, approximately 5% (Franz et al., 2015). This result has already been observed under similar conditions, but not during passive stretching, meaning that the activation of the soleus muscle also influences the elasticity of the transition region (Franz et al., 2015). This is particularly interesting for dynamic exercises, where the Achilles MTU muscles could act more like a series of valves that regulate how much of the work done by the large muscles of the thigh and hip is transferred to the ankle.

Other measurements speak of 4% maximum stretch before damage (Winnicki et al., 2020; Nuri et al., 2018), which is significantly lower than the values reported in Franz et al. (2015). In Nuri et al. (2018) an explanation for this big difference among measurements could be due to a difference of where the Achilles tendon begin and where it ends, with some authors measuring the elongation at the soleus muscle-tendon junction and others measuring at the gastrocnemius muscle-tendon junction (Nuri et al., 2018).

The change in volume during loading of the Achilles tendon has been measured *in vivo* as very little or nonexistent (Nuri et al., 2018; Obst et al., 2014). However, tendinopathy can alter this behavior significantly, resulting in a reduction in tendon volume of up to 28% during tension, which could be an important part of remodeling (Nuri et al., 2018). This change in the mechanical behavior is suggested to be linked to the fluid exudation (Nuri et al., 2018), a likely consequence of the repair process which includes local neovascularization and inflammation (Cook et al., 2004; Punchard, Whelan & Adcock, 2004).

The strain distribution in the Achilles tendon was multiple times observed as inhomogeneous. There are four main sources of inhomogeneity. First, the fact that the tendon fascicles and sub-tendons can slide. Second, the twisted geometry of sub-tendons and fascicles. Third, the change in position and orientation of the calcaneal tuberosity (Lersch et al., 2012). Fourth, the uneven activation of the three muscles attached to it (Franz et al., 2015; Farris et al., 2015). The interaction of these four phenomena can be seen in works such as Franz et al. (2015) and Laura Chernak Slane & Thelen (2014). Such works use ultrasound to track *in vivo* the position of various points inside the Achilles tendon. This allows a displacement field to be constructed and both works present results with clear non-uniform strain fields. This type of experiment has been used to compare elderly subjects to young subjects and it has been found that elderly subjects have a more uniform displacement field (*…defined as difference between deep and superficial portions of the free Achilles tendon…*)(Franz & Thelen, 2016). These results agree with the fact that tendons of elderly subjects have less sliding. With less sliding, forces in one fascicle are

transmitted to its neighbors through shear stresses, resulting in more uniform strain fields at points far from the tendon extremities, even when the boundary conditions are not uniform.

The sliding phenomenon may be an important factor in the inhomogeneous strain field of the Achilles tendon. Although not yet clear to the literature, the scenario outlined above indicates that uniformity of strain does not necessarily imply uniformity of stress. In fact, the opposite may be true. Nonuniformity of strain due to fascicle sliding may help the tendon to have more uniform and less intense stresses, as indicated by computational models (Shim et al., 2018).

When under load, the cross section of the tendon tends to become more cylindrical (Nuri et al., 2018; Obst et al., 2014) and rotate (Obst et al., 2014). The transverse strains of the Achilles tendon cross-sectional area, mediolateral diameter, and anteroposterior diameter where -5.5%, -8.7%, and 8.7%, respectively, with peak strains occurring near to the region with smaller cross-sectional area (Obst et al., 2014).

Some subjects have stress-shielded regions within their Achilles tendon. Stress shielding leads to local tissue adaptation due to the local absence of loading or even for the presence of compressive loads, forming cartilage-like changes (Maganaris, Narici & Almekinders L. C. Maffulli, 2004). Such compressive loads have been observed in experiments with human Achilles tendons in vitro (Lersch et al., 2012). Similarly, non-uniform strain patterns have been observed *in vivo* (Bogaerts et al., 2017) and by computer simulation (Shim et al., 2018). The shielded region could then eventually be subjected to high levels of tension due to a sport-related gesture and injuries could occur. This etiological pathway shows a paradoxical relationship where some lesions that are thought to be caused by overuse are actually caused by underuse (Maganaris, Narici & Almekinders L. C. Maffulli, 2004; Edama et al., 2016).

The contrary is also true. Tendinopathies can cause inhomogeneities in the strain field. Aging is known to affect sliding capabilities (Yin et al., 2021b), causing the tendon to behave less like a bundle of independent fibers and more like a beam (i.e., with non-negligible resistance to bending). Beam-like behavior was observed in elderly subjects (Lersch et al., 2012) where the strain field had regions less stressed than others due to the rotation of one of its ends. Similarly, calcific tendinopathy and insertional calcific tendinopathy are localized deposits of calcium in the substance of the tendon. Such deposits are known to add stiffness to the tissue and, as a consequence, changes in the strain field near them (Oliva, Via & Maffulli, 2012). The response of the body includes surrounding the deposits with cartilage-like material (Oliva, Via & Maffulli, 2012), a probable adaptation to the compressive stresses that typically are present around a stiff inclusion in soft materials under tension.

3.4   Rope modelling and similarities with tendons.

Having established that the Achiles tendon's subtendons present an heterogeneous strain field, that they present a sliding mechanism, and that the subtendons' muscles can be activated individually, it is then reasonable to establish a parallel to the behavior of ropes, since ropes are also made up of bundles of thin and long twisted substructures that can slide.

Paper	Software	Contact	Material	Element
(Song et al., 2019)	Ansys Abaqus	Frictional	Structural steel NL (bilinear)	Mostly Hexa.
(Wokem, Joseph & Curley, 2018)	Abaqus	Frictional	Elastic linear	C3D10M Modified tetrahedral
(Du et al., 2017)	Abaqus	Frictional	Elastic linear	C3D8I Hex
(Vukelic & Vizentin, 2017)	Ansys	Frictionless	Bilinear	Brick 20 node
(Abdullah et al., 2016)	-	Frictional	Elastic plastic	Hexahedral
(Jiang & Henshall, 1999)	Ansys	Frictional contact elements	Bilinear	Brick
(Kastratović et al., 2014)	Ansys	Bonded Frictional	Bilinear	Brick
(Wang et al., 2013)	Abaqus	Frictional	Elastic and Elastoplastic	Brick
(Kastratović & Vidanović, 2013)	Ansys	Frictional	Bilinear	Brick 20 node
(Jiang, 2012)	Ansys	Frictional	Bilinear	Hexa
(Vargas & Beltra, 2012)	Ansys	Frictional	-	Solid45
(Stanova et al., 2011)	Abaqus explicit	Frictional	Elastic linear	Brick
(Erdonmez & Imrak, 2011)	Abaqus	Frictional	Bilinear	Quadratic Brick
(Erdönmez & İmrak, 2011)	Abaqus	-	Frictional	Quadratic Brick C3D8R
(Páczelt & Beleznai, 2011)	Custom	Homemade	Linear elastic	Beam
(Ma, Ge & Zhang, 2008)	Ansys	Frictionless	Elastic linear	Solid45

Table 1 – Summary of literature review on rope simulation using commercial software.

With these similarities in mind, a literature search was conducted focusing on papers that used FEM to model the behavior of ropes. The search aimed to answer four main questions: What software was used? How was the contact included? What material model was used? And what element was used? The results are summarized in Table 1.

In the Table 1 it is possible to see that the approach used in rope modeling is quite simple. With the exception of one work, all works used well-known commercial software (Ansys or Abaqus). The contact strategies followed the same trend, most of the works used well established contact formulations already implemented in commercial software. Material formulations varied from elastic linear to elasto-plasticity. Finally, most elements were hexahedra, some linear and

some of higher order, one work used tetrahedral elements and another used beam elements.

3.5   Computational Models for Tendons

The use of the Finite Element Method for the simulation of tendons, although not new, is quite initial. Especially when compared to the intervertebral disk, which is also made of soft tissue and has a similar geometric complexity, but a much more developed body of work (Malandrino, Noailly & Lacroix, 2011; Galbusera et al., 2014; Ferguson, Ito & Nolte, 2004; Yao & Gu, 2007; Gu et al., 2014). Works that aim to adjust the parameters of a given constitutive model are quite common in tendons (Carniel & Fancello, 2017; Böl et al., 2015; Pinto, 2014; Natali et al., 2005; Pioletti et al., 1998; Johnson et al., 1996), but works representing the tendon geometry are not so common. Some examples of the application of the Finite Element Method to the simulation of the macroscopic structure of tendons are highlighted below.

In Shim et al. (2014) the Achilles tendon is simulated. The geometry of ten subjects is built based on the measurement of markers. The work focuses on the comparison with the mechanical test scenario. The work concludes that there is a large variation among the specimens, and that the rupture location is more dependent on the geometry, while the rupture load is more dependent on the material properties. From the same group, the works presented in Shim et al. (2018) and Shim et al. (2019) used a complex three-dimensional geometry, local fiber orientation, sliding, and fiber twist. The tendon geometry is limited by two transversal cuts, one proximal and one distal, and simple boundary conditions are imposed on these surfaces (displacement on one side, force on the other). The code used is said to be freely available for academic use.

In Roux et al. (2016) and Yamamura et al. (2014) the focus was on the whole muscle-tendon unit. In Roux et al. (2016), the Discrete Element Method is used to visualize the variation of the pennation angle during loading. In Yamamura et al. (2014), the Achilles muscle-tendon unit is simulated, focusing on the effect of the tendon stiffness on force generation. Different material parameters for the Achilles tendon from different sources are tested. The mechanical properties for the muscles are kept constant. The stiffest tendon resulted in up to 1.45 times more force output for the unit.

Obrezkov, Finni & Matikainen (2022) and Obrezkov et al. (2022) based their geometry on images of tendon cross sections, taking into account the actual geometry of the tendon and it's subtendons. However, they did not base their cross sections on multiple images, but rather used one of the cross section schematic drawings presented in Edama et al. (2015) as a reference and built all the geometry based on it. The proposal focuses on the use of high order beam elements instead of solid elements as a way to drastically reduce the number of degrees of freedom in the model.

Knaus & Blemker (2021) created a 3D model which uses a transverse isotropic constitutive model with twisted fiber directions. Different levels of twist were compared while under loads representing the act of walking. The length of the twisted fibers was measured and compared to the length of the "free tendon" and between different levels of twist. The amount of energy

stored in the tendon was measured and, counterintuitively, it was found that for the same load, tendons with more twist stored less energy. The geometry was constructed by lofting it between two elliptical cross sections.

In Handsfield et al. (2017), the external geometry of the Achilles tendon was constructed by outlining with cubic splines medical images obtained by MRI from a live subject. The internal geometry of the subtendons was modeled based on images from the literature. Frictionless contact was used to model the interaction between the subtendons. The muscles were included, but simplified as elastic one-dimensional elements with passive stiffness. The study goes on to investigate the non uniformity of the displacement in different regions/subtendons. The model presented is among the most complete found in the literature. However, the use of the external real geometry of one subject with a single internal subtendon geometry of another (literature) is a major limitation.

Similarly, Diniz et al. (2023b) also based their geometry on MRI images from living subjects. However, the subtendon twist was not obtained from the images. Subtendon twist was added by proposing two different degrees of twist severity based on the findings of Edama et al. (2015).

Yin et al. (2021b) used a series of photographs of dissected Achilles tendons to construct a computational model that takes into account the actual geometry of the tendon and its subtendons. They used multiple photographs of the cross section of dissected human Achilles tendons as a reference to delineate the cross section of each subtendon. The cross section was then used to form the solids. The study proceeds to investigate the influence of different levels of sliding on the peak stress magnitude and distribution in the tendon by changing the parameters of a frictional contact interaction between the subtendons.

With the exception of Knaus & Blemker (2021) and Obrezkov, Finni & Matikainen (2022), all of these works have in common the fact that they use a geometry that captures the tortuosity of the Achilles tendon to some extent. They included in their geometries the general external silhouette of the Achilles tendon with its misalignments and even some of its topography. In addition, in these works, the interface is usually represented as a contact interaction with zero thickness.

4   Computational model of the Achilles tendon

This work proposes an approach inspired by the path taken by the works with the intervertebral disk, where the geometry of the disk is significantly simplified and complexity is added incrementally as results are obtained (Malandrino, Noailly & Lacroix, 2011; Galbusera et al., 2014; Ferguson, Ito & Nolte, 2004; Yao & Gu, 2007; Gu et al., 2014). As an example, a list with some of the works of one group is provided (Lai, Hou & Mow, 1991; Gu, Lai & Mow, 1998; Sun et al., 1999; Yao & Gu, 2004; Yao & Gu, 2006; Yao & Gu, 2007; Huang & Yong, 2008; Jackson, Huang & Gua, 2011; Jackson et al., 2011; Zhu et al., 2012; Wu et al., 2013; Zhu, Gao & Gu, 2014; Gu et al., 2014; Zhu et al., 2016b; Zhu et al., 2016a; Zhu et al., 2020).

Inspired by the above path, this work chose to start with a simplified geometry. The geometry is fully parametrized as a series of parallel and concentric ellipses spaced apart. This approach was chosen as a way to avoid the presence of misalignments and misinterpretation of the numerical results of the finite element analysis, with minimal influence of artifacts on the simulation fields. In addition, a scalar field is proposed in order to incorporate the variation of material parameters in the domain, allowing for the representation of muscle-tendon transition and lesioned tissue. Details are presented in the next sections.

The geometry of the model and the subtendons was constructed using an in-house code in MATLAB, and the softwares MeshLab and SolidWorks. The FEM parameters and meshing were included in the model using another in-house code in MATLAB and the Abaqus graphic user interface. The simulation was run in Abaqus.

4.1   Geometry

The first major set of simplifications adopted concerns what geometries are not being represented. Many structures surrounding the Achilles tendon that may influence its mechanical behavior are not represented. Some examples include: The paratenon, the retrocalcaneal bursa, the skin, other muscle-tendon units (e.g., plantaris, flexor digitorum longus, and flexor hallucis longus), and the presence of footwear or sports-related accessories for the ankle (e.g., bandages wraps and compression socks). In addition, a significant portion of the muscle tissue is not represented in the geometry.

4.1.1   Elipsoidal cross section

The geometry of the tendon was idealized as a set of elliptical sections parallel to the transverse plane of the body and connected by their center to the tendon axis. This axis was defined as the straight line passing through the geometric center of the tendon and parallel to its longest dimension. The most distal point of the geometry was defined as the origin (Fig. 3).

The assumption of ellipsoidal cross section for tendons can be found in the literature being used to: calculate the cross section of the branches of the deep digital flexor tendons of the domestic pig (Carniel et al., 2019; Pinto, 2014) and mouse tail tendons (Eriksen et al., 2014), as statements regarding it as a good approximation (Wren et al., 2001), and cross section approximations of the patellar tendon (Svensson et al., 2012), rat tail tendon (Safa et al., 2020), and the Achilles tendon (Knaus & Blemker, 2021).

Each ellipse has one of its principal axis parallel to the frontal plane (medial-lateral aspect) and the other parallel to the sagittal plane (anterior-posterior aspect). The dimensions of each transversal section of the first half of the model (from $z = 0$ mm to $z = 60$ mm) follow the spline curves that approximate the measurements obtained in Obst et al. (2014). The spline curves used to define the ellipses are shown in Fig. 3, which represent the MLR (Medial Lateral Radius) and APR (Anterior Posterior Radius) measurements. Extra points were manually added to represent a transition region portion proximal to the soleus MTJ (from $z = 60$ mm to $z = 120$ mm).

Figure 3 – Representation of the ellipsoidal cross sections and the curves used as guide for the principal axis of each ellipse. Achilles tendon cross section medial-lateral radius (MLR). Achilles tendon cross section anterior-posterior radius (APR). $z = 0$ mm to $z = 60$ mm (green dashed line) represent the free tendon region (adapted from Obst et al. (2014)). $z = 60$ mm to $z = 120$ mm represent the transition to muscle region.
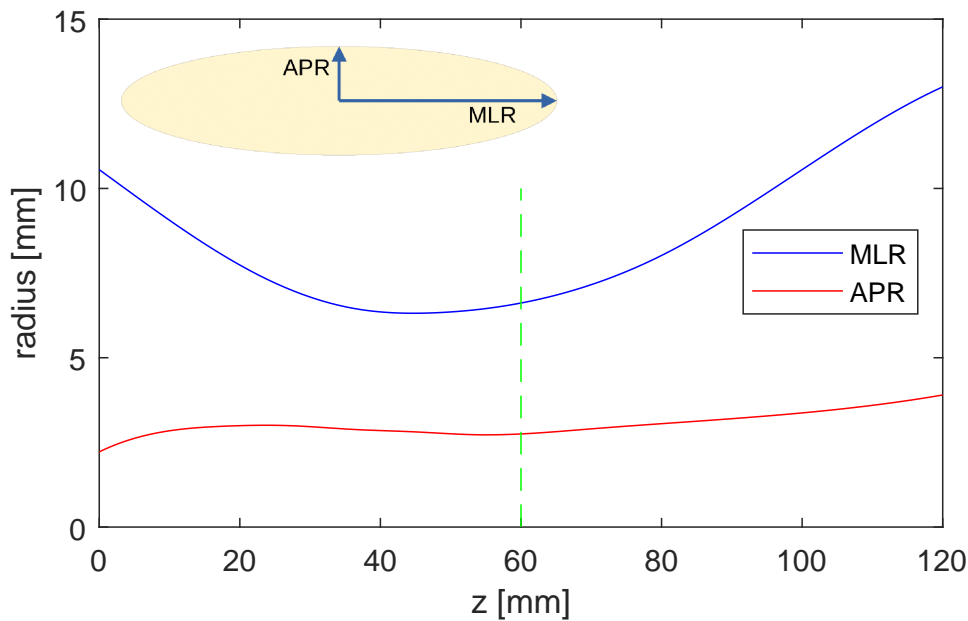
4.1.2   Internal division

The interior of the ellipses has been divided into three main regions, one for each subtendon. They are separated from each other by an interface of finite thickness (Fig. 4). The area fraction of the cross section occupied by each subtendon was kept constant over the entire length of the tendon. The area fraction of the soleus subtendon was 0.5, while the area fraction

Figure 4 – Elipsoidal cross section showing the internal division for different values of the Z coordinate.
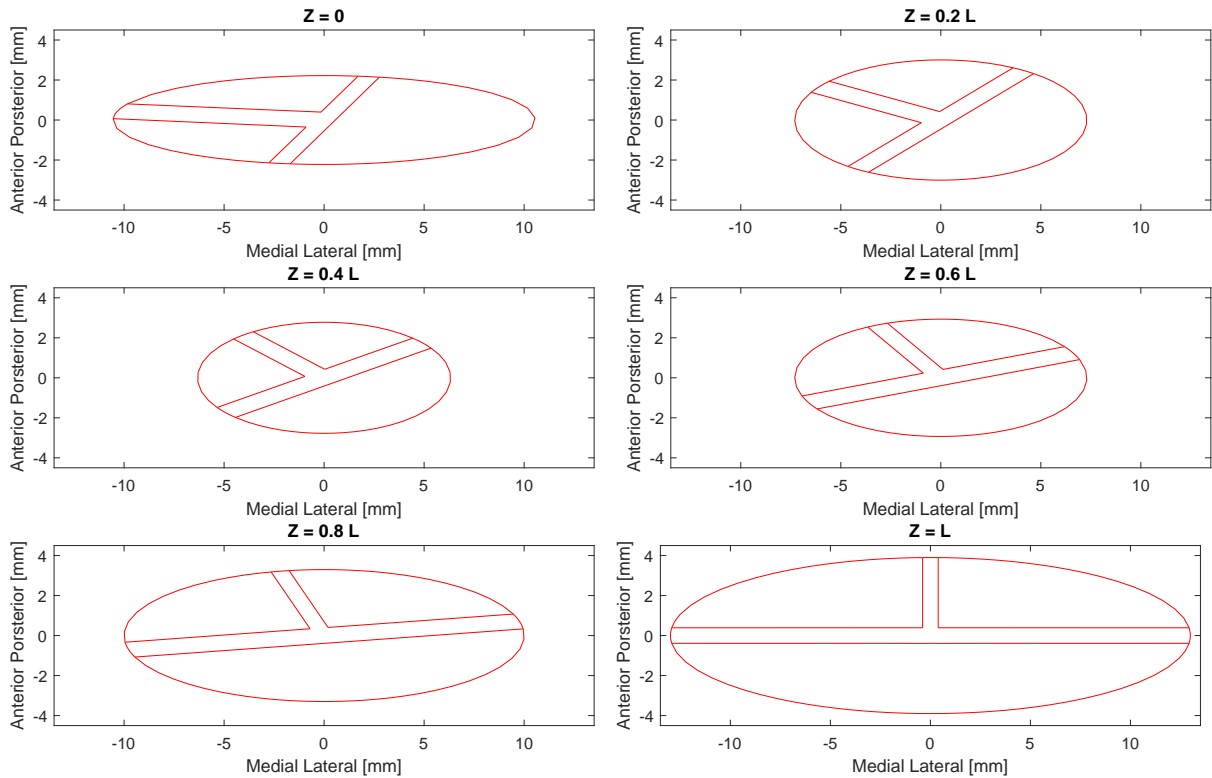
of each gastrocnemius subtendon was 0.25. The area fraction of each subtendon shows great variability among subjects (Yin et al., 2021b). The fractions were chosen in order to represent a possible tendon configuration ((Pekala et al., 2017; Śmigielski, 2008) and specimen 78 F in Yin et al. (2021b)) and to facilitate the interpretation of the results.

The assumption that there is an interface region of non-negligible thickness separating the subtendons is both useful and realistic, as shown by MRI in Szaro et al. (2020). This region is filled with a membrane-like material that facilitates the separation of the Achilles tendon into subtendons during dessication (Szaro et al., 2020). The resistance to shear of this region is assumed to be even lower than that of the subtendons, making the sliding mechanism a consequence of an interface region susceptible to high shear strains.

The shape of each region has been simplified as an ellipse sector. The actual shape of the internal divisions can be quite complex (Edama et al., 2016; Yin et al., 2021a).

4.1.3   Subtendon twist

To represent the internal twist of the subtendons, the internal configuration, but not the ellipse, was gradually rotated in each layer. The rotation was performed by rotating the interface portion separating the soleus and the medial gastrocnemius subtendon (Fig. 4). The other interface portions were rotated so that the area fractions remained unchanged. The rotation followed a variable pitch. The angle varied with the axial position, following a quadratic curve passing through three points. The angle was set to zero at the most proximal position and to the

full rotation at the most distal position. A third angle at the midpoint was set to one-third of the total rotation. The pith is then minimum at the most distal position and maximum at the most proximal position.

In this work, all models had a left hand twist, making the model a representation of an Achilles tendon of the right leg.

4.1.4   Representation of the tendon-muscle transition

The tendon length was represented by two regions. One representing the intramuscular part, where muscle and tendon share the same cross section, and the other representing the free tendon part, where there is no muscle tissue in the cross section (Winnicki et al., 2020).

The free tendon portion begins proximally, where the muscle tissue ceases to be present, and ends at the calcaneal insertion. The length of the free tendon region, as defined, varies considerably among subjects in Pichler et al. (2007) 12.5 % of subjects had a length less than 2.54 cm, while 70 % were between 2.54 and 7.62 cm, and 17.5 % were greater than 7.62 cm. In (Nuri et al., 2018) a similar definition was used and healthy tendons presented a similar length (70 ± 19 mm) with no significant differences when compared with tendons with tendinopathy and their contralateral. Similarly Pekala et al. (2017) measured 60.77 ± 14.15 mm. However, the muscle-tendon junction is not well defined for the entire tendon; each subtendon transitions for its muscle at different points. In particular, the most distal muscle fiber of both gastrocnemii could be more than 200 mm proximal to the calcaneal bone (Morrison, Dick & Wakeling, 2015). Given this scenario, the free tendon length was defined as 60 mm as in Knaus & Blemker (2021) and the muscle transition was represented up to 60 mm proximal to the free tendon end, resulting in a model with a total length of 120 mm (Fig. 5).

4.2   Boundary Conditions

The boundary conditions for the proposed model were divided into three regions: The peritendon, the muscle-tendon interface, and the bone-tendon interface.

The peritendon is assumed to be a free surface and the boundary condition is given by the trivial condition $\mathbf{t} = \sigma \mathbf{n} = 0$ in the peritendon.

The distal extremity is formed by a surface whose normal is 30° to the tendon axis (Fig. 5). It had all its nodes tied to the motion of a single reference point (RP). The RP was positioned close to the surface in order to represent the distal bone insertion of the TSMTU.

The proximal face had its nodes separated in four regions, one for each of the three subtendons and one for the interface region. The nodes on the areas of the proximal extremity of each subtendon had their translation and rotation coupled to a different RP (using the structural coupling method in Abaqus (Smith, 2009)) where independent forces act in the longitudinal direction z (tendon longitudinal axis) (Fig. 5). The displacements were set to zero in the directions perpendicular to the tendon axis, but it was kept free to rotate around the

RPs in all directions. No force were imposed on the nodes attached to the interface. The RPs were positioned at the origins of the TSMTU. The RP of the medial gastrocnemius subtendon was positioned at $\mathbf{x} = [20,\ 10,\ 400]$ mm, the RP of the lateral gastrocnemius subtendon was positioned at $\mathbf{x} = [-20,\ 10,\ 400]$ mm, and the RP of the soleus subtendon was positioned at $\mathbf{x} = [0,\ -10,\ 300]$ mm. The position of these RPs represent the origins of the triceps surae on the right leg.

Figure 5 – Schematic representation of the model. Arrows represent the proximal boundary conditions applied individually to the area of the proximal extremity of each subtendon. The proximal 60 mm is a region of transition of material properties from muscle tissue (color red) to tendon tissue (color blue). The position 52 mm proximal to the bone insertion mark the smallest cross section of the model. The upper figure is the representation of the lateral view of the model. The surface formed by the cut of 30° on the distal extremity is where the distal boundary condition was imposed.
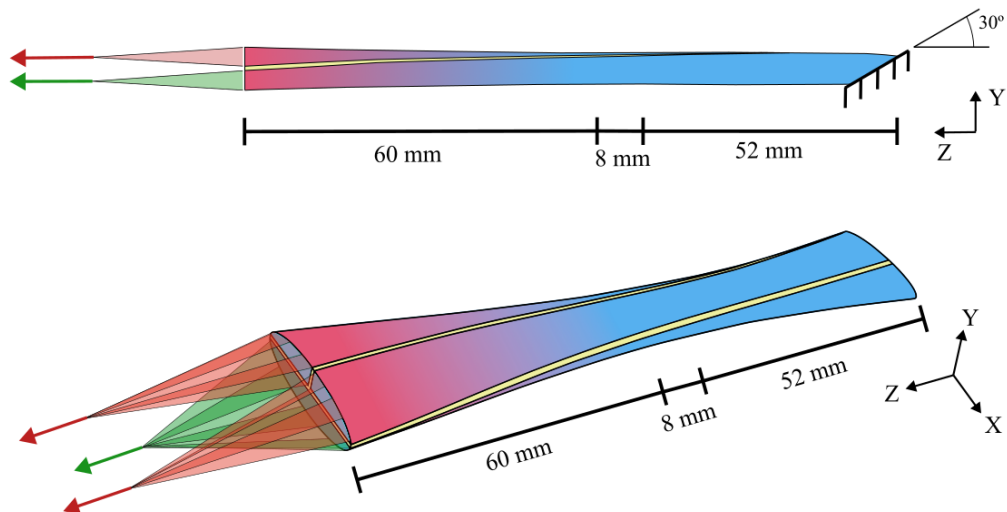
4.3 Constitutive models

The use of constitutive models presents a number of interesting challenges. In general, tendons are neither elastic nor isotropic and can often experience physiological strains greater than 3%, i.e., the use of small strain formulations is not sufficient. In addition, tendons exhibit a non-linear stress-strain curve with the presence of a toe region before an approximately linear region (Fung, 1993). Under progressive cyclic loading, tendons exhibit an hysteresis behavior, losing a certain amount of energy in each cycle even at strain rates lower than 0.1 %/s (Fig. 6).

The use of infinitesimal strain models to represent tendons is not appropriate in most cases. The use of properties such as Young's modulus and Poisson's ratio to describe tendons, although sometimes useful, can lead to errors as with any other material that undergo large strains. In addition, the presence of a toe region makes the stress x strain relationship non linear. Due to these facts, it is recommended that the modeling of tendons should, at least, include the ability to properly represent large strains.
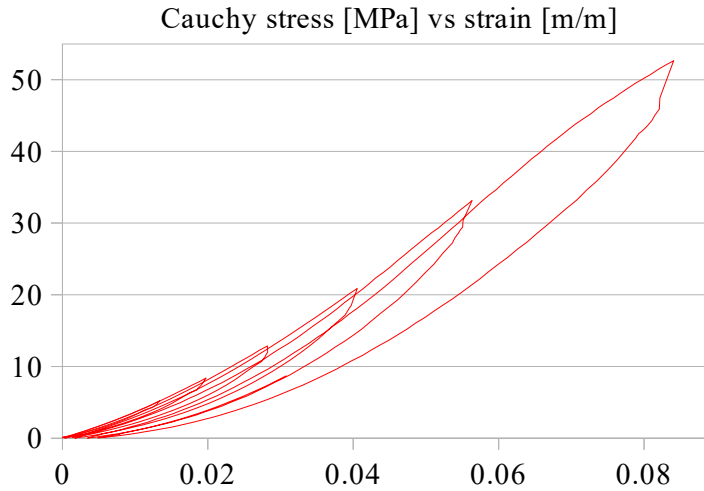
Figure 6 – Stress x strain curve of a hind limb swine deep digital flexor tendon under progressive trapezoidal cyclic loading. Toe region is not evident due to the use of pre-conditioning prior to the mechanical test. Strain rate was approximately than 0.075 %/s Adapted from Pinto (2014)

In continuum mechanics, the approach used to represent large strains starts by defining two categories of configurations. One is fixed in time (conventionally $t = 0$) and is called reference or undeformed configuration. Particles in this configuration have their position described by a position vector usually named $\mathbf{X}$. The other category includes every configuration and it is dependent of time. Particles will have their position described by a position vector that depends on time usually named $\mathbf{x}(\mathbf{X}, t)$. With the two configurations defined one can measure the displacement field $\mathbf{u}(\mathbf{X}, t)$ by subtracting one from the other, $\mathbf{u}(\mathbf{X}, t) = \mathbf{x}(\mathbf{X}, t) - \mathbf{X}$. With that, the deformation gradient is then defined as the tensor that results from the derivative of $\mathbf{x}$ with respect of $\mathbf{X}$ ($\mathbf{F}(\mathbf{X}, t) = \frac{\partial \mathbf{x}(\mathbf{X},t)}{\partial \mathbf{X}}$). However $\mathbf{F}$ is not yet useful as a strain measure since it is sensitive to rigid body rotations. One way to remove the rotations from $\mathbf{F}$ is to simply multiply its transpose by it, to get the Right Cauchy-Green deformation tensor $\mathbf{C} = \mathbf{F^T}\mathbf{F}$.

The tensor $\mathbf{C}$ is a measure that, for a given reference frame, only changes when the strain changes and changes whenever the strain changes. But it still changes whenever the reference frame change. To remove such dependence, the relations are not dependent on the tensor, but on its invariants, making the function an objective function.

When the constitutive function is given by a strain energy density function, i.e. the function results in a measure of energy per unit of volume dependent only on the invariants of a measure of strain such as $\mathbf{C}$, the constitutive function is named hyperelastic. In such cases a measure of stress can be obtained as the derivative of the strain energy density function with respect to a measure of strain, e.g. $\mathbf{S} = 2\frac{\partial W}{\partial \mathbf{C}}$, where W is the strain energy density function and $\mathbf{S}$ is the second Piola-Kirchhoff stress tensor. Among the many strain energy density functions, the Neo-Hookean (Bonet & Wood, 1997) is one of the most commonly used. As with others energy functions, it can be written in the form where the measure of volume change J is explicit separated,

$$W = C_{10}(\bar{I}_1 - 3) + \frac{1}{D}(J - 1)^2, \tag{4.1}$$

where I_1 is one invariant of $\mathbf{C}$ given by $I_1 = tr(\mathbf{C})$ and J is the determinant of $\mathbf{F}$, also an invariant of $\mathbf{C}$. C_{10} and D are material constants.

Similarly, one can define the behaviour of an hyperelastic anisotropic material with an anisotropic strain energy density function. One of such propositions is the Fung material. It can be found in Fung, Fronek & Patitucci (1979) for two-dimensional models, that can be generalized for three dimensions as presented in Humphrey (1995), arriving at the following strain energy density function

$$W = \frac{c}{2}e^Q; \quad Q = \mathbf{E{:}b{:}E}, \tag{4.2}$$

where $\mathbf{E} = \frac{1}{2}(\mathbf{C} - \mathbf{I})$ is another measure of strain, called Lagrangian finite strain tensor, c is a material constant and $\mathbf{b}$ is a dimensionless symmetric fourth-order tensor. Due to the symmetry of the tensors, we can write $\mathbf{E}$ as an one dimensional matrix and $\mathbf{b}$ as a two dimensional matrix (Voigt notation, (Reddy, 2013, p. 230)), allowing the visualization of the nine constants in $\mathbf{b}$ as:

$$Q = \begin{bmatrix} E_{11} & E_{22} & E_{33} & E_{12} & E_{23} & E_{13} \end{bmatrix} \begin{bmatrix} b_1 & b_4 & b_6 & 0 & 0 & 0 \\ b_4 & b_2 & b_5 & 0 & 0 & 0 \\ b_6 & b_5 & b_3 & 0 & 0 & 0 \\ 0 & 0 & 0 & b_7 & 0 & 0 \\ 0 & 0 & 0 & 0 & b_8 & 0 \\ 0 & 0 & 0 & 0 & 0 & b_9 \end{bmatrix} \begin{bmatrix} E_{11} \\ E_{22} \\ E_{33} \\ E_{12} \\ E_{23} \\ E_{13} \end{bmatrix} \tag{4.3}$$

Another material model used for the tendons is the Holzapfel-Gasser-Ogden HGO (Gasser, Ogden & Holzapfel, 2006), a hyperelastic fiber-reiforced model which is defined by the following strain energy potential:

$$W = C_{10}(\bar{I}_1 - 3) + \frac{1}{D}\left(\frac{(J)^2 - 1}{2} - \ln J\right) + \frac{k_1}{2k_2}\sum_{\alpha=1}^{N}\{\exp\left[k_2\langle\bar{E}_\alpha\rangle^2\right] - 1\}, \tag{4.4}$$

with

$$\bar{E}_\alpha \overset{\mathsf{def}}{=} \kappa(\bar{I}_1 - 3) + (1 - 3\kappa)(\bar{I}_{4(\alpha\alpha)} - 1), \tag{4.5}$$

where C_{10}, D, k_1, k_2 and κ are material parameters, $\bar{I}_1$ is the first invariant of the distortional part of the Right Cauchy-Green strain ($\bar{\mathbf{C}}$), $\bar{I}_{4(\alpha\alpha)}$ is the fourth invariant of the distortional part of the Right Cauchy-Green strain ($\bar{\mathbf{C}}$) in the direction of the fiber family α, and N is the total

number of fiber families. If only one fiber family is used ($N=1$), the model becomes transversely isotropic, consequently eq. 4.4 and eq. 4.5 become:

$$W = C_{10}(\bar{I}_1 - 3) + \frac{1}{D}\left(\frac{(J)^2 - 1}{2} - \ln J\right) + \frac{k_1}{2k_2}\left[\exp\left(k_2\langle\bar{E}\rangle^2\right) - 1\right], \tag{4.6}$$

with

$$\bar{E} \stackrel{\mathsf{def}}{=} \kappa(\bar{I}_1 - 3) + (1 - 3\kappa)(\bar{I}_4 - 1). \tag{4.7}$$

Both the Fung model (eq. 4.2) and the HGO model (eq. 4.4) are readily found in commercial software and were made specifically for biomechanics applications. Comparing both, the HGO model with $N=1$ (eq. 4.6) was chosen for this work due to three main characteristics. First, it is a transversely isotropic model with an exponential energy function in the fiber directions. Second, the portion of the energy function related to the fiber elastic energy acts only in tension. This characteristic is given by the operator $\langle \cdot \rangle = \frac{1}{2}(|\cdot| + \cdot)$, that basically turns off the energy accumulation of fibers under compression. Third, it is of easy interpretation since by simply considering $\kappa = 0$ one can readily see that C_{10} and D are analogous to a Neo-Hookean compressible solid and that k_1 and k_2 are the parameters for the exponential energy function of the fiber reinforcement.

The material model used for the interface was the Neo-Hookean model (eq. 4.1). This choice was made in order to represent the interface material as a region where the fiber reinforcement of the collagen fibers is negligible. As a consequence, the interface is isotropic. The Neo-Hookean model was chosen because it is similar to the isotropic component of the HGO model.

The concept of strain energy density function can be extrapolated to include dissipative capabilities. It is counterintuitive to use energy potentials to define a dissipative process, but this strategy has been shown to be useful in many works such as Fancello, Ponthot & Stainier (2006). In such works the potential depends not only on the strains, but also on a set of internal variables, making it not truly a potential but a pseudo-potential. Through this strategy it is possible to include in the model dissipative behaviors observed in tendons such as viscoelasticity (Fancello, Ponthot & Stainier, 2006) or damage (Vassoler, Reips & Fancello, 2012).

Another known dissipative process in tendons is the displacement of the fluid and its coupling with the solid kinematics. To account for this, a constitutive relationship is not always sufficient and it is sometimes useful to modify the entire system of equations. Such problems are called poromechanical problems or biphasic problems and are usually based heavily on the formulation proposed in Biot (1941). However, the formulation proposed in Biot (1941) is for small strains and the use of poromechanics in soft tissues requires more advanced models that consider finite strain theory. Examples of such models can be found in Lai, Hou & Mow (1991) and Klahr et al. (2023).

A local coordinate system was assigned to each element in the FEM mesh. The local

x direction was set to be parallel to the imaginary helix, formed by the subtendon twist, at the centroid of the element. The local *y* direction was set to be perpendicular to the local *x* direction and pointing to the tendon axis, and the local *z* direction was defined as the cross product of the first two forming orthogonal right-hand local coordinates. In other words, the local fiber direction followed the same twist pattern as the subtendons. In Pekala et al. (2017) it is shown that the fibers of the subtendons do not necessarily follow the rotation of the subtendons. In the case presented in Pekala et al. (2017), they rotate within the subtendon, producing a secondary rotation that is not equal among the subtendons. Thus, the assumption that the fiber rotation follows the subtendon rotation is yet another simplification of the observations reported in the literature. An interesting strategy was used by Knaus & Blemker (2021), where Laplacian simulations were used to solve for the fiber directions as an analogy to streamlines in flow simulations. The streamline technique appears to yield similar results to the strategy used in this work.

4.3.1 Mechanical Properties and aging

The measurement of the mechanical properties of tendons presents a large variation of values in the literature. The reported Young's modulus of the Achilles tendon has measured values ranging from 0.3 GPa to 1.5 GPa (Winnicki et al., 2020; Wunderli et al., 2018; Stenroth et al., 2012; Arya & Kulig, 2010; Vankan et al., 1996; Grytz & Meschke, 2009). Other measurements show similar variation, e.g.: ultimate tendon stress (20-110 MPa) (Winnicki et al., 2020; Maganaris, Narici & Maffulli, 2008), ultimate tendon strain (5-8%) (Winnicki et al., 2020; Franz et al., 2015) , maximal tendon forces (200-3800 N), elongation (2-24 mm), and stiffness (17-760 N/mm) (Winnicki et al., 2020). The reason for such variation is partly due to subject to subject variation, but other important sources have been reported such as: experimental technique (Carniel et al., 2019), the use of models richer than the data set (Klahr et al., 2023; Klahr et al., 2021), differences in nomenclature (Nuri et al., 2018), and the presence of time-dependent behavior (Kay & Blazevich, 2009).

When tested separately from the tendon, fibrils show a similar variation for measurements of the elastic modulus. The reported values are between 0.12 - 1.6 GPa (Shen et al., 2011; Reese, Maas & Weiss, 2010; Szczesny & Elliott, 2014).

Aging affects the mechanical characteristics of tendons. Young subjects generally present tendons with higher resistance to fatigue (Thorpe et al., 2014), lower longitudinal modulus and higher tensile rupture stresses (Winnicki et al., 2020). The sliding capabilities are affected by aging through the higher presence of cross-links in elderly tendons (Thorpe et al., 2012a; Muench, Thelen & Henak, 2020; Gautieri et al., 2017), then it is expected that elderly subjects would present higher resistance to shear (higher shear modulus). An interesting term used in such studies is "tendon age" (Yin et al., 2021a), which suggests that the tendon may exhibit age-dependent behavior that is different from the actual age of the person. Because glycation is so strongly associated with age-related characteristics, it is understandable that it would increasingly become a clock-like parameter, where the age of various body structures would be

determined by the level of glycation (*i.e.*, resistance to shear). Glycation can also be affected by diet and an increase in the shear modulus of tendons due to diet induced glycation was verified experimentally in a rat model (Grasa et al., 2013). Given that aging affects the rupture stress and the resistance to shear, it is viable to hypothesize that high shear modulus has a causal relationship with lower rupture stresses in tendons. Such a hypothesis is within the scope of traditional solid mechanics and could be tested using a computational model.

The sex of the person is sometimes strongly correlated with mechanical properties (Winnicki et al., 2020). While this is true, it can lead to a misinterpretation of the phenomenon. Other studies show that the correlation is actually with muscle strength and not the sex of the person (Muraoka et al., 2005; Morrison, Dick & Wakeling, 2015) and muscle strength is known to be correlated with the sex of the person (Nuzzo, 2023). This distinction is important because it helps in the search for the causality of the difference. The results of (Muraoka et al., 2005; Morrison, Dick & Wakeling, 2015) suggest that the causality is more likely related to adaptation to the environment (training) than to genetic or hormonal causes. In summary, tendon stiffness increases with strength (Muraoka et al., 2005; Morrison, Dick & Wakeling, 2015).

Aging was included in the model by the manipulation of the shear modulus. Sliding was represented by simply spacing the isotropic shear modulus of the HGO and Neo-Hookean models from the fiber parameters of the HGO, as it will be shown in the next sections.

4.3.2   The tendon as a functionally graded material.

The material parameters varied with their position in the domain. A scalar predefined field is proposed as a function of position $\phi(\mathbf{x})$, where $\mathbf{x} = [x, y, z]$, and the material parameters vary as a function of the scalar predefined field. The field was defined analytically as an explicit function of the material coordinates of a point in the domain.

Two phenomena were represented simultaneously by varying the material parameters with the position. The first one is the variation in the properties of the Achilles tendon as it becomes more proximal and transitions into muscle tissue. The second is the representation of lesions such as calcifications, scar tissue and other localized abnormalities.

The proposed scalar function has three important values. When $\phi(\mathbf{x}) = 0$ it represents muscle tissue. When $\phi(\mathbf{x}) = 1$ it represents healthy tendon tissue and when $\phi(\mathbf{x}) = 2$ it represents pathological tendon tissue. If $0 < \phi(\mathbf{x}) < 1$ it means that the region is partially healthy tendon tissue and partially muscle tissue. If $1 < \phi(\mathbf{x}) < 2$ it means that the region is partially healthy tendon and partially pathological tendon. The mechanical properties at a given point in the transitions are obtained by interpolation, weighted by the value of $\phi(\mathbf{x})$.

The function $\phi(\mathbf{x})$ is then constructed as the sum of two parts, one related to the transition to muscle tissue ($\phi_m(\mathbf{x})$) and the other related to the transition to pathological tissue ($\phi_p(\mathbf{x})$),

$$\phi(\mathbf{x}) = 1 - \phi_m(\mathbf{x}) + \phi_p(\mathbf{x}), \tag{4.8}$$

where $\phi_m(\mathbf{x})$ is written as,

$$\phi_m(\mathbf{x}) = \frac{|z - l_m| + (z - l_m)}{2(l_0 - l_m)}, \tag{4.9}$$

and $\phi_p(\mathbf{x})$ is written as,

$$\phi_p(\mathbf{x}) = (1 + \phi_m(\mathbf{x})) \left(\frac{1}{e_{rr}}\right)^{\psi(\mathbf{x})}, \tag{4.10}$$

where

$$\psi(\mathbf{x}) = -\bar{r}(\mathbf{x})^n. \tag{4.11}$$

In the previous equation, z is the global coordinate aligned with the tendon axis (Fig. 5), the parameter l_m is the value of z above which the free tendon ends and the transition begins (Fig. 7), and l_0 is the total length of the model, e_{rr} is a tolerance parameter greater than zero and less than one, n is a parameter greater than zero and $\bar{r}$ is a normalized radius based on an ellipsoid with its three main axis aligned with the global coordinate system of the model, and it is given by the following equation,

$$\bar{r}(\mathbf{x}) = \sqrt{\left(\frac{x - x_0}{r_x}\right)^2 + \left(\frac{y - y_0}{r_y}\right)^2 + \left(\frac{z - z_0}{r_z}\right)^2}. \tag{4.12}$$

Note that $\bar{r}(\mathbf{x})$ is written so that $\bar{r}(\mathbf{x}) = 1$ defines an ellipsoid surface centered at $\mathbf{x_0} = (x_0, y_0, z_0)$ and with the length of its three main axes given by r_x, r_y, r_z.

The surface $\bar{r}(\mathbf{x}) = 1$ defines an ellipsoidal zone of influence of the lesion with $\phi_p(\mathbf{x_0}) = (2 - \phi_m(\mathbf{x}))$ in the geometric center of the ellipsoid ($\mathbf{x} = \mathbf{x_0}$), and $\phi_p(\mathbf{x}) = e_{rr}(1 - \phi_m(\mathbf{x}))$ in the surface $\bar{r}(\mathbf{x}) = 1$. As the value of $\bar{r}(\mathbf{x})$ grows, $\phi_p(\mathbf{x})$ tends to zero asymptotically.

Fig. 7 presents an 1D visualization of the scalar function ϕ. The mechanical properties of the distal half of the model represent the tendon with the lesion region. The proximal half represent the transition region $z > l_m$. The material properties varied linearly with the position in the tendon axis transitioning from tendon tissue parameters to muscle tissue parameters. The material parameter values for intermediate values of $\phi(\mathbf{x})$ are calculated by linear interpolation weighted by the value of $\phi(\mathbf{x})$. The scalar function is added to the model as a temperature and the material parameters change the same way as they would in a material with temperature dependent properties. This technique is known as the virtual temperature technique, more details can be seen in Rousseau & Tippur (2000) and in Martínez-Pañeda & Gallego (2015).

4.4 Numerical Test Setup 1. Simple tension test simulation

In Peltonen et al. (2013) *in vivo* experiments were performed in humans, with the subject sitting in a custom-built ankle dynamometer. The movement of the Achilles tendon was captured

Figure 7 – Representation of the scalar function for the tendon-muscle transition region ($z > l_m$ and $\phi(\mathbf{x}) < 1$) and pathological tissue ($\phi(\mathbf{x}) > 1$).
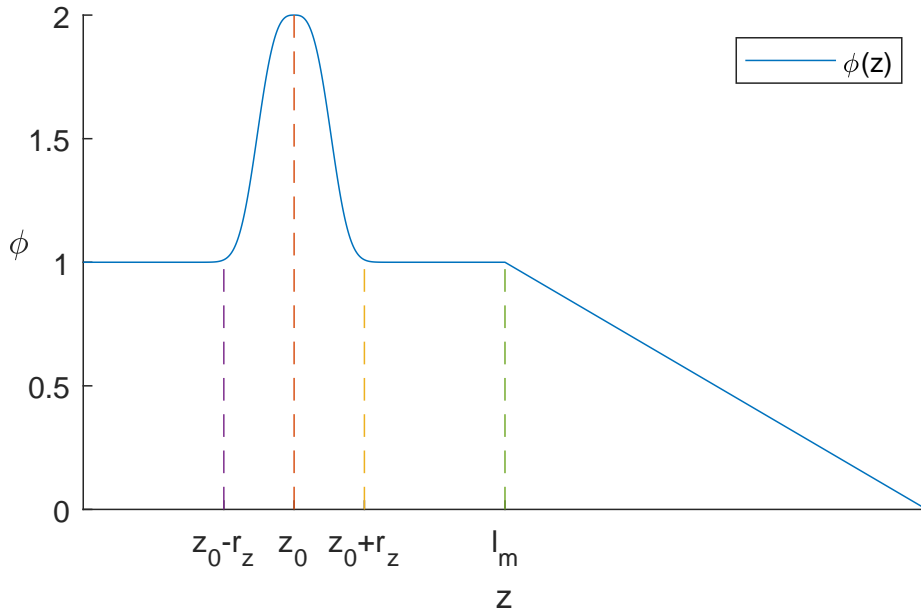
using motion capture assisted ultrasonography. Subjects were asked to perform contractions in the calf muscles to stretch and release the tendon. By taking into account the geometry of the subjects' anatomy, this procedure was able to generate force-elongation curves of the Achilles tendon.

In this first study, the goal was to be able to reproduce the curve presented in Peltonen et al. (2013). The distal RP was not allowed to either translate or rotate. The proximal RPs were axially loaded (total force = 2500 N as in the experiment). Each RP received a force proportional to the area fraction of the corresponding subtendon. *i.e.* 25% for each gastrocnemius subtendon and 50% for the soleus subtendon.

The total subtendon twist for this model was 90° (60° in the free tendon and 30° in the muscle-tendon transition zone). No pathology was included ($\phi_p(\mathbf{x}) = 0$). The parameters for $\phi_m(\mathbf{x})$ were $l_m = 60$ mm and $l_0 = 120$ mm. A set of six different material parameters was tested as shown in the Table 2. The elongation of the free tendon was measured at the position $z = 60$ mm.

The results of this test setup can be found in subsection 5.1

4.5   Numerical Test Setup 2. Non uniform load

A series of experimental tests performed in Lersch et al. (2012) were used to identify a group of parameters that define the numerical model: material constants of the constitutive models and twist angle of the subtendons (Fig. 4). In such study 5 different load cases and 4 calcaneal bone rotations were evaluated, totaling 9 experiments (1 standard and 8 variations, see Tab. 3). Each of these tests were performed on $n = 5$ human TSMTU specimens. Length

Table 2 – Parameters for the material models used for the Numerical Test Setup 1. The parameter k_2 is dimentionless, D is given in MPa^{-1}, C_{10} and k_1 are given in MPa.

	Tendon				Muscle				Interface	
	C_{10}	D	k_1	k_2	C_{10}	D	k_1	k_2	C_{10}	D
Model 0	10	0.001	60	0.8	1	0.5	6	0.5	0.1	0.01
Model 1	10	0.001	27	0.8	1	0.5	5.4	0.5	0.1	0.01
Model 2	10	0.001	30	0.8	1	0.5	6	0.5	0.1	0.01
Model 3	9	0.001	30	0.8	0.9	0.5	6	0.5	0.1	0.01
Model 4	10	0.001	24	0.8	1	0.5	4.8	0.5	0.1	0.01
Model 5	10	0.001	21	0.8	1	0.5	4.2	0.5	0.1	0.01

measurements were made at 5 different samples of the surface. The length L of the sample achieved by each of the 8 experiment variations was compared with the length L_{st} of the same sample achieved at the standard experiment, providing the following strain measure:

$$\tilde{\varepsilon} = \frac{L - L_{st}}{L_{st}}. \tag{4.13}$$

In order to measure the values of L and L_{st} in the model, samples were defined as the distance between markers on the surface of the model. Four markers were placed on the ventral side of the tendon (the surface facing the bone), which were spaced in order to form a 2x2 grid. The two distal markers were placed at $z = 40$ mm and the two proximal markers were placed at $z = 60$ mm. The lateral and medial markers were equally spaced from the center of the model, with the distance between the two markers being 70% of the model width at that position. The dorsal aspect of the tendon (the surface facing the skin) has six markers, spaced in order to form a 2x3 grid. The two distal markers were placed at $z = 15$ mm and the three proximal markers were placed at $z = 60$ mm. The lateral and medial markers were spaced exactly as in the ventral aspect and an additional central marker was added in order to reproduce the measurement strategy used in Lersch et al. (2012). The positions of the markers were estimated using the photos presented in Lersch et al. (2012) as a reference, since their actual positions were not provided by the author.

The same loads and boundary conditions used in the experimental setup were applied to the present model, totaling 9 simulations for a given set of model parameters.

Fourteen sets of model parameters (material parameters and tendon twists configurations) were tested (see Tab. 4). For such simulations, no material pathology was included in the model ($\phi_p(\mathbf{x}) = 0$).

To simplify the comparison between simulations and experimental results the following normalized residual is proposed:

$$R = \frac{\tilde{\varepsilon}_s - \tilde{\varepsilon}_e}{\Delta\varepsilon_e}, \tag{4.14}$$

where $\tilde{\varepsilon}_s$ is the simulation value and $\tilde{\varepsilon}_e = (\varepsilon_e^{max} + \varepsilon_e^{min})/2$ is the midpoint between the maximum ε_e^{max} and minimum ε_e^{min} experimental measurements. Finally, $\Delta\varepsilon_e = (\varepsilon_e^{max} - \varepsilon_e^{min})/2$. Residual R assumes that $\tilde{\varepsilon}_e$ represents the target value and $\Delta\varepsilon_e$ represents a unitary deviation score for

Table 3 – Load cases for the parameter identification corresponding to the lowest load
level in the experiment made by Lersch et al. (2012).

Case	Forces [N]			Rotation
	Soleus	Medial G.	Lateral G.	
0 - Standard	300	200	100	0°
1 - Variation 1	300	100	200	0°
2 - Variation 2	300	100	100	0°
3 - Variation 3	300	100	0	0°
4 - Variation 4	300	0	100	0°
5 - Eversion 7.5º	300	200	100	7.5º
6 - Eversion 15º	300	200	100	15º
7 - Inversion 7.5º	300	200	100	-7.5º
8 - Inversion 15º	300	200	100	-15º

Table 4 – Parameters for the models of the parameter identification process.The parameter
k_2 is dimentionless, D is given in MPa^{-1}, C_{10} and k_1 are given in MPa.

	Model	Tendon				Muscle				Interface	
		C_{10}	D	k_1	k_2	C_{10}	D	k_1	k_2	C_{10}	D
twist = 45°	A1	10	0.001	24	0.8	1	0.5	4.8	0.5	5	0.001
	A2	10	0.001	36	0.8	1	0.5	7.2	0.5	1.25	0.001
	A3	10	0.001	36	0.8	1	0.5	7.2	0.5	0.25	0.001
	A4	10	0.001	36	0.8	1	0.5	7.2	0.5	5	0.001
	A5	10	0.001	36	0.8	1	0.5	7.2	0.5	20	0.001
	A6	10	0.001	60	0.8	1	0.5	6	0.5	5	0.001
twist = 90°	B1	0.1	0.0001	36	0.8	0.1	0.5	7.2	0.5	0.25	0.001
	B2	10	0.001	36	0.8	1	0.5	7.2	0.5	1.25	0.001
	B3	0.1	0.001	120	0.8	0.1	0.05	12	0.5	0.25	0.001
	B4	1	0.001	120	0.8	0.1	0.05	12	0.5	0.25	0.001
	B5	10	0.001	120	0.8	0.1	0.05	12	0.5	0.25	0.001
	B6	30	0.001	120	0.8	0.1	0.05	12	0.5	0.25	0.001
	B7	100	0.001	120	0.8	0.1	0.05	12	0.5	0.25	0.001
	B8	500	0.001	120	0.8	0.1	0.05	12	0.5	0.25	0.001

that data point ($R = 1$). A value R is computed at each sample allowing the calculation of a
mean value $\bar{R}$:

$$\bar{R} = \frac{1}{n} \sum_{i=1}^{n} |R_i|, \tag{4.15}$$

where $n = 40$ is the number of samples. An ideal result is achieved when $\bar{R}$ is null, meaning that
the model has all of its values of $\tilde{\varepsilon}_s = \tilde{\varepsilon}_e$.

For the this case, the goal is to obtain a set of parameters with a normalized residual $\bar{R}$
less than one. It is then assumed that a set of parameters with $\bar{R} < 1$ represents a viable tendon,
since its results deviate from the target value, in average, less than the maximum deviations
observed in the experiments.

The fourteen rows of table 4 represent the educated sequence of model parameters used
to achieve a residual value $R < 1$.

The results of this test setup can be found in subsection 5.2

4.6 Numerical Test Setup 3. Pathology

For this study, the set of parameters B7 was chosen to represent the elderly tendon since it reached a mean normalized residual lower than one ($\bar{R} < 1$), as it will be shown in the Results section, and because most of the tendons tested in Lersch et al. (2012) are from 72–86 years elderly subjects. Young tendons, on the other side, are chosen to differ from elderly ones on the shear parameter C_{10} that was set to be $\frac{1}{10}$ of the former. This ratio in C_{10} is in agreement that reported in (Grasa et al., 2013) in rat models. Such a difference is attributed to the glycation phenomenon that augment the density of cross-link bonds between collagen molecules and consequently augment the shear stiffness (Gautieri et al., 2017).

Properties of the muscle tissue are mostly determined by the C_{10} and k_1 (fiber) parameters, both of them set up $\frac{1}{10}$ of that of healthy tendons, which is in accordance to that found in the literature (Lv et al., 2010; Stenroth et al., 2012; Arya & Kulig, 2010; Calvo et al., 2010).

The parameters for the pathological tendon are that of the young tendon with decreasing values of C_{10} and k_1, the last representing less collagen fibers, driving it to a less organized structure, both characteristics that fit the description of tendinosis (Aicale, Tarantino & Maffulli, 2019).

The interface was represented by a isotropic material with low resistance to shear but still with an incompressible behavior, since in this region it is expected a higher presence of water and a lower presence and organization of collagen type I (Thorpe et al., 2016). The list with all parameters can be seen in Tab. 5.

Table 5 – Parameters for the numerical test setup models. The parameter k_2 is dimentionless, D is given in MPa^{-1}, C_{10} and k_1 are given in MPa.

Model	Tendon				Muscle				Interface	
	C_{10}	D	k_1	k_2	C_{10}	D	k_1	k_2	C_{10}	D
elderly (B7)	100	0.001	120	0.8	0.1	0.05	12	0.5	0.25	0.001
young	10	0.001	120	0.8	0.1	0.05	12	0.5	0.25	0.001
pathology	10	0.001	18	0.8	-	-	-	-	-	-

All cases were tested with a total load of 600 N applied at the proximal reference points as in the standard case of the experiment made in Lersch et al. (2012) (Tab. 3), *i.e.*, 300 N at the soleus, 200 N at the medial gastrocnemius and 100 N at the lateral gastrocnemius.

In order to emulate a local pathology, also known as tendinosis (Docking, Ooi & Connell, 2015), in the central part of the tendon, the function $\phi_p(\mathbf{x})$ described in Section 4.3.2 was activated. The localization of the pathological tissue was chosen in order to reproduce the worst-case scenario for the model, *i.e.*, the region with the smallest cross-sectional area ($z = 52$ mm).

Three different levels of pathology severity were simulated by varying the percentage of compromised cross section as follows: the low case, with a 20% of the cross section compromised; the medium case, with 50% compromised and the high case, with 80% compromised. The parameters for the scalar function $\phi(\mathbf{x})$ are presented in Table 6. A visualization of the three $\phi(\mathbf{x})$ distributions is shown in Fig. 8.

The pathology was modeled solely by a local change in mechanical properties. Without any local change in volume due to inflammation. In addition, since the model is unable to represent fluid exudation, the parameters for the pathological tendon were kept close to incompressible as in the young and elderly tendon parameters.

Table 6 – Parameters for $\phi(\mathbf{x})$ for the pathological case. e_{rr} and n are dimensionless, all the other parameters are given in millimeters.

Severity	$\phi(\mathbf{x})$									
	l_m	l_0	e_{rr}	n	x_0	y_0	z_0	r_x	r_y	r_z
80%	60	120	0.1	6	0	0	52	5.1	20	2.55
50%	60	120	0.1	6	0	0	52	3.2	20	1.6
20%	60	120	0.1	6	0	0	52	1.3	20	0.65

Figure 8 – Visualization of $\phi(\mathbf{x})$ for three sizes of lesion.
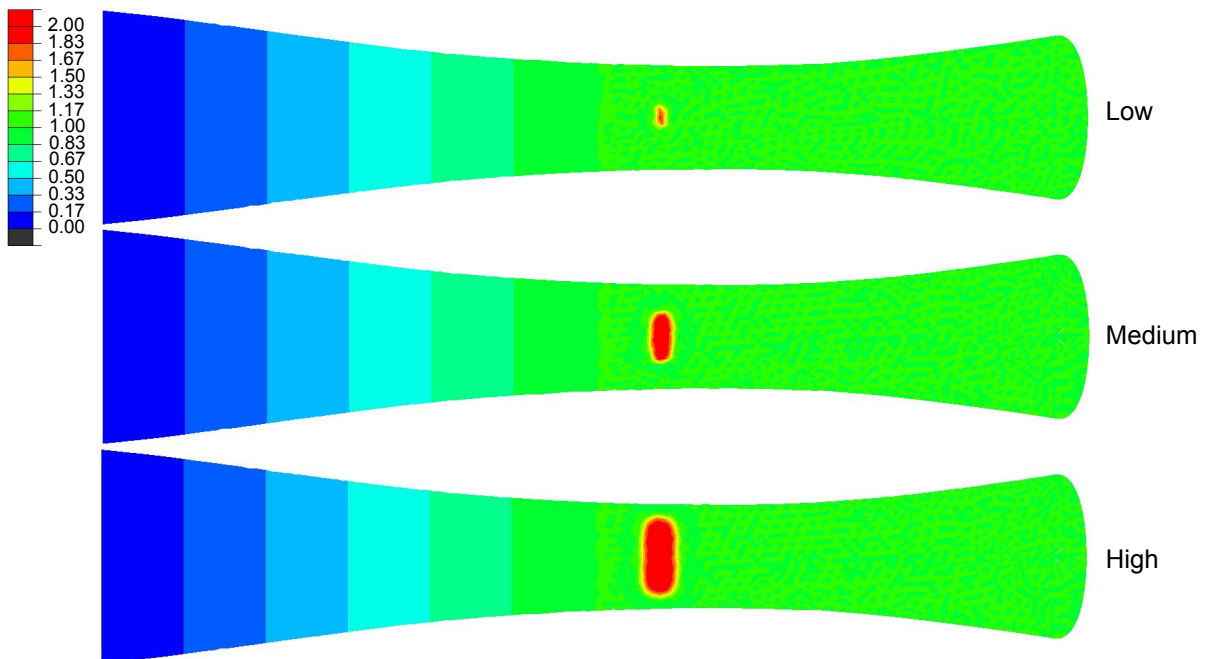
The results of this test setup can be found in subsection 5.3

4.7   Numerical Test Setup 4. Suture evaluation

In this study, a repair technique is simulated by adding to the model the geometry of three suture strands representing the Achillon technique. The purpose of this study was to compare the loads on the different suture strands before before and after the last knot is tied.

The knot tying pattern studied was the 123 pattern, meaning that the surgeon would first tie the small suture strand (strand 1), then tie the medium strand (strand 2), and finally the long strand (strand 3). The simulation was designed to test the hypothesis that after tying the last knot, the force in the first two knots would decrease significantly.

4.7.1 Suture modeling

The geometry of the three suture strands was constructed as three rectangular perimeters with rounded corners and circular cross section (Fig. 9). The dimensions of each rectangle are shown in the Table 7. The cross section of the sutures has a diameter of 0.44 mm which corresponds to a USP (United States Pharmacopeia) size 1 suture which is commonly used in tendon repair (Byrne & Aly, 2019).

Table 7 – Parameters for the geometries of the suture strands. Values are given in mm.

Strand	height	width	filet radius
1	25	14	2
2	40	16	2
3	55	18	2

Figure 9 – Visualization of the suture geometries. Doted lines represent the spring elements used to model a portion of the suture.
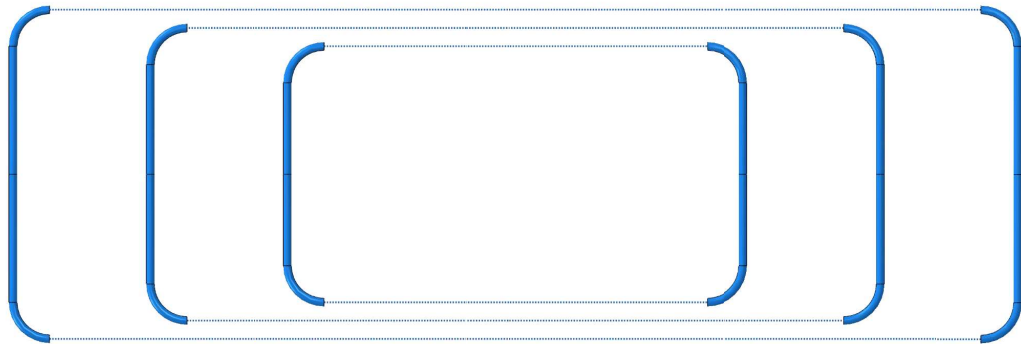
The three rectangles were positioned concentrically and oriented parallel to the zy plane passing through $x = 0$. Their center has the coordinates $\mathbf{x} = (48, 0, 0)$. After positioning, the geometry of the sutures was subtracted from the geometry of the tendon by a Boolean operation, creating cavities that exactly matched the geometry of the sutures (Fig. 10 and Fig. 11).

Figure 10 – Visualization of the model assembled with the suture geometries.
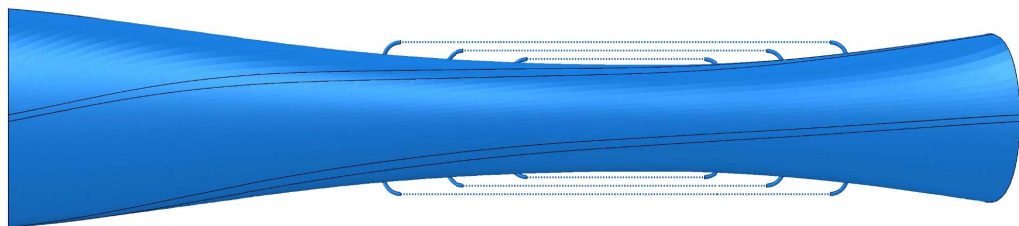
Figure 11 – Detail of the spring elements representing a section of the suture strands in a cut on the frontal plane showing the internal position of the suture.
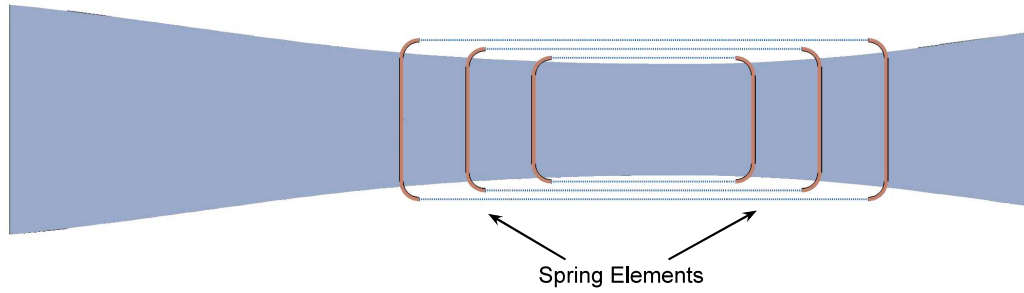
The suture material aimed to represent the properties of the Ethibond suture, which is commonly used in tendon repair (Byrne & Aly, 2019). The material of the suture was represented using the HGO model.

The parameter k_1 was used to represent the longitudinal stiffness of the suture. Reported values of initial Young's modulus for Ethibond sutures are $1.2 - 6.5$ GPa (Chu, 2013), so $k_1 = 3000$ MPa was chosen.

An indirect strategy was used for the determination of the shear modulus by considering infinitesimal strain. In Chen et al. (2015), the bending stiffness of silk sutures shows a behavior expected for a material with 3 orders of magnitude less Young's modulus than the reported longitudinal modulus of silk ($E = 8.4 - 12.9$ GPa considering longitudinal stiffness (Chu, 2013) vs $E \approx 30$ MPa considering bending stiffness (Chen et al., 2015)). The bending stiffness is defined for the cantilever beam as in Chen et al. (2015):

$$B = \frac{Fl^3}{3f}, \tag{4.16}$$

where $B = EI$, E is the Young's modulus of the beam material and I is the moment of inertia of the beam, F is the load applied at the end of the beam, l is the length of the beam, and f is the deflection of the beam at the load position. Chen et al. (2015) reported values of bending stiffness varying between $0.015 - 0.04$ cN $\cdot$ cm^2 for silk sutures with different coatings. The test was performed on 2-0 commercially available braided silk sutures. By considering the smallest diameter for a 2-0 suture (0.3 mm), it is possible to calculate the moment of inertia of the suture ($I = \pi d^4/64 = 0.0004$ mm^4) and then the perceived Young's Modulus of the suture during bending using $B = 0.02$ cN $\cdot$ cm^2 would be $E = 50$ MPa.

This value is significantly lower than the longitudinal initial Young's Modulus reported for silk sutures of $8400 - 12900$ MPa (Chu, 2013). By considering that the lower bending stiffness in the braided silk suture is caused by the sliding between the braided fibers, it is possible to propose a material with a behavior similar to a fiber reinforced material with longitudinal initial tangent modulus of 10000 MPa and an initial isotropic shear modulus of 16.66 MPa (one third of the perceived Young's Modulus during bending).

Assuming that the Ethibond suture would have a similar behavior, we can transpose the

same ratio for an Ethibond suture, which, in this work is represented with a longitudinal initial Young's Modulus of 3000 MPa, resulting in a initial shear modulus of 5 MPa. This values were used as reference values to construct the material parameters for the HGO constitutive model of the suture. The material parameters of the suture are summarized in the table 8.

Table 8 – Parameters for the material model of the suture.The parameter k_2 is dimentionless, D is given in MPa^{-1}, C_{10} and k_1 are given in MPa.

C_{10}	D	k_1	k_2
5	0.001	3000	1

4.7.2   Suture boundary conditions and interactions with the tendon model

The external portion of the suture geometry was cropped after the geometry of the suture was assembled in the Achilles tendon model. The cropped portion was then replaced by a linear spring element (Fig. 9 and Fig. 11).

In a first simulation, no stiffness was assigned to any of the six spring elements and a force of 25 N was applied to one of the strands to simulate tying the first knot. Only one reference in the literature was found for suture knot loads and it reported a value of 10-15 N for sutures USP size 3-0 in flexor tendons (Vanhees et al., 2013). However, since the suture size used in Achilles tendon repair is usually larger (e.g. USP size 0 (Assal, 2024), USP size 1 (Byrne & Aly, 2019) and even USP size 2 (Adames et al., 2023)), the value of 25 N was chosen.

At the end of the simulation, the position of the loaded suture extremities was used as reference to obtain the parameters of the first pair of linear springs. This procedure was repeated for the second knot, now with the first knot already loaded by the newly defined spring element, and the results were used to define the second pair of linear springs. Finally, a third simulation is performed resulting in a load of 25 N in the final knot and a different load in the previous two knots.

A frictionless contact interaction was used to model the interaction between the suture strands and the tendon.

4.7.3   Tendon model modifications

For this case, the proximal boundary conditions were replaced by a series of linear springs in the direction of the z axis in order to represent the passive stiffness of the different muscles of the TSMTU (Fig. 12). The value of the stiffness was approximated by using the value of torsional stiffness of the ankle joint presented in (Walker et al., 2022) and the moment arm of 35 mm measured by Olszewski, Dick & Wakeling (2015)). In addition, a simulation was performed with the tendon model in order to measure the average stiffness of the model and consider it in the calculation of the muscle stiffness. The result was a muscle stiffness of 46.7 N/mm (23.35 N/mm for the soleus muscle and 11.675 N/mm for each subtendon.).

Figure 12 – Detail of the position of the spring elements representing the muscle passive
stiffness.

The rupture was modeled as a transversal cut in the tendon. A similar rupture model is used in *in vitro* suture biomechanical testing (Diniz et al., 2023a; Demetracopoulos et al., 2014; Heitman et al., 2011). The cut was represented by a significant loss of mechanical properties in the central cross section of the model. Such loss was implemented by using the $\phi_p(\mathbf{x})$ function (Fig. 13).

Figure 13 – Visualization of $\phi(\mathbf{x})$ used to model the rupture of the tendon.
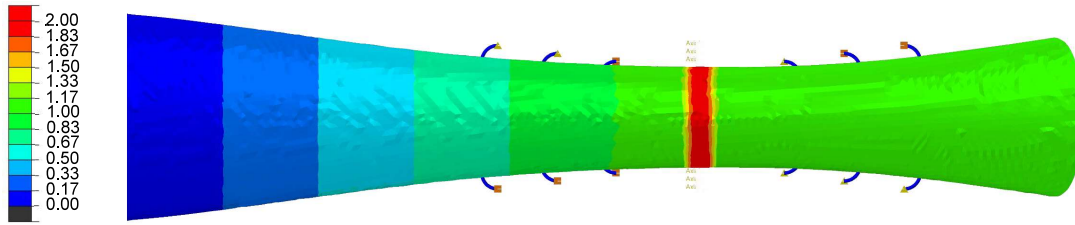
An explicit dynamic formulation was used in order to enable the simulation. The time increment was set to change automatically in order to never cross the minimum element-by-element stable time increment defined as:

$$\Delta t_{stable} = \frac{L_e}{C_d}, \tag{4.17}$$

where Δt_{stable} is the maximum stable time increment for a given element, L_e is the element length, and C_d is the element wave speed (Smith, 2009).

A mass scaling strategy was used, where the material density ρ of each element was automatically updated every 100 time increments in order to achieve a target value of Δt_{stable}. The result of this strategy is that each element would have a different material density ρ and that it would likely change every 100 time increments. This means that ρ could change significantly during the simulation. In order to be able to minimize the influence of the change of ρ on the model behavior, the target value of Δt_{stable} was set small enough to make the simulation behave close to a quasi-static process (Smith, 2009). This minimized the influence of inertial forces on the overall model behavior.

The number of elements in the model was significantly increased to reduce the number of distorted elements in the mesh. Therefore, first-order tetrahedral elements were used instead of second-order elements to reduce the total number of degrees of freedom in the simulation.

The results of this test setup can be found in subsection 5.4

5 Results and specific discussions

5.1 Numerical Test Setup 1

The following results regard the comparison of the model with the simple tension *in vivo* tests made by Peltonen et al. (2013) (the methodology can be found in subsection 4.4).

Six different sets of material properties were tested, as shown in Table 2. This resulted in six different force-displacement curves, as shown in Figure 14. The displacement measurements were taken at the beginning of the transition region ($z = 60$ mm).

Figure 14 – Force-displacement curves for different material properties compared to experimental results from Peltonen et al. (2013).
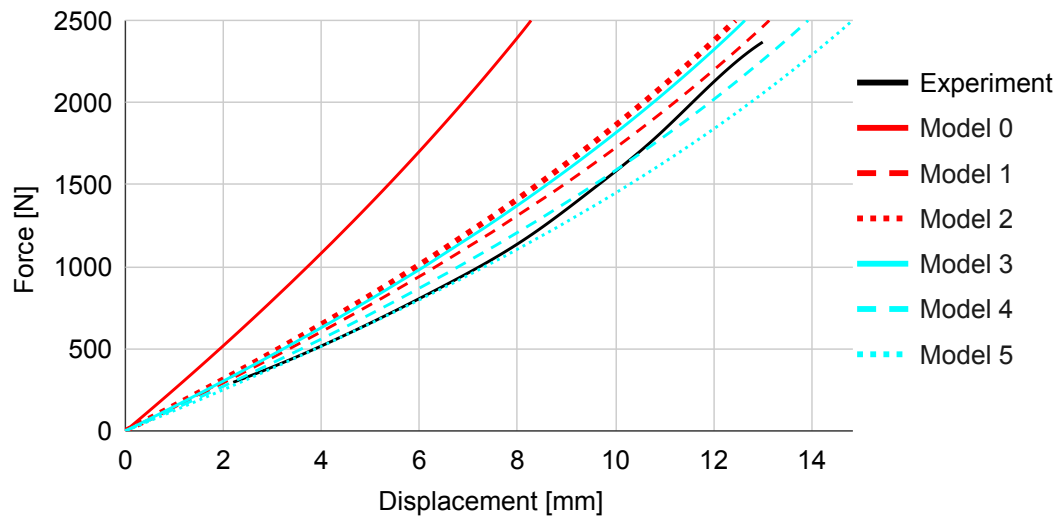
For the simple tensile test, it can be seen that the general behavior was captured with all curves. However, model 0 did not correctly represent the amplitude of the curve.

Both the experimental and simulation curves do not show the S-shape curve (Fig. 1). This can be explained by the fact that in the experiment the subjects were asked to perform a round of 10 warm-up/practice contractions, in *in vitro* experiments this procedure is similar to preconditioning (Pinto, 2014), such procedure can minimize the presence of the region (I) of the S-shape curve. Additionally, the subjects were asked to perform 80% of maximum voluntary contraction and the Achilles tendon is able to withstand forces up to three times the maximum voluntary contraction (Olszewski, Dick & Wakeling, 2015; Schepsis, Jones & Haas, 2002). i.e. the experiment is likely far from the region III.

5.2   Numerical Test Setup 2

The following results are a compilation of the comparison of the model behavior with the various measurements obtained in Lersch et al. (2012). In this test setup the load distribution in the muscles and the ankle rotation were varied and strain measurements were taken in 5 different segments of the tendon (the methodology can be found in subsection 4.5).

The relative strain measurements were compared one by one with the results presented in Lersch et al. (2012). For each model result set, a value for $\bar{R}$ is shown in Table 9 as explained in subsection 4.5. This result set was processed considering only the first load level of the experiment.

Table 9 – Values of $\bar{R}$ obtained for the models in Tab. 4

Twist	$\bar{R}$							
	A1	A2	A3	A4	A5	A6	-	-
45°	2.21	1.94	1.87	1.84	1.73	1.45	-	-
	B1	B2	B3	B4	B5	B6	B7	B8
90°	2.77	1.83	1.71	1.27	1.10	1.05	0.96	0.96

Fourteen different combinations of material parameters and subtendon twist were simulated and compared with the experiments presented in Lersch et al. (2012). The results show a large variability in the values of $\bar{R}$. Only two models had values of $\bar{R}$ lower than one. The combination of properties that fit the experiment better were those with higher C_{10}, which is a material parameter analogous to the shear modulus in the Neo-Hookean material model.

It is possible that the "demand" for high levels of shear resistance could be a consequence of factors such as: the advanced age of most experiment specimens (72-86 years elderly specimens with only one 20 year elderly specimen), the fact that the specimens were frozen prior to the experiments, the deregulation of the metabolism post-mortem, the removal of the specimen from the body and possible loss of water to the environment. However, to confirm the need for high levels of shear resistance in order to adjust the parameters for these specimens, a more thorough investigation would have to be done, taking into account the actual geometry of each specimen and running many more simulations so that the the envelope of viable values for C_{10} could become visible.

Furthermore, it is clear that an automatic optimization procedure can be used to improve the residual minimization, e.g. using PSO (particle swarm optimization) approaches (Kuhl et al., 2013).

The comparison made in this test setup was much richer than in Numerical Test Setup 1 because each set of material parameters was compared with 40 different measurements. Load variations including non-uniform muscle activation and calcaneal bone rotation were taken into account, as well as non-homogeneity in the displacement field. However, the values obtained for $\bar{R}$ were quite high. The general behavior of most load variations was satisfactorily captured, with the exception of the load variation 3. If load variation 3 were removed from the data set the new table for $\bar{R}$ would improve for all models except model B8 (Tab. 9).

Table 10 – Values of $\bar{R}$ for Numerical Test Setup 2. After removing load variation 3 from the data set.

Twist	$\bar{R}$							
	A1	A2	A3	A4	A5	A6	-	-
45°	1.50	1.39	1.30	1.28	1.21	1.07	-	-
	B1	B2	B3	B4	B5	B6	B7	B8
90°	1.86	1.32	1.29	1.02	0.94	0.93	0.93	0.98

In summary, two of the tested models can be considered a viable tendon since their value of $\bar{R}$ was lower than one. Model B7 was also able to represent most of the inhomogeneities due to calcaneal rotation, uneven muscle loading, and non-negligible shear stresses. However, the model still requires improvements before it can be considered fully validated.

In addition, the Achilles tendon model was able to present some of the behaviors observed in Lersch et al. (2012):

Lersch et al. (2012) observed that "*...changes in frontal plane calcaneus position resulted in higher strain differences within the tendon than variations of triceps muscle force ratios...*". That is, the range of rotations of the experiments caused more change in the measured strain field than the range of variation in muscle activation. The same pattern was observed in the simulations. Figures 15 and 16 show that, when compared to the standard case, Load Variation 1 produces a strain field visibly closer to the Standard case field than the Eversion 15° and Inversion 15° cases.

Lersch et al. (2012) observed that "*...During eversion and inversion unilateral increase and contra-lateral decrease of tendon strain could be observed as well on the dorsal as on the ventral tendon aspect...*". The same can be seen in figures 15 and 16. This general behavior suggests a beam-like behavior caused by non-negligible shear stresses.

Lersch et al. (2012) observed that:

> "[...]AT strain patterns that occurred with inversion and eversion of the calcaneus did not show the same behavior with regard to proximal versus distal tendon strain on the dorsal tendon aspect. During inversion lateral and intermedial tendon aspects experienced an increase in strain while medial tendon strain decreased in relation to the baseline condition. During eversion the distal tendon aspect showed the mirror-inverted pattern while proximal tendon strain also decreased in medial and intermedial aspects...[...]" (Lersch et al., 2012).

In Figures 17 and 18, the color scale has been changed in order to compare the results of model B7 with this observation. The dorsal aspect can be seen in Figure 17 and 15, where it is possible to see that in the distal portion of the eversion and inversion cases the strain fields mirror each other, with similar proportions of compression zones (blue and dark gray) and tension zones (red and light gray). However, when looking at the proximal region of the free tendon (near the region with the smallest cross section) the mirroring is not present, this is more evident in figure

Figure 15 – Results for model B7. Logarithmic strain in the fiber direction on the anterior surface of the model for the Standard, Variation 1, Inversion 15°, and Eversion 15°, ordered from top to bottom.
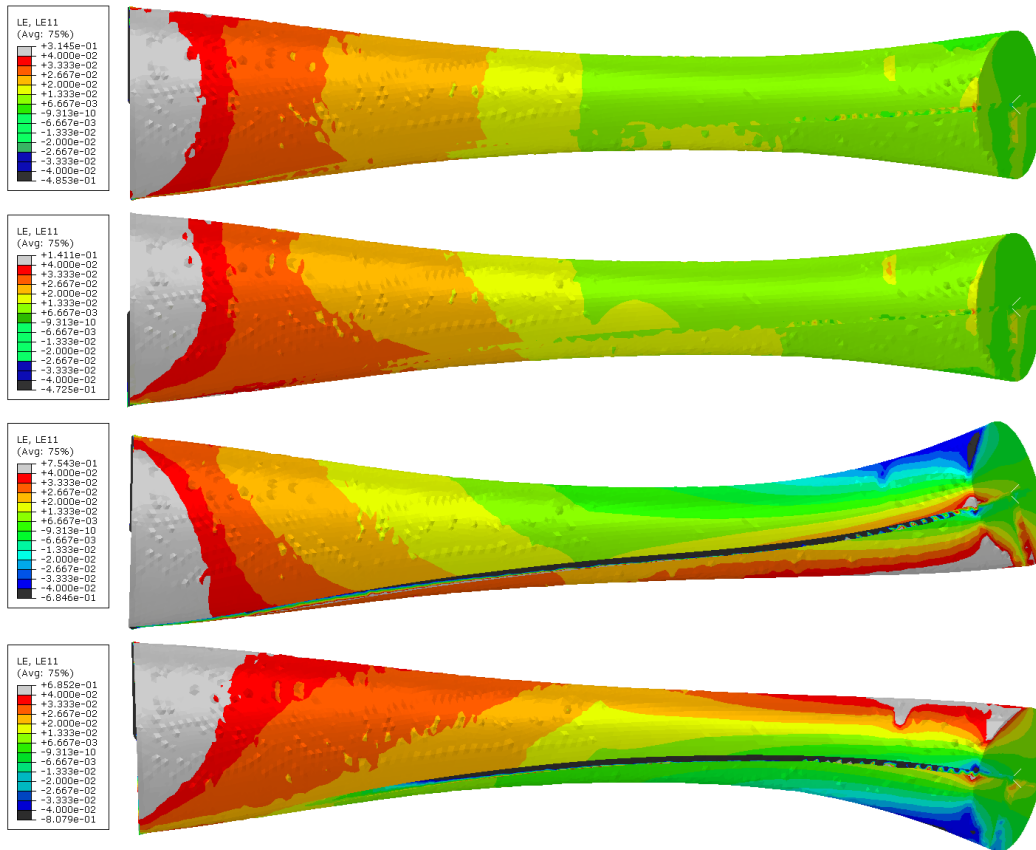
17 where it can be seen that at the smallest cross section the strains due to inversion are mainly light blue, with a small region in red, while the strains due to eversion present a pattern similar to the distal region. Although this is a result where the proximal portion of the free tendon is not mirrored, the pattern presented is not the same as the one presented in Lersch et al. (2012), where the posterior aspect would be dominated with strains lower than the standard case in eversion and not in inversion.

In addition, a tendency for rotation of the proximal portion of the tendon was observed (Fig. 19). This tendency has also been commented in Lersch et al. (2012) as a reason for why there is differences in the proximal and distal strain fields. While some of this rotation may play a role in the strain distribution within the tendon, the complete restriction of this behavior becomes more unrealistic as a given Achilles tendon model chooses to represent a shorter portion of the TSMTU, since the anchor points that could resist such rotation would be incrementally further away, making the equivalent torsional stiffness of the ignored portion of the TSMTU incrementally lower. In addition, the three joints that the TSMTU crosses (knee, talocrural, and subtalar) have some allowance for rotation in the transverse plane due to them not being perfectly rigid (even though such rotation is not one of their main degrees of freedom), so it could be the case that this rotation is not only absorbed by the soft tissues of the TSMTU, some of it could result in relative rotation of the attachment points of the TSMTU.
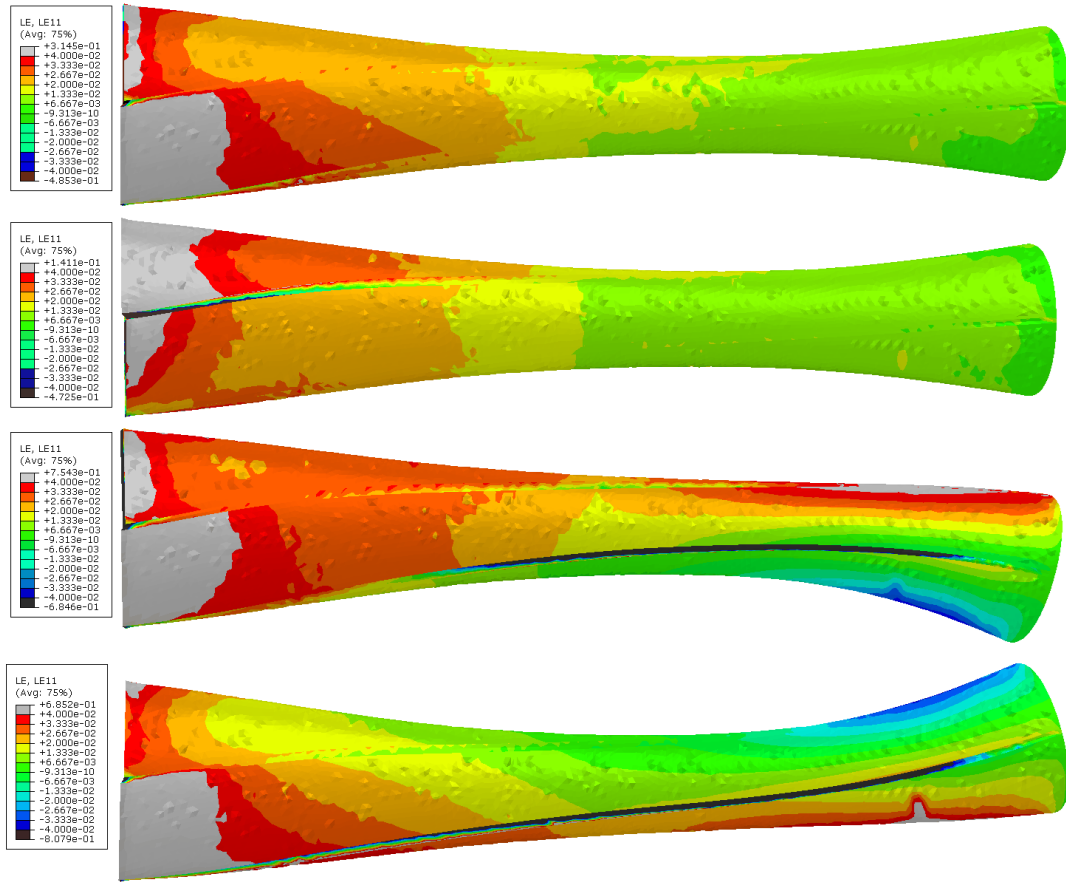
Figure 16 – Results for model B7. Logarithmic strain in the fiber direction on the posterior surface of the model for the Standard, Variation 1, Inversion 15°, and Eversion 15°, ordered from top to bottom.

5.3 Numerical Test Setup 3

The following results refer to the comparison of the behavior of an elderly and an young tendon with tendinosis of different sizes (the methodology can be found in subsection 4.6).

The results obtained in this test are shown in terms of the (locally) axial Cauchy stress field, i.e. σ_{11} being $\mathbf{e}_1$ the local direction of the fibers. To facilitate interpretation, the color red was chosen to represent stresses of 32 MPa, which is approximately three times the average tensile stress (total axial force of 600 N divided by the smallest cross-sectional area of 54.9 mm^2).

Figure 20 show σ_{11} for the elderly and young tendons with no lesion. The same field is presented for the low, medium and high severity cases in Figures 21, 22 and 23, respectively.

Figure 20 shows that even for a non-pathological tendon (standard case), the stress distribution is not completely homogeneous. As expected due to its low stiffness, the interface material presents low stress. Moreover, both tendons, elderly and young show similar results.

The low severity case (Fig. 21) presents little changes when compared to the standard case. The small lesion had very little influence on the stress fields of both, young and elderly tendons. Just a small region of low stress is visible near the pathological tissue but not enough to create any substantial stress concentrations.

Figure 17 – Results for model B7. Logarithmic strain in the fiber direction on the anterior surface of the model for the Standard, Variation 1, Inversion 15°, and Eversion 15°, ordered top to bottom. Colors have been manually scaled so that green represents the average strain in the proximal region of the tendon for the standard case ($0.012 < \varepsilon < 0.015$), yellow, red, and light gray represent increasingly larger strains, while light blue, dark blue, and dark gray represent increasingly smaller strains.
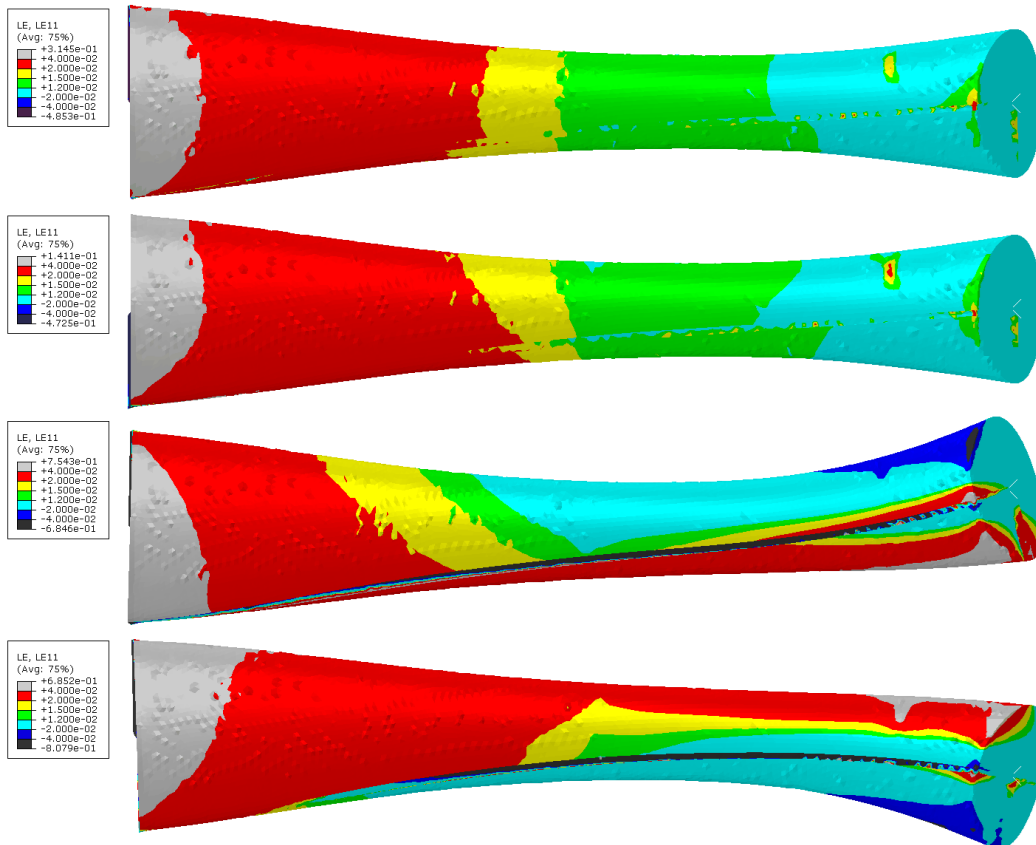
The case of medium severity (Fig. 22) presents a substantial change in the stress fields of both tendons. The lesion region exhibits a dark blue spot, indicating its low capacity to bear forces. Stress concentrations are particularly noted in the lateral portion of the medial gastrocnemius subtendon. Most importantly, the stress concentration level of the elderly tendon is substantially higher than than that of the young tendon.

The case of high severity, displayed in Fig. 23, presents significant changes in the stress field when compared to the standard case. Low stresses are found in the central region as a direct consequence of the loss of stiffness with the expected load transfer to the tendon sides and consequent stress concentration. The level of the stress concentration appears to be slightly lower in the young subject, specially in the medial portion of the tendon but with results much more similar than the differences found in the medium severity case.

The increase in the size of the pathological region produces a stress field pattern with stress concentration at the sides of the affected region. However, and that is the point raised up in this study, the geometric and material characteristics of the tendon allows for different

Figure 18 – Results for model B7. Logarithmic strain in the fiber direction on the posterior surface of the model for the Standard, Variation 1, Inversion 15°, and Eversion 15°, ordered top to bottom. Colors have been manually scaled so that green represents the average strain in the proximal region of the tendon for the standard case ($0.012 < \varepsilon < 0.015$), yellow, red, and light gray represent increasingly larger strains, while light blue, dark blue, and dark gray represent increasingly smaller strains.
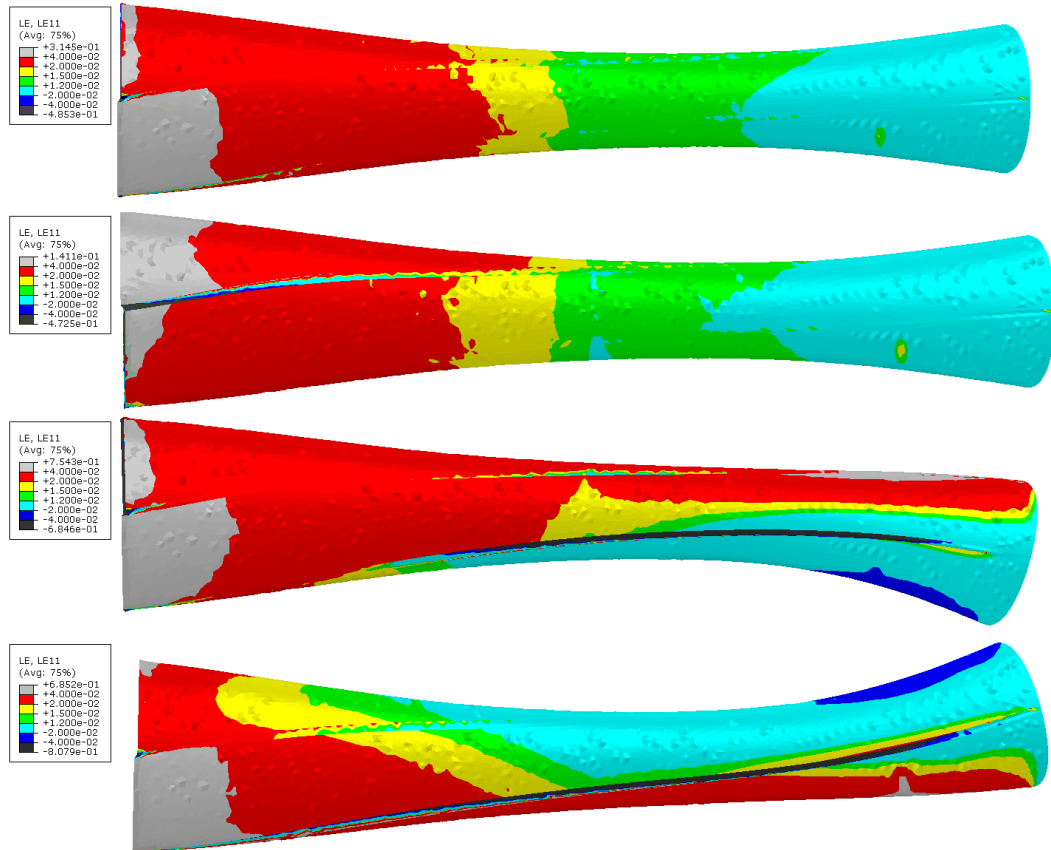
Figure 19 – Rotation of the proximal portion of the model relative to the distal end.
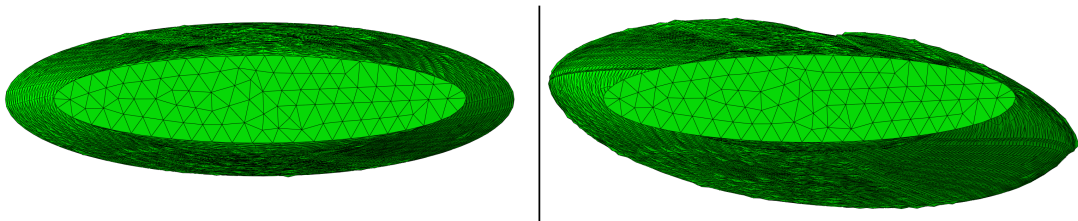
kinematic accommodations depending on the shear stiffness of the tendon tissue.

For the medium severity level (Fig. 22), the young tissue results show a stress concentration region smaller than that of the elderly tissue. The most important issue to be highlighted here is that such result was achieved by just changing the C_{10} shear parameter. Moreover, such result is not that obvious, since the same change operating on low and high pathological severity levels do not bring the same contrasting result.

The lower shear modulus of the young tendon allows for a better (homogeneous) dis-

Figure 20 – Stress in the local direction of the fibers for the standard case (no lesion).
        Upper image is from the young subject and lower image is from the elderly
        subject.

Figure 21 – Stress in the local direction of the fibers for the lesion of low level of severity
        case. Upper image is from the young subject and lower image is from the
        elderly subject.
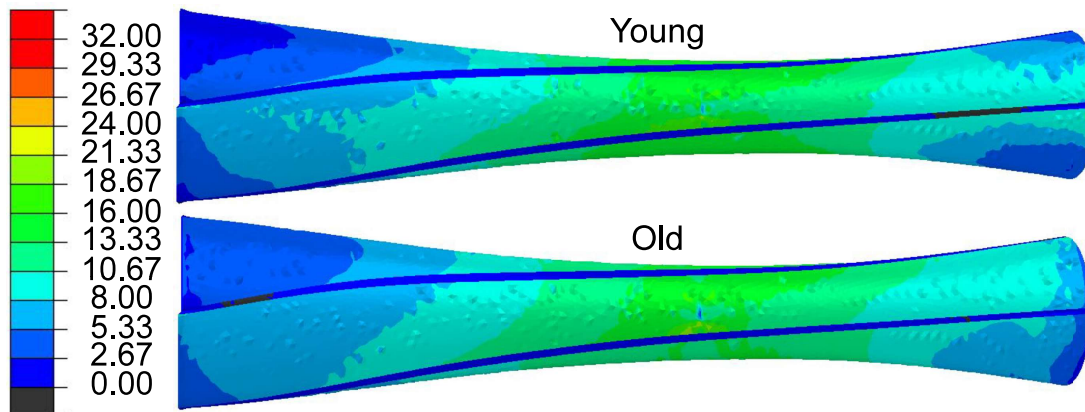
tribution of the axial loads across the fibers, which is clearly not achieved in the stiffer tissue.
This result shows a possible mechanism linking aging to an increased likelihood of acute Achilles
tendon rupture due to overload, without the need to propose a lower local failure stress or any
other dependence of damage-related properties on age.

It can also be seen that, for low and high levels of severity (Fig. 21 and Fig. 23), there
is no clear difference between young and elderly subjects. This indicates that if the lesion is
small enough, both tendons have stress distributions similar to the standard case and can be
considered as in a safe condition. On the other hand, if the lesion is large enough, both would
have a very inhomogeneous stress field and would be equally at risk of acute rupture.

The results show that the lesion size dominates the phenomenon at small ($\approx 20\%$ of
the cross section) and large ($\approx 80\%$ of the cross section) lesions, since at this levels there is
no sensible effect of the differences in C_{10}. However, the C_{10} shear parameter impacts in the
determination of the critical size of the lesion. The results indicate that when tendinosis size
increases, the risk of a acute lesion arrives first for tendons with more shear stiffness.

Figure 22 – Stress in the local direction of the fibers for the lesion of medium level of severity case. Upper image is from the young subject and lower image is from the elderly subject.
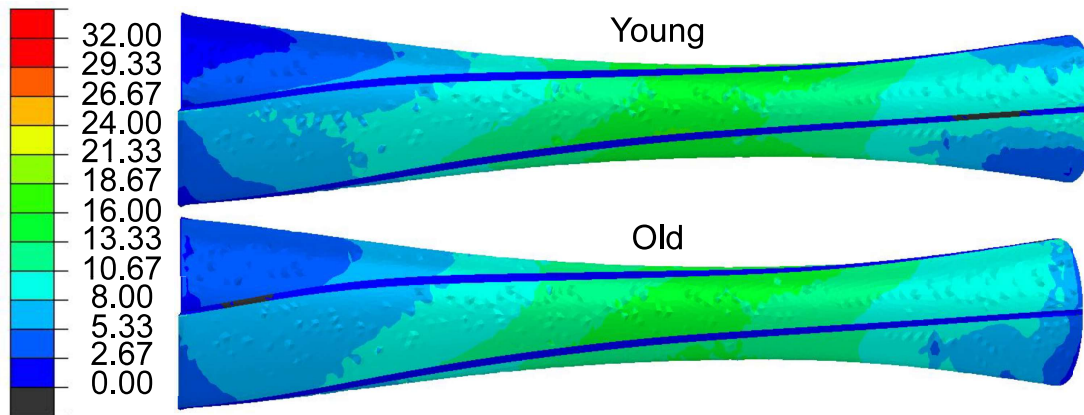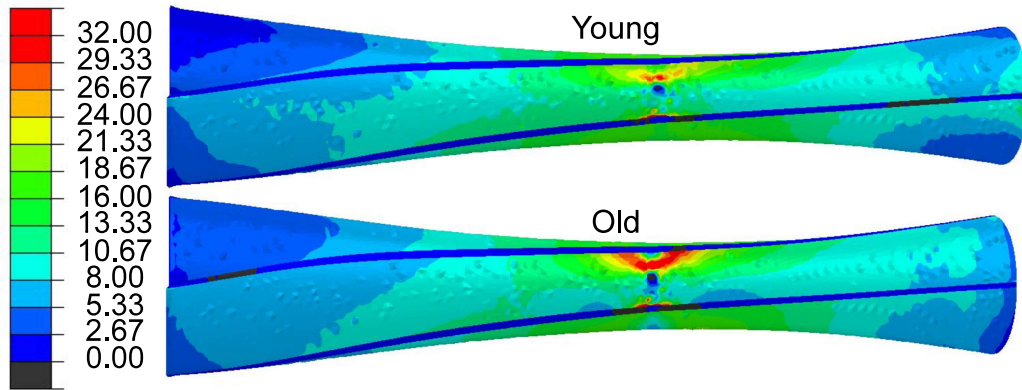

Figure 23 – Stress in the local direction of the fibers for the lesion of high level of severity case. Upper image is from the young subject and lower image is from the elderly subject.
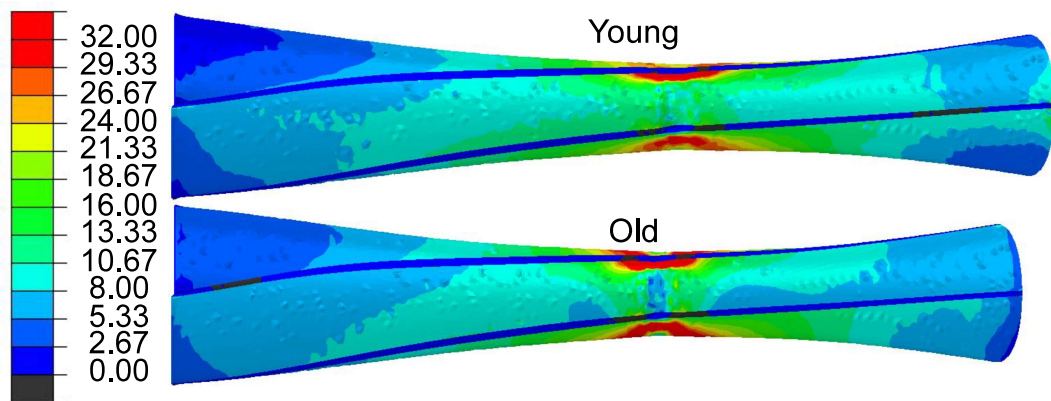
In addition, this finding suggests that for higher values of C_{10} the tendinosis has, potentially, a higher probability to grow, since higher values of C_{10} amplify the stress concentration near the tendinosis. The regions with stress concentrations could then suffer a series of microruptures making a new tendonosis area at the site of the stress concentration. If the process just described occurs in a faster pace than the tendon recovery speed, then the tendinosis will grow. This mechanism could be one of the causes for elderly tendons being more sensitive to fatigue (Thorpe et al., 2014).

The model was able to represent a possible underlying failure mechanism that differentiates the resistance of elderly and young tendons to an acute rupture. To suport this point is important to differentiate tendinosis from tendinopathy since, in this work, the same tendinosis (localized material alterations) provoked different levels of tendonopathy (the perceived level of impact of the tendinosis on the tendon health). This observation agrees with the observations of Sun et al. (2015) where the lack of sliding capabilities can lead to more tendinopaties. By assuming a correlation of sliding capabilities with age, this results also agree with Thorpe et al. (2012a) since elderly tendons were shown as more sensitive to a given tendinosis and with Thorpe et al.

(2014) since the higher stress concentrations in the elderly case could help to explain the lower fatigue resistance of elderly tendons.

5.4   Numerical Test Setup 4.

The following results regard the study of the suture technique Achillon described in subsection 4.7.

The results of this test are shown as the forces on the sutures' spring elements at the end of each knot tying simulation (Tab. 11).

Table 11 – Forces in the different suture strands at the end of the knot tying simulation.

Strand		
1	2	3
16.5 N	21.0 N	25 N

In addition, a buckling like behavior was observed (Fig. 24). Figures 24 and 25 show a central region with compressive strains. This region is the region where the material properties have been lowered in order to represent the tendon rupture. The compression and the buckling-like behavior shown in these figures indicate that a significant portion of the force from the sutures is internally balanced. This is confirmed by the difference between the total reaction forces in the muscles (≈ 90 N) and the total force in the six suture spring elements (≈ 125 N), i.e. approximately 35 N is absorbed by the compression of the ruptured segment.

This behavior can be seen in images of Achilles tendon repair and sometimes results in overlapping of the two tendon stumps, a phenomenon known as bayoneting (Heitman et al., 2011).

Figure 24 – Lateral view of the tendon after the knot tying simulation. Colors represent the minimum principal strain (maximum compression). The detail show the buckling-like behavior of the central portion of the model.
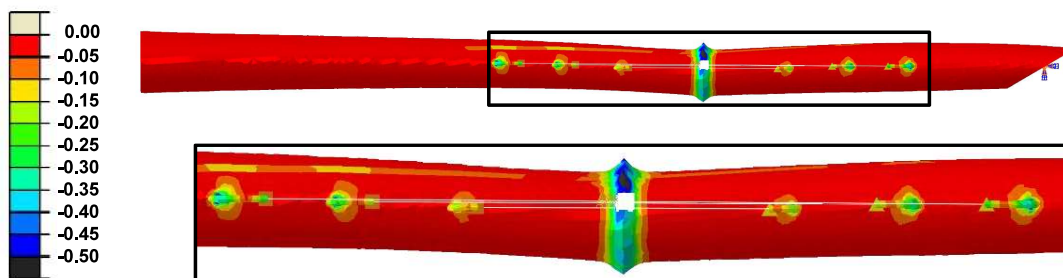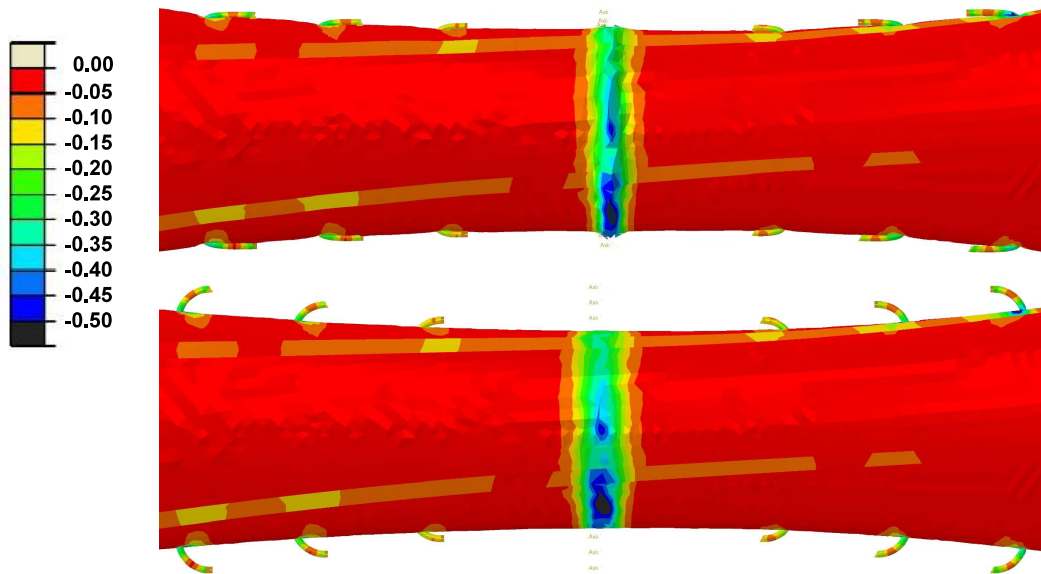
Figure 25 – Posterior view of the tendon after the knot tying simulation. Colors represent the minimum principal strain (maximum compression). The top image shows the deformed configuration and the bottom image shows the same strain field but in the undeformed configuration in order to better visualize the movement of the suture geometries.

6 General discussion and future work

This dissertation presented a model of the Achilles tendon as a strategy to investigate the behavior of the tendon under different conditions.

The simplified geometry proved to be an asset of the proposition since there were very few moments in the results interpretation process where a particular irregularity or misalignment interfered, when they did they were caused by the meshing process and could be corrected, or they were caused by model parameters and they were there by design.

The proposition of an internal interface proved to be successful. The model was able to replicate a complex set of experimental results presented in Lersch et al. (2012).

A remark must be made about the interface and the choice of material models. Their proposition should not be confused with the proposition of non existence or negligible dissipative interactions between the subtendons or even within the subtendons. The experiment in Lersch et al. (2012) used much slower strain rates than the physiological loading rates, and it is expected that a model with no dissipation would be able to fit it since for this particular scenario dissipation can probably be neglected. Tendons, including energy-storing tendons, are known to dissipate energy during movement, and if the experiment protocol in Lersch et al. (2012) used faster loads, it is possible that some dissipation mechanism would have to be added to the model in order to achieve results similar to those presented in this work.

The proposition of a transition region between the MTJ of the soleus and the MTJ of the gastrocnemius also proved to be advantageous, since it shifted the boundary conditions away from the critical area of the tendon (smaller cross section at $z = 52$ mm). The presence of this additional region allowed the investigation of lesions in the critical area. Without the additional region, the results of this research would likely be affected by the proximity of the boundary condition, which could make interpretation difficult.

The use of local fiber orientation combined with the use of a transversely isotropic material model allowed for the representation of the internal fiber sliding. Because of this feature, the shear and longitudinal behaviors of the model are uncoupled and the individual manipulation of these behaviors is straightforward. However, the orientation of the fibers followed the twist of the subtendons and it has been observed in the literature that this may not be the case.

The implementation of a generic parameterized scalar function for the variation of the material properties of the model adds the possibility of simulating different conditions on the tendon. An example of its aplication for the investigation of tendinopathies is shown, where the lesioned region is represented as a tissue with lower collagen content and hence lower longitudinal stiffness, but scenarios with different changes in properties such as local calcifications could also be easily tested.

The first and second investigations in this work were aimed at validating the model

by comparing it with experimental data and adjusting its parameters in order to get as close as possible to the sample of the population being tested in the experiment. With the results presented in this work, it is not possible to claim that the model is fully validated, but the model was able to represent the general behavior observed in the experiments.

The third investigation aims to demonstrate the potential capabilities of the model for clinical applications. In this investigation, a taylored numerical model of the Achilles tendon is used to investigate the hypothesis of existence of a causal relation among tissue sliding and tendinopathy, and, by associating sliding with aging, it also proposes a causal explanation to the correlation of aging with tendinopathy.

The fourth investigation also aimed to demonstrate the potential capabilities of the model for clinical applications. In this investigation, the Achilles tendon model is complemented with a model of the Achillon suture technique. The simulation was designed to test the hypothesis that after tying the last knot, the force in the first two knots would decrease significantly. The maximum decrease in force was as expected in the first suture strand (from 25 N to 16.5 N), but the value of the decrease was not as significant as expected.

As a second remark, it is important to highlight the fact that, although the model is competent in representing the general behavior of the Achilles tendon, the model used in the third investigation is not fully validated. The results were able to show how shear resistance can make a tendon more prone to acute ruptures when an injury is present, but caution must be taken when extrapolating the numerical results presented in this work to clinical scenarios. As an example, the results of this work should not be used clinically to determine what lesion size is safe for a young tendon, but they can be used to conclude that a lesion size that was considered safe in a young tendon may not be safe in an elderly tendon. In addition, the results indicate that a lesion size that is safe for an elderly tendon may be also safe for a younger tendon.

6.1   Limitations

This work has a number of important limitations, which are addressed in the following paragraphs.

The use of material models without dissipation, limits the model to situations where the loading rate is sufficiently slow to keep the model in equilibrium with its boundary conditions at all times. Tendons are known to dissipate energy even at slower than physiological loading rates (Pinto, 2014), so the determination of how slow is slow enough must be made on a case-by-case basis. Incorporating viscoelastic dissipation into the model is straightforward, but tendons are also known to dissipate energy through fluid motion, making the use of poroviscoelastic models a more appropriate choice. Either way, the use of those material models would make the parameter identification process significantly more costly and for that reason they were not used at this moment.

The geometry of the tendon, the geometry of the subtendons, the amount of twisting, and the experimental mechanical behavior were not obtained from the same sample. This could

lead to a validation procedure where the behavior is satisfactorily approximated for a given data set, but the end result is a nonexistent tendon, because the geometry of the tendon which the mechanical behavior was measured may be significantly different from the geometry used to model it. An ideal scenario would have all data (geometry, twist, mechanical behavior) coming from the same tendon, but unfortunately such data has not been found in the literature.

The geometry of the transition region to the muscle tissue was defined by simply extrapolating the geometry of the free tendon region. Ideally, the geometry of the whole TSMTU, including the surrounding tissue and the bones, would be represented. However, due to computational and labor constraints, it is common to limit the geometry to the scope of the investigation by cropping it and removing the surrounding tissue. A more accurate way to achieve this would be to start with the geometry of the entire TSMTU and crop it so that the transition region has its geometry represented more accurately.

The thickness and material model of the interface were added as a hypothesis, and were not based on a specific measurement. Again, it would be ideal to have the measurement of these parameters, but the data has not yet been found in the literature.

Above all, the main limitation of this work, and of all the works found in the literature trying to model the Achilles tendon, is the the lack of a formal and extensive validation. The Achilles tendon presents a great variability of measured mechanical behavior and is usually treated as a material. Proper modeling of the tendon should look at it more like a part with non homogeneous material properties, where different Achilles tendons could behave as different parts do. The tendon of one subject can differ significantly from the tendon of another to the point that the whole model would have to be completely different. This is the most intimidating aspect of modeling the Achilles tendon and it is the greatest obstacle to the clinical use of such models. Proper validation of an Achilles tendon model should include a procedure in which the geometry, material, and boundary conditions are all derived from the same tendon, and that the range of mechanical behaviors observed from that tendon is sufficiently rich so that all the material parameters are determined. In addition, to be clinically viable, this procedure should be performed *in vivo*, since, although some useful conclusions could be drawn from it, there is no direct clinical application for a model of a dead tendon.

6.2 Conclusion

This work presents a novel computational model of the Achilles tendon with a new strategy to represent sliding among subtendons, the geometry of the tendon and its subtendons, to represent the proximal boundary conditions of the Achilles tendon and to represent lesions in the tendon. All these mentioned features were put in service to test the hypothesis of existence of a causal relationship between changes in the shear behavior due to aging and the lowering of the perceived tensile rupture stress of the Achilles tendon.

Numerical Test Setup 1 showed that the model is able to reproduce the general behavior of the tendon in a tensile test. The results of Numerical Test Setup 2 showed that the model is

able to achieve reasonable agreement with non-homogeneous displacement fields, presenting good levels of normalized residual ($\bar{R}$) for some sets of material properties. In addition, the model is able to represent inhomogeneities due to calcaneal rotation and non-negligible shear stresses.

The results of Numerical Test Setup 3 show a possible mechanism for a causal relationship between aging and an increase in the incidence of acute ruptures. The increase in shear resistance associated with aging due to the increased presence of advanced glycation end products and other mechanisms of protein adhesion associated with aging can weaken the "immunity" of the tendon to stress concentrations. In other words, the lower shear modulus of younger subjects can result in stronger Achilles tendons. Numerical Test Setup 4 demonstrates the feasibility of modeling suture techniques using the model, and its results showed some loss of suture tension during the knot tying procedure of the Achillon repair technique. At this point, however, more information is needed to determine whether this decrease in tension is significant.

6.3   Next steps

Below are some suggestions for future work, some of which are already being worked on, while the others are listed because they were perceived by the author as low cost compared to the expected return.

Automation of the parameter identification procedure could potentially reduce the residual of the validation procedures shown in this work. The automation of the material parameters and their incorporation into an optimization algorithm would take some time, but it is a common procedure. The automation of the twisting level will probably require more work as it would involve geometry generation and meshing automation, a procedure that is not as common as the classical material parameter identification through optimization.

The effect of the subtendon twist on the mechanics of the Achilles tendon was investigated by several authors. However, as mentioned in the text above, none of these works is free from limitations. In addition, the strategy used in this work represents the subtendon sliding through a purely elastic phenomenon (interface with a hyperelastic material model) rather than purely dissipative phenomenon (frictional or frictionless contact), which is the strategy used by the other works found. This difference alone allows the possibility of adding new insights to the current discussion in the literature.

Inclusion of the calcaneal bone geometry would likely improve the distal boundary condition and it is already being worked on. Inclusion of the calcaneus would complete the geometry of a portion of the tendon and allow for new investigations related to the enthesis, the retrocalcaneal bursa, and even footwear use.

Currently, the transition region geometry was created by extrapolating the tendon geometry. This was pointed above as a limitation and it could be eliminated by using medical images or measurements to create the geometry of this region. This improvement would allow for investigations of interesting problems such as the very common tendinopathies in the proximal portion of the medial gastrocnemius subtendon.

The inclusion of material models with dissipation or even damage can be easily done and would improve the evelope of mechanical behaviors that the model is able to represent. For example, the simulation of dynamic gestures such as running and jumping. However, the validation of such models would be much more complex. A similar observation can be made regarding the inclusion of fluid flow in the model. Its inclusion would allow investigations of tendon metabolism and even improve the improve the fidelity of the model's results, since fluid mechanics is known to influence tendon kinematics.

The model is already being used to investigate other clinical applications. An investigation of repair techniques by including the representation of the suture and the lesion at different stages of healing is already underway. This investigation involves the use of explicit dynamic solution strategies and contact and has the potential to improve the ongoing discussion regarding the comparison of suturing techniques.

The proposition and execution of more advanced *in vitro*, *in situ*, and, above all, *in vivo* experimental setups can potentially improve the validation of all models of the Achilles tendon that are currently being worked on. The generation of abundant experimental data for the Achilles tendon is not only an interesting line of work. It is an obvious necessity for the community working with computational models of the Achilles tendon.

This work proposes the existence of an interface of non-negligible thickness separating the subtendons of the Achilles tendon. However, this proposition could be expanded since at the moment no measurement of its thickness and very little data on its shape and mechanical behavior were found.

The investigation of the influence of neighboring structures (bursa, other muscle tendon unities, footwear, sportswear, etc) can open a line of investigation where new features would be progressively added to the model by incrementally adding new structures to the model. This line of work could eventually result in a model of the whole lower limb.

Bibliography

ABDULLAH, A. B. M. et al. An investigation on stressing and breakage response of a prestressing strand using an efficient finite element model. *Engineering Structures*, Elsevier Ltd, vol. 123, p. 213–224, 2016. ISSN 0141-0296. Cited on page 51.

ADAMES, M. K. et al. Biomechanical comparison of shoelace suture technique for repairing calcaneal tendon. *Injury*, vol. 54, n. 12, p. 111134, 2023. ISSN 00201383. Cited 2 times on pages 43 and 73.

AICALE, R.; TARANTINO, D.; MAFFULLI, N. Non-insertional achilles tendinopathy: State of the art. In: *Sports Injuries of the Foot and Ankle: A Focus on Advanced Surgical Techniques.* [S.l.]: Springer Berlin Heidelberg, 2019. p. 359–367. ISBN 9783662587041. Cited 3 times on pages 41, 42, and 69.

ALFREDSON, H.; ÖHBERG, L.; FORSGREN, S. Is vasculo-neural ingrowth the cause of pain in chronic Achilles tendinosis? An investigation using ultrasonography and colour Doppler, immunohistochemistry, and diagnostic injections. *Knee Surgery, Sports Traumatology, Arthroscopy*, Springer Verlag, vol. 11, n. 5, p. 334–338, 2003. ISSN 09422056. Cited on page 42.

ARYA, S.; KULIG, K. Tendinopathy alters mechanical and material properties of the achilles tendon. *Journal of Applied Physiology*, vol. 108, n. 3, p. 670–675, 2010. ISSN 8750-7587, 1522-1601. Cited 4 times on pages 46, 47, 63, and 69.

ASSAL, M. 2024. Accessed: 08/02/2024. Available from Internet:<https://fischermedical.dk/wp-content/uploads/Achillon.pdf>. Cited 2 times on pages 44 and 73.

AZIZI, E.; BRAINERD, E. L.; ROBERTS, T. J. Variable gearing in pennate muscles. *Proceedings of the National Academy of Sciences*, vol. 105, n. 5, p. 1745–1750, 2008. ISSN 0027-8424, 1091-6490. Cited on page 33.

AZZONI, R.; CABITZA, P. Achilles tendon pathology: The role of ultrasonography. *Journal of Orthopaedics and Traumatology*, vol. 5, n. 3, p. 172–177, dec 2004. ISSN 15909921. Cited on page 42.

BAAR, K. Stress Relaxation and Targeted Nutrition to Treat Patellar Tendinopathy. *International Journal of Sport Nutrition and Exercise Metabolism*, 2018. Cited on page 40.

BALLAL, M. S.; WALKER, C. R.; MOLLOY, A. P. The anatomical footprint of the Achilles Tendon. *Bone and Joint Journal*, vol. 96B, n. 10, p. 1344–1348, 2014. ISSN 20494408. Cited on page 38.

BENJAMIN, M. et al. The anatomy of the achilles tendon. *The Achilles Tendon*, Springer London, vol. 3, p. 5–16, 2007. Cited 2 times on pages 36 and 37.

BIOT, M. A. General Theory of ThreeDimensional Consolidation. *Journal of Applied Physics*, vol. 12, n. 155, 1941. Cited on page 62.

BOGAERTS, S. et al. Evaluation of tissue displacement and regional strain in the achilles tendon using quantitative high-frequency ultrasound. *PLoS ONE*, Public Library of Science, vol. 12, 7 2017. ISSN 19326203. Cited on page 50.

BÖL, M. et al. Tissue-scale anisotropy and compressibility of tendon in semi-confined compression tests. *Journal of Biomechanics*, Elsevier, vol. 48, n. 6, p. 1092–1098, 2015. ISSN 18732380. Cited on page 52.

BONET, J.; WOOD, R. D. *Nonlinear continuum mechanics for finite element analysis*. [S.l.]: Cambridge university press, 1997. Cited on page 60.

BUDDECKE, D. Acute achilles tendon ruptures. *Clinics in Podiatric Medicine and Surgery*, vol. 38, n. 2, p. 201–226, 2021. ISSN 08918422. Cited 2 times on pages 43 and 44.

BYRNE, M.; ALY, A. The surgical suture. *Aesthetic Surgery Journal*, vol. 39, p. S67–S72, 2019. ISSN 1090-820X, 1527-330X. Cited 3 times on pages 71, 72, and 73.

CALVO, B. et al. Passive nonlinear elastic behaviour of skeletal muscle: Experimental results and model formulation. *Journal of Biomechanics*, vol. 43, n. 2, p. 318–325, 2010. ISSN 00219290. Cited on page 69.

CARNIEL, T. A.; FANCELLO, E. A. A transversely isotropic coupled hyperelastic model for the mechanical behavior of tendons. *Journal of Biomechanics*, vol. 54, p. 49–57, mar. 2017. ISSN 00219290. Cited on page 52.

CARNIEL, T. A. et al. An experimental and numerical study on the transverse deformations in tensile test of tendons. *Journal of Biomechanics*, vol. 87, p. 120–126, 2019. ISSN 00219290. Cited 5 times on pages 46, 47, 48, 56, and 63.

CHEN, W. et al. Epidemiology of insertional and midportion achilles tendinopathy in runners: A prospective cohort study. *Journal of Sport and Health Science*, p. S2095254623000376, 2023. ISSN 20952546. Cited on page 27.

CHEN, X. et al. Quantitative physical and handling characteristics of novel antibacterial braided silk suture materials. *Journal of the Mechanical Behavior of Biomedical Materials*, vol. 50, p. 160–170, 2015. ISSN 17516161. Cited on page 72.

CHU, C. Types and properties of surgical sutures. In: *Biotextiles as Medical Implants*. [S.l.]: Elsevier, 2013. p. 231–273. ISBN 978-1-84569-439-5. Cited on page 72.

CHUTKAN, N. B. Surgical versus nonsurgical treatment of acute achilles tendon rupture: A meta-analysis of randomized trials. *Orthopedics*, vol. 36, n. 2, p. 136–137, 2013. ISSN 0147-7447, 1938-2367. Cited on page 43.

CLANTON, T. O. et al. A biomechanical comparison of an open repair and 3 minimally invasive percutaneous achilles tendon repair techniques during a simulated, progressive rehabilitation protocol. *The American Journal of Sports Medicine*, vol. 43, n. 8, p. 1957–1964, 2015. ISSN 0363-5465, 1552-3365. Cited on page 43.

COOK, J. L. et al. Neovascularization and Pain in Abnormal Patellar Tendons of Active Jumping Athletes:. *Clinical Journal of Sport Medicine*, vol. 14, n. 5, p. 296–299, set. 2004. ISSN 1050-642X. Cited 2 times on pages 41 and 49.

CSAPO, R. et al. On muscle, tendon and high heels. *Journal of Experimental Biology*, vol. 213, n. 15, p. 2582–2588, 2010. ISSN 00220949. Cited on page 45.

CURTIS, L. Nutritional research may be useful in treating tendon injuries. *Nutrition*, Elsevier Ltd, vol. 32, n. 6, p. 617–619, 2016. ISSN 18731244. Cited on page 40.

DALEFFE, M. R. et al. Avaliação biomecânica de técnicas cirúrgicas para reparo da ruptura de tendão calcâneo: Estudo laboratorial em bovinos. *Journal of the Foot & Ankle*, vol. 17, n. 3, p. 163–169, 2023. ISSN 2675-2980. Cited on page 43.

DEMETRACOPOULOS, C. A. et al. Limited-open achilles tendon repair using locking sutures versus nonlocking sutures: An in vitro model. *Foot & Ankle International*, vol. 35, n. 6, p. 612–618, 2014. ISSN 1071-1007, 1944-7876. Cited on page 74.

DINIZ, P. et al. Modified triple kessler with least risk of elongation among achilles tendon repair techniques: a systematic review and network meta-analysis of human cadaveric studies. *Knee Surgery, Sports Traumatology, Arthroscopy*, vol. 31, n. 5, p. 1644–1657, 2023. ISSN 0942-2056, 1433-7347. Cited on page 74.

DINIZ, P. et al. Design and validation of a finite element model of the aponeurotic and free achilles tendon. *J Orthop Res.*, vol. 41, n. 3, p. 534–545, 2023. Cited 2 times on pages 29 and 53.

DOCKING, S. I.; OOI, C. C.; CONNELL, D. Tendinopathy: Is imaging telling us the entire story? *Journal of Orthopaedic and Sports Physical Therapy*, Movement Science Media, vol. 45, n. 11, p. 842–852, nov 2015. ISSN 01906011. Cited 2 times on pages 42 and 69.

DU, W. et al. Finite element analysis on the stress state of rope hoisting equipment based on the ABAQUS. In: *2017 8th International Conference on Mechanical and Intelligent Manufacturing Technologies (ICMIMT)*. Cape Town: IEEE, 2017. p. 84–88. ISBN 978-1-5386-0377-2. Cited on page 51.

EDAMA, M. et al. The twisted structure of the human achilles tendon. *Scandinavian Journal of Medicine and Science in Sports*, vol. 25, p. e497–e503, 2015. ISSN 16000838. Cited 8 times on pages 30, 35, 37, 38, 46, 47, 52, and 53.

EDAMA, M. et al. Structure of the achilles tendon at the insertion on the calcaneal tuberosity. *Journal of Anatomy*, vol. 229, p. 610–614, 2016. ISSN 14697580. Cited 5 times on pages 36, 37, 38, 50, and 57.

EDAMA, M. et al. Classification by degree of twisted structure of the fetal Achilles tendon. *Surgical and Radiologic Anatomy*, Springer-Verlag Italia s.r.l., vol. 43, n. 10, p. 1691–1695, oct 2021. ISSN 12798517. Cited 2 times on pages 37 and 38.

ERDONMEZ, C.; IMRAK, C. E. A finite element model for independent wire rope core with double helical geometry subjected to axial loads. *Sadhana*, vol. 36, n. 6, p. 995–1008, dez. 2011. ISSN 0256-2499, 0973-7677. Cited on page 51.

ERDöNMEZ, C.; İMRAK, C. E. Modeling Techniques of Nested Helical Structure Based Geometry for Numerical Analysis. *Strojniški vestnik – Journal of Mechanical Engineering*, vol. 57, n. 04, p. 283–292, abr. 2011. ISSN 00392480. Cited on page 51.

ERIKSEN, C. et al. Systemic stiffening of mouse tail tendon is related to dietary advanced glycation end products but not high-fat diet or cholesterol. *Journal of Applied Physiology*, vol. 117, n. 8, p. 840–847, out. 2014. ISSN 8750-7587, 1522-1601. Cited on page 56.

FANCELLO, E.; PONTHOT, J. P.; STAINIER, L. A variational formulation of constitutive models and updates in non-linear finite viscoelasticity. *International Journal for Numerical Methods in Engineering*, vol. 65, n. 11, p. 1831–1864, 2006. ISSN 00295981. Cited on page 62.

FARRIS, D. J. et al. The role of human ankle plantar flexor muscle-tendon interaction & architecture in maximal vertical jumping examined *in vivo. Journal of Experimental Biology*, p. jeb.126854, 2015. ISSN 1477-9145, 0022-0949. Cited 3 times on pages 45, 47, and 49.

FERGUSON, S. J.; ITO, K.; NOLTE, L. P. Fluid flow and convective transport of solutes within the intervertebral disc. *Journal of Biomechanics*, vol. 37, n. 2, p. 213–221, 2004. ISSN 00219290. Cited 2 times on pages 52 and 55.

FINNI, T.; LICHTWARK, G. A. *Rise of the tendon research.* [S.l.]: Blackwell Munksgaard, 2016. 992–994 p. Cited on page 36.

FRANZ, J. R. et al. Non-uniform in vivo deformations of the human Achilles tendon during walking. *Gait and Posture*, Elsevier B.V., vol. 41, n. 1, p. 192–197, 2015. ISSN 18792219. Cited 5 times on pages 45, 47, 48, 49, and 63.

FRANZ, J. R.; THELEN, D. G. Imaging and simulation of Achilles tendon dynamics: Implications for walking performance in the elderly. *Journal of Biomechanics*, Elsevier, vol. 49, n. 9, p. 1403–1410, 2016. ISSN 18732380. Cited on page 49.

FUNAKOSHI, T. et al. Lubricin distribution in the goat infraspinatus tendon: A basis for interfascicular lubrication. *Journal of Bone and Joint Surgery - Series A*, vol. 90, n. 4, p. 803–814, 2008. ISSN 00219355. Cited 2 times on pages 40 and 48.

FUNG, Y. C. *Biomechanics Mechanical Properties of Living Tissues.* 2nd. ed. [S.l.]: Springer New York, 1993. Cited 3 times on pages 29, 39, and 59.

FUNG, Y. C.; FRONEK, K.; PATITUCCI, P. Pseudoelasticity of arteries and the choice of its mathematical expression. *American Journal of Physiology - Heart and Circulatory Physiology*, vol. 6, n. 5, 1979. ISSN 03636135. Cited on page 61.

GALBUSERA, F. et al. Inverse numerical prediction of the transport properties of vertebral endplates in low back pain patients. *Biomedizinische Technik*, vol. 59, n. 5, p. 385–397, 2014. ISSN 00135585. Cited 2 times on pages 52 and 55.

GASSER, T.; OGDEN, R.; HOLZAPFEL, G. Hyperelastic modelling of arterial layers with distributed collagen fibre orientations. *J R Soc Interface*, vol. 22, p. 15–35, 2006. Cited on page 61.

GAUTIERI, A. et al. Advanced glycation end-products: Mechanics of aged collagen from molecule to tissue. *Matrix Biology*, vol. 59, p. 95–108, 2017. ISSN 0945053X. Cited 2 times on pages 63 and 69.

GELSE, K.; POSCHL, E.; AIGNER, T. Collagens — structure , function , and biosynthesis. *Advanced Drug Delivery Reviews*, vol. 55, p. 1531–1546, 2003. Cited on page 39.

GILS, C. C. V.; STEED, R. H.; PAGE, J. C. Torsion of the human Achilles tendon. *Journal of Foot and Ankle Surgery*, American College of Foot and Ankle Surgeons, vol. 35, n. 1, p. 41–48, 1996. ISSN 10672516. Cited 2 times on pages 35 and 37.

Giuseppe Longo, U.; RONGA, M.; MAFFULLI, N. Achilles Tendinopathy. *Sports Med Arthrosc Rev*, vol. 17, n. 2, 2009. Cited 2 times on pages 41 and 42.

GRANT, T. M. et al. Elastic fibres are broadly distributed in tendon and highly localized around tenocytes. *Journal of Anatomy*, vol. 222, n. 6, p. 573–579, 2013. ISSN 00218782. Cited on page 39.

GRASA, J. et al. Variations in tendon stiffness due to diets with different glycotoxins affect mechanical properties in the muscle-tendon unit. *Annals of Biomedical Engineering*, vol. 41, n. 3, p. 488–496, 2013. ISSN 00906964. Cited 3 times on pages 40, 64, and 69.

GRYTZ, R.; MESCHKE, G. Constitutive modeling of crimped collagen fibrils in soft tissues. *Journal of the Mechanical Behavior of Biomedical Materials*, Elsevier Ltd, vol. 2, n. 5, p. 522–533, 2009. ISSN 1751-6161. Cited on page 63.

GU, W. et al. Simulation of the progression of intervertebral disc degeneration due to decreased nutritional supply. *Spine*, vol. 39, n. 24, p. E1411—-E1417, 2014. ISSN 15281159. Cited 2 times on pages 52 and 55.

GU, W. Y.; LAI, W. M.; MOW, V. C. A Mixture Theory for Charged-Hydrated Soft Tissues Containing Multi-electrolytes: Passive Transport and Swelling Behaviors. *Journal of Biomechanical Engineering*, vol. 120, n. 2, p. 169–180, 1998. ISSN 15288951. Cited on page 55.

HAGEMAN, P. A.; BLANKE, D. J. Comparison of gait of young women and elderly women. *Physical Therapy*, vol. 66, n. 9, p. 1382–1387, 1986. ISSN 0031-9023, 1538-6724. Cited on page 45.

HANDSFIELD, G. G. et al. A 3d model of the achilles tendon to determine the mechanisms underlying nonuniform tendon displacements. *Journal of Biomechanics*, Elsevier Ltd, vol. 51, p. 17–25, 1 2017. ISSN 18732380. Cited 2 times on pages 37 and 53.

HANNAFIN, J. A.; ARNOCZKY, S. P. Effect of cyclic and static tensile loading on water content and solute diffusion in canine flexor tendons: An in Vitro study. *Journal of Orthopaedic Research*, vol. 12, n. 3, p. 350–356, 1994. ISSN 1554527X. Cited on page 38.

HARALDSSON, B. T. et al. Lateral force transmission between human tendon fascicles. *Matrix Biology*, vol. 27, n. 2, p. 86–95, 2008. ISSN 0945053X. Cited on page 47.

HARKNESS-ARMSTRONG, C. et al. Effective mechanical advantage about the ankle joint and the effect of achilles tendon curvature during toe-walking. *Frontiers in Physiology*, vol. 11, p. 407, 2020. ISSN 1664-042X. Cited on page 46.

HARRIS, C. A.; PEDUTO, A. J. Achilles tendon imaging. *Australasian Radiology*, vol. 50, n. 6, p. 513–525, dec 2006. ISSN 00048461. Cited on page 42.

HEITMAN, D. E. et al. Biomechanical comparison of the achillon® tendon repair system and the krackow locking loop technique. *Foot & Ankle International*, vol. 32, n. 9, p. 879–887, 2011. ISSN 1071-1007, 1944-7876. Cited 4 times on pages 43, 44, 74, and 84.

HUANG, C.-y.; YONG, W. Effects of mechanical compression on metabolism and distribution of oxygen and lactate in intervertebral disc. *Journal of biomechanics*, vol. 41, p. 1184–1196, 2008. Cited on page 55.

HUMPHREY, J. D. *Mechanics of the arterial wall: Review and directions*. 1995. 1–162 p. Cited on page 61.

ISMAIL, M. et al. The achillon® achilles tendon repair: Is it strong enough? *Foot & Ankle International*, vol. 29, n. 8, p. 808–813, 2008. ISSN 1071-1007, 1944-7876. Cited 2 times on pages 43 and 44.

JACKSON, A. R.; HUANG, C. Y.; GUA, W. Y. Effect of endplate calcification and mechanical deformation on the distribution of glucose in intervertebral disc: A 3D finite element study. *Computer Methods in Biomechanics and Biomedical Engineering*, vol. 14, n. 2, p. 195–204, 2011. ISSN 10255842. Cited on page 55.

JACKSON, A. R. et al. 3D finite element analysis of nutrient distributions and cell viability in the intervertebral disc: Effects of deformation and degeneration. *Journal of Biomechanical Engineering*, vol. 133, n. 9, p. 1–7, 2011. ISSN 01480731. Cited on page 55.

JAY, G. D.; WALLER, K. A. The biology of Lubricin : Near frictionless joint motion. *Matrix Biology*, Elsevier B.V., vol. 39, p. 17–24, 2014. ISSN 0945-053X. Cited on page 39.

JIANG, W.-g. International Journal of Mechanical Sciences A concise finite element model for pure bending analysis of simple wire strand. *International Journal of Mechanical Sciences*, Elsevier, vol. 54, n. 1, p. 69–73, 2012. ISSN 0020-7403. Cited on page 51.

JIANG, W. G.; HENSHALL, J. L. The analysis of termination effects in wire strand using the finite element method. *The Journal of Strain Analysis for Engineering Design*, vol. 34, n. 1, p. 31–38, jan. 1999. ISSN 0309-3247, 2041-3130. Cited on page 51.

JOHNSON, G. A. et al. A Single Integral Finite Strain Viscoelastic Model of Ligaments and Tendons. *Journal of Biomechanical Engineering*, vol. 118, n. May 1996, 1996. Cited on page 52.

JUNQUEIRA, L. C.; CARNEIRO, J. *Histologia Básica Texto e Atlas*. [S.l.]: Guanabara Koogan, 2013. 1–527 p. ISSN 1098-6596. ISBN 9788527723114. Cited 3 times on pages 33, 39, and 40.

KARATHANASOPOULOS, N.; HADJIDOUKAS, P. TendonMech: An open source high performance code to compute the mechanical behavior of tendon fascicles. *SoftwareX*, Elsevier B.V., vol. 9, p. 324–327, 2019. ISSN 23527110. Cited on page 28.

KASTRATOVIć, G.; VIDANOVIć, N. 3D finite element modeling of sling wire rope in lifting and transport processes. *TRANSPORT*, vol. 30, n. 2, p. 129–134, out. 2013. ISSN 1648-4142, 1648-3480. Cited on page 51.

KASTRATOVIć, G. et al. On finite element analysis of sling wire rope subjected to axial loading. *Ocean Engineering*, vol. 88, p. 480–487, set. 2014. ISSN 00298018. Cited on page 51.

KAY, A. D.; BLAZEVICH, A. J. Isometric contractions reduce plantar flexor moment, achilles tendon stiffness, and neuromuscular activity but remove the subsequent effects of stretch. *Journal of Applied Physiology*, vol. 107, n. 4, p. 1181–1189, 2009. ISSN 8750-7587, 1522-1601. Cited 3 times on pages 48, 49, and 63.

Khan K.M. et al. Histopathology of Common Tendinopathies: Update and Implications for Clinical Management. *Sports Medicine*, vol. 27, n. 6, p. 393–408, 1999. Cited on page 42.

KHAN, R. J. Treatment of acute achilles tendon RupturesA meta-analysis of randomized, controlled trials. *The Journal of Bone and Joint Surgery (American)*, vol. 87, n. 10, p. 2202, 2005. ISSN 0021-9355. Cited 2 times on pages 43 and 44.

KJÆR, M. Role of Extracellular Matrix in Adaptation of Tendon and Skeletal Muscle to Mechanical Loading. *Physiological Reviews*, vol. 84, n. 2, p. 649–698, 2004. ISSN 00319333. Cited on page 39.

KLAHR, B. et al. On the contribution of solid and fluid behavior to the modeling of the time-dependent mechanics of tendons under semi-confined compression. *Journal of the Mechanical Behavior of Biomedical Materials*, vol. 148, p. 106220, dez. 2023. ISSN 17516161. Cited on page 63.

KLAHR, B. et al. Cell mechanics: Are poroviscoelastic parameters reliable? *Mechanics Research Communications*, vol. 118, p. 103793, dez. 2021. ISSN 00936413. Cited on page 63.

KLAHR, B. et al. A variational RVE-based multiscale poromechanical formulation applied to soft biological tissues under large deformations. *European Journal of Mechanics - A/Solids*, vol. 99, p. 104937, 2023. ISSN 09977538. Cited on page 62.

KLIFTO, C. S.; BOOKMAN, J.; PAKSIMA, N. Postsurgical Rehabilitation of Flexor Tendon Injuries. *Journal of Hand Surgery*, Elsevier Inc, vol. 44, n. 8, p. 680–686, 2019. ISSN 15316564. Cited on page 44.

KNAUS, K. R.; BLEMKER, S. S. 3D Models Reveal the Influence of Achilles Subtendon Twist on Strain and Energy Storage. *Frontiers in Bioengineering and Biotechnology*, Frontiers Media S.A., vol. 9, feb 2021. ISSN 22964185. Cited 6 times on pages 28, 52, 53, 56, 58, and 63.

KOHRS, R. T. et al. Tendon fascicle gliding in wild type, heterozygous, and lubricin knockout mice. *Journal of Orthopaedic Research*, vol. 29, n. 3, p. 384–389, 2011. ISSN 07360266. Cited 2 times on pages 39 and 48.

KOMOLAFE, O. A.; DOEHRING, T. C. Fascicle-scale loading and failure behavior of the achilles tendon. *Journal of Biomechanical Engineering*, vol. 132, n. 2, p. 1–5, 2010. ISSN 01480731. Cited on page 46.

KUHL, A. et al. Modeling nonlinear viscoelastoplastic behavior of high density polyethylene (hdpe) using particle swarm optimization (pso). In: *XXXIV Ibero-Latin American Congress on Computational Methods in Engineering*. [S.l.: s.n.], 2013. Cited on page 76.

KUJALA, U. M.; SARNA, S.; KAPRIO, J. Cumulative incidence of achilles tendon rupture and tendinopathy in male former elite athletes. *Clinical Journal of Sport Medicine*, vol. 15, n. 3, p. 133–135, 2005. ISSN 1050-642X. Cited 2 times on pages 27 and 47.

LAI, W. M.; HOU, J. S.; MOW, V. C. A triphasic theory for the swelling and deformation behaviors of articular cartilage. *Journal of Biomechanical Engineering*, vol. 113, n. 3, p. 245–258, 1991. ISSN 15288951. Cited 3 times on pages 39, 55, and 62.

Laura Chernak Slane; THELEN, D. G. Non-Uniform Displacements within the Achilles Tendon observed during Passive and Eccentric Loading. *Bone*, vol. 23, n. 1, p. 1–7, 2014. ISSN 15378276. Cited 2 times on pages 45 and 49.

LEMME, N. J. et al. Epidemiology of achilles tendon ruptures in the united states: Athletic and nonathletic injuries from 2012 to 2016. *Orthopaedic Journal of Sports Medicine*, vol. 6, n. 11, p. 232596711880823, 2018. ISSN 2325-9671, 2325-9671. Cited on page 27.

LERSCH, C. et al. Influence of calcaneus angle and muscle forces on strain distribution in the human achilles tendon. *Clinical Biomechanics*, vol. 27, p. 955–961, 2012. Cited 16 times on pages 21, 36, 45, 46, 47, 48, 49, 50, 66, 67, 68, 69, 76, 77, 78, and 87.

LOHRER, H. et al. The Achilles tendon insertion is crescent-shaped: An in vitro anatomic investigation. *Clinical Orthopaedics and Related Research*, vol. 466, n. 9, p. 2230–2237, 2008. ISSN 15281132. Cited on page 38.

LOUIS-UGBO, J.; LEESON, B.; HUTTON, W. C. Tensile properties of fresh human calcaneal (achilles) tendons. *Clinical Anatomy*, vol. 17, n. 1, p. 30–35, 2004. Cited on page 47.

LV, S. et al. Designed biomaterials to mimic the mechanical properties of muscles. *Nature*, vol. 465, n. 7294, p. 69–73, 2010. ISSN 0028-0836, 1476-4687. Cited on page 69.

LYNCH, H. A. Effect of Fiber Orientation and Strain Rate on the Nonlinear Uniaxial Tensile Material Properties of Tendon. *Journal of Biomechanical Engineering*, vol. 125, n. 5, p. 726, 2003. ISSN 0148-0731. Cited on page 39.

MA, J.; GE, S.-r.; ZHANG, D.-k. Distribution of wire deformation within strands of wire ropes. *Journal of China University of Mining and Technology*, vol. 18, n. 3, p. 475–478, set. 2008. ISSN 10061266. Cited on page 51.

MAGANARIS, C. N.; NARICI, M. V.; ALMEKINDERS L. C. MAFFULLI, N. Biomechanics and pathophysiology of overuse tendon injuries: ideas on insertional tendinopathy. *Sports Med.*, vol. 34(14), p. 1005–17, 2004. Cited 2 times on pages 47 and 50.

MAGANARIS, C. N.; NARICI, M. V.; MAFFULLI, N. Biomechanics of the Achilles tendon. *Disability and Rehabilitation*, vol. 30, n. 20-22, p. 1542–1547, jan. 2008. ISSN 0963-8288, 1464-5165. Cited 2 times on pages 47 and 63.

MAHAN, J. et al. *Achilles tendon complex: The anatomy of its insertional footprint on the calcaneus and clinical implications.* [S.l.]: Reed Elsevier India Pvt. Ltd., 2020. 221–227 p. Cited 2 times on pages 38 and 42.

MALANDRINO, A.; NOAILLY, J.; LACROIX, D. The effect of sustained compression on oxygen metabolic transport in the intervertebral disc decreases with degenerative changes. *PLoS Computational Biology*, vol. 7, n. 8, 2011. ISSN 1553734X. Cited 2 times on pages 52 and 55.

MARTINI, F. et al. *Fundamentals of anatomy and physiology.* 12th edition. ed. [S.l.]: Pearson Education, Inc., 2024. ISBN 978-0-13-785431-8. Cited on page 33.

MARTíNEZ-PAñEDA, E.; GALLEGO, R. Numerical analysis of quasi-static fracture in functionally graded materials. *International Journal of Mechanics and Materials in Design*, vol. 11, n. 4, p. 405–424, 2015. ISSN 1569-1713, 1573-8841. Cited on page 65.

MILLER, T. L.; SHEMORY, S. Insertional Achilles Tendon Injuries in the Athlete. *Operative Techniques in Sports Medicine*, W.B. Saunders, vol. 25, n. 2, p. 87–98, jun 2017. ISSN 15579794. Cited on page 43.

MORRISON, S. M.; DICK, T. J.; WAKELING, J. M. Structural and mechanical properties of the human Achilles tendon: Sex and strength effects. *Journal of Biomechanics*, vol. 48, n. 12, p. 3530–3533, set. 2015. ISSN 00219290. Cited 2 times on pages 58 and 64.

MUENCH, J. R.; THELEN, D. G.; HENAK, C. R. Interfibrillar shear behavior is altered in aging tendon fascicles. *Biomechanics and Modeling in Mechanobiology*, vol. 19, n. 3, p. 841–849, 2020. ISSN 1617-7959, 1617-7940. Cited on page 63.

MURAOKA, T. et al. Elastic properties of human achilles tendon are correlated to muscle strength. *J Appl Physiol*, vol. 99, 2005. Cited on page 64.

NATALI, A. et al. Anisotropic elasto-damage constitutive model for the biomechanical analysis of tendons. *Medical Engineering and Physics*, vol. 27, apr 2005. ISSN 1350-4533. Cited on page 52.

NUNLEY, J. A. (Ed.). *The Achilles tendon: treatment and rehabilitation.* [S.l.]: Springer, 2009. ISBN 978-0-387-79205-7 978-0-387-79206-4. Cited on page 43.

NURI, L. et al. Three-dimensional morphology and volume of the free achilles tendon at rest and under load in people with unilateral mid-portion achilles tendinopathy. *Experimental Physiology*, Blackwell Publishing Ltd, vol. 103, p. 358–369, 3 2018. ISSN 1469445X. Cited 5 times on pages 46, 49, 50, 58, and 63.

NUZZO, J. L. Narrative review of sex differences in muscle strength, endurance, activation, size, fiber type, and strength training participation rates, preferences, motivations, injuries, and neuromuscular adaptations. *Journal of Strength and Conditioning Research*, vol. 37, n. 2, p. 494–536, 2023. ISSN 1064-8011. Cited on page 64.

OBREZKOV, L. et al. Approximation of pre-twisted Achilles sub-tendons with continuum-based beam elements. *Applied Mathematical Modelling*, Elsevier Inc., vol. 112, p. 669–689, dec 2022. ISSN 0307904X. Cited on page 52.

OBREZKOV, L. P.; FINNI, T.; MATIKAINEN, M. K. Modeling of the achilles subtendons and their interactions in a framework of the absolute nodal coordinate formulation. *Materials*, vol. 15, n. 24, 2022. ISSN 1996-1944. Cited 4 times on pages 29, 30, 52, and 53.

OBST, S. J. et al. Three-dimensional deformation and transverse rotation of the human free Achilles tendon in vivo during isometric plantarflexion contraction. *Journal of Applied Physiology*, vol. 116, n. 4, p. 376–384, 2014. ISSN 87507587. Cited 4 times on pages 17, 49, 50, and 56.

OCHEN, Y. et al. Operative treatment versus nonoperative treatment of achilles tendon ruptures: systematic review and meta-analysis. *BMJ*, p. k5120, 2019. ISSN 0959-8138, 1756-1833. Cited on page 43.

ÖHBERG, L.; LORENTZON, R.; ALFREDSON, H. Neovascularisation in Achilles tendons with painful tendinosis but not in normal tendons: An ultrasonographic investigation. *Knee Surgery, Sports Traumatology, Arthroscopy*, vol. 9, n. 4, p. 233–238, 2001. ISSN 09422056. Cited on page 42.

OLIVA, F.; VIA, A.; MAFFULLI, N. Physiopathology of intratendinous calcific deposition. *BMC Med 10*, vol. 95, 2012. Cited 2 times on pages 42 and 50.

OLSZEWSKI, K.; DICK, T. J.; WAKELING, J. M. Achilles tendon moment arms: The importance of measuring at constant tendon load when using the tendon excursion method. *Journal of Biomechanics*, vol. 48, n. 6, p. 1206–1209, 2015. ISSN 00219290. Cited 5 times on pages 46, 48, 49, 73, and 75.

PÁCZELT, I.; BELEZNAI, R. Nonlinear contact-theory for analysis of wire rope strand using high-order approximation in the FEM. *Computer and Structures*, vol. 89, 2011. Cited on page 51.

PARK, Y. H. et al. Quantitative magnetic resonance imaging analysis of the common site of acute achilles tendon rupture: 5 to 8 cm above the distal end of the calcaneal insertion. *American Journal of Sports Medicine*, SAGE Publications Inc., vol. 47, p. 2374–2379, 8 2019. ISSN 15523365. Cited 2 times on pages 28 and 41.

PEEK, A.; MALAGELADA, F.; CLARK, C. The achilles tendon. *Orthopaedics and Trauma*, vol. 30, n. 1, p. 1–7, 2016. ISSN 18771327. Cited 2 times on pages 41 and 43.

PEKALA, P. A. et al. The twisted structure of the achilles tendon unraveled: A detailed quantitative and qualitative anatomical investigation. *Scandinavian Journal of Medicine and Science in Sports*, Blackwell Munksgaard, vol. 27, p. 1705–1715, 12 2017. ISSN 16000838. Cited 6 times on pages 36, 37, 38, 57, 58, and 63.

PELTONEN, J. et al. Viscoelastic properties of the achilles tendon in vivo. *SpringerPlus*, vol. 2, n. 1, p. 212, 2013. ISSN 2193-1801. Cited 4 times on pages 18, 65, 66, and 75.

PICHLER, W. et al. Anatomic variations of the musculotendinous junction of the soleus muscle and its clinical implications. *Clinical Anatomy*, vol. 20, n. 4, p. 444–447, 2007. ISSN 0897-3806, 1098-2353. Cited 2 times on pages 36 and 58.

PINTO, O. T. *Estudo Numérico Experimental de Tecido Conjuntivo Mole Submetido a Deformações Finitas*. Dissertação (Mestrado) — Universidade Federal de Santa Catarina, 2014. Cited 8 times on pages 17, 29, 30, 52, 56, 60, 75, and 88.

PIOLETTI, D. P. et al. Viscoelastic constitutive law in large deformations: application to human knee ligaments and tendons. *Journal of biomechanics*, vol. 31, n. 8, p. 753–7, aug 1998. ISSN 0021-9290. Cited on page 52.

PROSENZ, J. et al. The twist of the achilles tendon - associations of torsions in the lower extremity. *Clin Anat*, vol. 31, p. 1085–1091, 2018. Cited on page 37.

PUNCHARD, N. A.; WHELAN, C. J.; ADCOCK, I. The Journal of Inflammation. *Journal of Inflammation*, vol. 1, n. 1, p. 1, 2004. ISSN 14769255. Cited 2 times on pages 41 and 49.

PURSLOW, P. P. The shear modulus of connections between tendon fascicles. In: *2009 IEEE Toronto International Conference Science and Technology for Humanity (TIC-STH)*. Toronto, ON, Canada: IEEE, 2009. p. 134–136. ISBN 978-1-4244-3877-8. Available from Internet:<http://ieeexplore.ieee.org/document/5444520/>. Cited on page 47.

REBECCATO, A. et al. Repair of the achilles tendon rupture: A functional comparison of three surgical techniques. *The Journal of Foot and Ankle Surgery*, vol. 40, n. 4, p. 188–194, 2001. ISSN 10672516. Cited on page 43.

REDDY, J. N. *An Introduction to Continuum Mechanics, Second Edition*. 2. ed. [S.l.]: Cambridge University Press, 2013. ISBN 978-1-139-17895-2. Cited on page 61.

REESE, S. P.; MAAS, S. a.; WEISS, J. a. Micromechanical models of helical superstructures in ligament and tendon fibers predict large Poisson's ratios. *Journal of biomechanics*, Elsevier, vol. 43, n. 7, p. 1394–400, may 2010. ISSN 1873-2380. Cited on page 63.

RIBBANS, W. J.; COLLINS, M. Pathology of the tendo Achillis. *The Bone & Joint Journal*, vol. 95-B, n. 3, p. 305–313, 2013. ISSN 2049-4394. Cited on page 41.

RILEY, G. Tendinopathy—from basic science to treatment. *Nature Clinical Practice Rheumatology*, vol. 4, n. 2, p. 82–89, 2008. ISSN 1745-8382, 1745-8390. Cited on page 42.

ROBERTS, J. R. InFocus: Tendon Injuries of the Hand: Flexor Tendon. *Emergency Medicine News*, vol. 33, n. 11, p. 26–28, 2011. ISSN 1054-0725. Cited on page 44.

ROUSSEAU, C.-E.; TIPPUR, H. Compositionally graded materials with cracks normal to the elastic gradient. *Acta Materialia*, vol. 48, n. 16, p. 4021–4033, 2000. ISSN 13596454. Cited on page 65.

ROUX, A. et al. Influence of muscle-tendon complex geometrical parameters on modeling passive stretch behavior with the Discrete Element Method. *Journal of Biomechanics*, Elsevier, vol. 49, n. 2, p. 252–258, 2016. ISSN 18732380. Cited 2 times on pages 28 and 52.

SAFA, B. N. et al. Evaluation of transverse poroelastic mechanics of tendon using osmotic loading and biphasic mixture finite element modeling. *Journal of Biomechanics*, Elsevier LTD, vol. 109, p. 109892, 2020. ISSN 18732380. Cited on page 56.

SCHEPSIS, A. A.; JONES, H.; HAAS, A. L. Achilles tendon disorders in athletes. *American Journal of Sports Medicine*, vol. 30, n. 2, p. 287–305, 2002. ISSN 03635465. Cited 7 times on pages 37, 38, 41, 43, 44, 46, and 75.

SCHÖFFL, V.; HEID, A.; KÜPPER, T. Tendon injuries of the hand. *World Journal of Orthopaedics*, vol. 3, n. 6, p. 62–69, 2012. ISSN 22185836. Cited on page 44.

SCHULZE-TANZIL, G. G. et al. Tendon healing: a concise review on cellular and molecular mechanisms with a particular focus on the achilles tendon. *Bone & Joint Research*, vol. 11, n. 8, p. 561–574, 2022. ISSN 2046-3758. Cited on page 28.

SCREEN, H. R. C. et al. Tendon functional extracellular matrix. *Journal of Orthopaedic Research*, vol. 33, n. 6, p. 793–799, 2015. ISSN 1554527X. Cited 2 times on pages 34 and 41.

SCREEN, H. R. C. et al. The influence of noncollagenous matrix components on the micromechanical environment of tendon fascicles. *Annals of Biomedical Engineering*, vol. 33, n. 8, p. 1090–1099, 2005. ISSN 00906964. Cited 4 times on pages 28, 40, 41, and 44.

SHEN, Z. L. et al. Viscoelastic properties of isolated collagen fibrils. *Biophysical Journal*, Biophysical Society, vol. 100, n. 12, p. 3008–3015, 2011. ISSN 15420086. Cited on page 63.

SHIM, V. B. et al. Subject-specific finite element analysis to characterize the influence of geometry and material properties in achilles tendon rupture. *Journal of Biomechanics*, Elsevier, vol. 47, p. 3598–3604, 2014. ISSN 18732380. Cited 2 times on pages 30 and 52.

SHIM, V. B. et al. Combining in silico and in vitro experiments to characterize the role of fascicle twist in the achilles tendon. *Scientific Reports*, vol. 8, p. 1–12, 2018. Cited 6 times on pages 28, 30, 37, 46, 50, and 52.

SHIM, V. B. et al. Influence of altered geometry and material properties on tissue stress distribution under load in tendinopathic achilles tendons - a subject-specific finite element analysis. *J Biomech.*, vol. 82, p. 142–148, 2019. Cited 2 times on pages 30 and 52.

SINGH, R. et al. A review of current concepts in flexor tendon repair: Physiology, biomechanics, surgical technique and rehabilitation. *Orthopedic Reviews*, vol. 7, n. 4, p. 101–105, 2015. ISSN 20358164. Cited 2 times on pages 40 and 44.

ŚMIGIELSKI, R. Management of Partial Tears of the Gastro-Soleus Complex. *Clinics in Sports Medicine*, vol. 27, n. 1, p. 219–229, 2008. ISSN 02785919. Cited 3 times on pages 45, 47, and 57.

SMITH, M. *ABAQUS/Standard User's Manual, Version 6.9*. United States: Dassault Systèmes Simulia Corp, 2009. Cited 2 times on pages 58 and 74.

SONG, B. et al. Distributions of stress and deformation in a braided wire rope subjected to torsional loading. *The Journal of Strain Analysis for Engineering Design*, vol. 54, n. 1, p. 3–12, jan. 2019. ISSN 0309-3247, 2041-3130. Cited on page 51.

STANOVA, E. et al. Advances in Engineering Software Computer modelling of wire strands and ropes part II : Finite element-based applications. *Advances in Engineering Software*, Elsevier Ltd, vol. 42, n. 6, p. 322–331, 2011. ISSN 0965-9978. Cited on page 51.

STENROTH, L. et al. Age-related differences in Achilles tendon properties and triceps surae muscle architecture in vivo. *Journal of Applied Physiology*, vol. 113, n. 10, p. 1537–1544, 2012. ISSN 87507587. Cited 4 times on pages 46, 47, 63, and 69.

SUN, D. N. et al. A Mixed Finite Element Formulation of Triphasic Mechano-Eletrochemical Theory for Charged, Hydrated Biological Soft Tissues. *International Journal for Numerical Methods in Engineering*, p. 1375–1402, 1999. Cited on page 55.

SUN, Y. L. et al. Lubricin in human achilles tendon: The evidence of intratendinous sliding motion and shear force in achilles tendon. *Journal of Orthopaedic Research*, vol. 33, n. 6, p. 932–937, 2015. ISSN 1554527X. Cited 5 times on pages 39, 40, 45, 48, and 83.

SVENSSON, R. B. et al. Mechanical properties of human patellar tendon at the hierarchical levels of tendon and fibril. *Journal of Applied Physiology*, vol. 112, p. 419–426, 2012. ISSN 87507587. Cited on page 56.

SZARO, P. et al. Distribution of the subtendons in the midportion of the achilles tendon revealed in vivo on mri. *Scientific Reports*, Nature Research, vol. 10, 12 2020. ISSN 20452322. Cited 2 times on pages 37 and 57.

SZARO, P.; WITKOWSKI, G.; CISZEK, B. The twisted structure of the fetal calcaneal tendon is already visible in the second trimester. *Surgical and Radiologic Anatomy*, Springer-Verlag Italia s.r.l., vol. 43, n. 7, p. 1075–1082, jul 2021. ISSN 12798517. Cited on page 37.

SZARO, P. et al. Fascicles of the adult human Achilles tendon - An anatomical study. *Annals of Anatomy*, vol. 191, n. 6, p. 586–593, 2009. ISSN 09409602. Cited on page 37.

SZCZESNY, S. E.; ELLIOTT, D. M. Interfibrillar shear stress is the loading mechanism of collagen fibrils in tendon. *Acta Biomaterialia*, Acta Materialia Inc., vol. 10, n. 6, p. 2582–2590, 2014. ISSN 18787568. Cited on page 63.

TACK, C.; SHORTHOUSE, F.; KASS, L. The physiological mechanisms of effect of vitamins and amino acids on tendon and muscle healing: A systematic review. *International Journal of Sport Nutrition and Exercise Metabolism*, vol. 28, n. 3, p. 294–311, 2018. ISSN 15432742. Cited on page 40.

THORPE, C. T. et al. The role of the non-collagenous matrix in tendon function. *International Journal of Experimental Pathology*, vol. 94, n. 4, p. 248–259, 2013. ISSN 09599673. Cited on page 39.

THORPE, C. T. et al. The interfascicular matrix enables fascicle sliding and recovery in tendon, and behaves more elastically in energy storing tendons. *Journal of the Mechanical Behavior of Biomedical Materials*, Elsevier Ltd, vol. 52, p. 85–94, 2015. ISSN 18780180. Cited 2 times on pages 45 and 48.

THORPE, C. T. et al. Distribution of proteins within different compartments of tendon varies according to tendon type. *Journal of Anatomy*, vol. 229, n. 3, p. 450–458, 2016. ISSN 14697580. Cited on page 48.

THORPE, C. T. et al. Helical sub-structures in energy-storing tendons provide a possible mechanism for efficient energy storage and return. *Acta Biomaterialia*, Acta Materialia Inc., vol. 9, n. 8, p. 7948–7956, 2013. ISSN 18787568. Cited 3 times on pages 27, 34, and 46.

THORPE, C. T. et al. Anatomical heterogeneity of tendon: Fascicular and interfascicular tendon compartments have distinct proteomic composition. *Scientific Reports*, Nature Publishing Group, vol. 6, p. 1–12, 2016. ISSN 20452322. Cited on page 69.

THORPE, C. T. et al. Fascicles from energy-storing tendons show an age-specific response to cyclic fatigue loading. *Journal of The Royal Society Interface*, vol. 11, n. 92, p. 20131058, 2014. ISSN 1742-5689, 1742-5662. Cited 3 times on pages 63, 83, and 84.

THORPE, C. T. et al. Capacity for sliding between tendon fascicles decreases with ageing in injury prone equine tendons: A possible mechanism for age-related tendinopathy? *European Cells and Materials*, vol. 25, n. 0, p. 48–60, 2012. ISSN 14732262. Cited 5 times on pages 40, 47, 48, 63, and 83.

THORPE, C. T. et al. Specialization of tendon mechanical properties results from interfascicular differences. *Journal of the Royal Society Interface*, vol. 9, n. 76, p. 3108–3117, 2012. ISSN 17425662. Cited 3 times on pages 39, 47, and 48.

TOMLINSON, D. J. et al. Impact of Above-Average Proanabolic Nutrients Is Overridden by High Protein and Energy Intake in the Muscle-Tendon Unit Characteristics of Middle- to Older-Aged Adults. *Journal of Nutrition*, vol. 148, n. 11, p. 1776–1785, 2018. ISSN 15416100. Cited on page 40.

UQUILLAS, C. A. et al. Everything achilles: Knowledge update and current concepts in management: AAOS exhibit selection. *The Journal of Bone and Joint Surgery-American Volume*, vol. 97, n. 14, p. 1187–1195, 2015. ISSN 0021-9355. Cited on page 43.

VAISHYA, R. et al. Haglund ' s Syndrome : A Commonly Seen Mysterious Condition. *Cureus*, vol. 8, n. 10, 2016. Cited on page 38.

VANHEES, M. et al. The effect of suture preloading on the force to failure and gap formation after flexor tendon repair. *The Journal of Hand Surgery*, vol. 38, n. 1, p. 56–61, 2013. ISSN 03635023. Cited on page 73.

VANKAN, W. J. et al. Poroelasticity of saturated solids with an application to blood perfusion. *International Journal of Engineering Science*, vol. 34, n. 9, p. 1019–1031, 1996. ISSN 00207225. Cited on page 63.

VARGAS, D.; BELTRA, J. F. Effect of broken rope components distribution throughout rope cross-section on polyester rope response : Numerical approach. *International Journal of Mechanical Sciences*, vol. 64, p. 32–46, 2012. Cited on page 51.

VASSOLER, J. M.; REIPS, L.; FANCELLO, E. A. A variational framework for fiber-reinforced viscoelastic soft tissues. *International Journal for Numerical Methods in Engineering*, vol. 89, n. 13, p. 1691–1706, mar 2012. Cited on page 62.

VASSOLER, J. M.; STAINIER, L.; FANCELLO, E. A. A variational framework for fiber-reinforced viscoelastic soft tissues including damage. *International Journal for Numerical Methods in Engineering*, 2016. Cited on page 29.

VUKELIC, G.; VIZENTIN, G. Damage-Induced Stresses and Remaining Service Life Predictions of Wire Ropes. *applied sciences*, 2017. Cited on page 51.

WALKER, J. et al. Repeatability and sensitivity of passive mechanical stiffness measurements in the triceps surae muscle-tendon complex. *Scandinavian Journal of Medicine & Science in Sports*, vol. 32, n. 1, p. 83–93, 2022. ISSN 0905-7188, 1600-0838. Cited on page 73.

WALLIS, J. A. et al. A Systematic Review of Clinical Practice Guidelines for Physical Therapist Management of Patellofemoral Pain. *Physical Therapy*, vol. 101, n. 3, p. pzab021, mar. 2021. ISSN 0031-9023, 1538-6724. Cited on page 28.

WANG, D. et al. Finite element analysis of hoisting rope and fretting wear evolution and fatigue life estimation of steel wires. *Engineering Failure Analysis*, Elsevier Ltd, vol. 27, p. 173–193, 2013. ISSN 1350-6307. Cited on page 51.

WILLITS, K. et al. Operative versus nonoperative treatment of acute achilles tendon ruptures: A multicenter randomized trial using accelerated functional rehabilitation. *Journal of Bone and Joint Surgery*, vol. 92, n. 17, p. 2767–2775, 2010. ISSN 0021-9355, 1535-1386. Cited on page 43.

WINNICKI, K. et al. *Functional anatomy, histology and biomechanics of the human Achilles tendon — A comprehensive review.* [S.l.]: Elsevier GmbH, 2020. Cited 12 times on pages 28, 35, 39, 40, 41, 45, 46, 47, 49, 58, 63, and 64.

WOKEM, C.; JOSEPH, T.; CURLEY, M. Fatigue life prediction for cables in cyclic tension. *Journal of Strain Analysis*, 2018. Cited on page 51.

WREN, T. A. et al. Mechanical properties of the human achilles tendon. *Clinical Biomechanics*, vol. 16, p. 245–251, 2001. ISSN 02680033. Cited on page 56.

WU, Y. et al. Effect of Cartilage Endplate on Cell Based Disc Regeneration: A Finite Element Analysis. *Mol Cell Biomech*, vol. 10, n. 2, p. 159–182, 2013. Cited on page 55.

WUNDERLI, S. L. et al. Minimal mechanical load and tissue culture conditions preserve native cell phenotype and morphology in tendon—a novel ex vivo mouse explant model. *Journal of Orthopaedic Research*, vol. 36, n. 5, p. 1383–1390, 2018. ISSN 1554527X. Cited on page 63.

XU, Y.; MURRELL, G. A. The basic science of tendinopathy. *Clinical Orthopaedics and Related Research*, vol. 466, n. 7, p. 1528–1538, 2008. ISSN 15281132. Cited on page 42.

YAMAMURA, N. et al. Effect of tendon stiffness on the generated force at the Achilles tendon - 3D finite element simulation of a human triceps surae muscle during isometric contraction. *Journal of Biomechanical Science and Engineering*, vol. 9, n. 3, p. 1–11, 2014. ISSN 18809863. Cited on page 52.

YAO, H.; GU, W. Y. Physical signals and solute transport in cartilage under dynamic unconfined compression: Finite element analysis. *Annals of Biomedical Engineering*, vol. 32, n. 3, p. 380–390, 2004. ISSN 00906964. Cited on page 55.

YAO, H.; GU, W. Y. Physical signals and solute transport in human intervertebral disc during compressive stress relaxation: 3D finite element analysis. *Biorheology*, vol. 43, n. 3-4, p. 323–335, 2006. ISSN 0006355X. Cited on page 55.

YAO, H.; GU, W. Y. Three-dimensional inhomogeneous triphasic finite-element analysis of physical signals and solute transport in human intervertebral disc under axial compression. *Journal of Biomechanics*, vol. 40, n. 9, p. 2071–2077, 2007. ISSN 00219290. Cited 3 times on pages 39, 52, and 55.

YIN, N. H. et al. Individual variation in achilles tendon morphology and geometry changes susceptibility to injury. *eLife*, eLife Sciences Publications Ltd, vol. 10, p. 1–15, 2 2021. ISSN 2050084X. Cited 5 times on pages 27, 33, 37, 57, and 63.

YIN, N.-H. et al. Individual variation in achilles tendon morphology and geometry changes susceptibility to injury. *eLife*, eLife Sciences Publications, Ltd, vol. 10, p. e63204, feb 2021. ISSN 2050-084X. Cited 4 times on pages 29, 50, 53, and 57.

ZADRO, J.; O'KEEFFE, M.; MAHER, C. Do physical therapists follow evidence-based guidelines when managing musculoskeletal conditions? Systematic review. *BMJ Open*, vol. 9, n. 10, p. e032329, out. 2019. ISSN 2044-6055, 2044-6055. Cited on page 28.

ZHU, Q. et al. Effect of intervertebral disc degeneration on mechanical and electric signals at the interface between disc and vertebra. *Journal of Biomechanics*, Elsevier Ltd, vol. 104, 2020. ISSN 0021-9290. Cited on page 55.

ZHU, Q.; GAO, X.; GU, W. Temporal changes of mechanical signals and extracellular composition in human intervertebral disc during degenerative progression. *Journal of Biomechanics*, Elsevier, vol. 47, n. 15, p. 3734–3743, 2014. ISSN 18732380. Cited on page 55.

ZHU, Q. et al. Influences of nutrition supply and pathways on the degenerative patterns in human intervertebral disc. *Spine*, vol. 41, n. 7, p. 568–576, 2016. ISSN 15281159. Cited on page 55.

ZHU, Q. et al. Simulation of biological therapies for degenerated intervertebral discs. *Journal of Orthopaedic Research*, vol. 34, n. 4, p. 699–708, 2016. ISSN 1554527X. Cited on page 55.

ZHU, Q. et al. Cell viability in intervertebral disc under various nutritional and dynamic loading conditions: 3d Finite element analysis. *Journal of Biomechanics*, Elsevier, vol. 45, n. 16, p. 2769–2777, 2012. ISSN 00219290. Cited on page 55.

Appendix

APPENDIX A — Glossary

A.1   Terms that are specific to tendons.

Energy storing tendon: A category of tendons characterized by a relative lower level of energy dissipation and higher levels of elongation.

Positional tendon: A category of tendons characterized by a relative higher level of energy dissipation and lower levels of elongation.

Subtendon (Achilles): A subdivision of the Achilles tendon describing bundles of fascicles from the same muscle.

Flexor tendons: The tendons responsible for flexing the fingers of the hand or the toes of the foot.

Muscle-tendon junction: The position of the muscle-tendon unit where the muscle tissue stops and there is only tendon tissue or aponeurosis from this point to the insertion (i.e. the end of the muscle-tendon unit).

Muscle-tendon unit: The term used to describe the tendon and muscle as a single entity. It starts in the bone origin of the unit and ends at the bone insertion of the unit.

Pulley (tendon): Some tendons pass through special structures, usually in the form of small tunnels, which allow the tendon to curve and still transmit tension, similarly to normal pulleys. Such special structures are also called pulleys.

Insertional: Refers to phenomenon or regions close to the insertion of the tendon into the bone.

A.2   Terms that are specific to anatomy location.

Distal: Refers to something that further from the center of the body (Fig. 26). E.g. the ankle is distal to the knee.

Proximal: Refers to something that is closer to the center of the body (Fig. 26). E.g. the knee is proximal to the ankle.

Frontal plane: The plane that divides the body or other structures into front and back (Fig. 26).

Saggital plane: The plane that divide the body or other structures into right and left (Fig. 26).

Transverse plane: The plane that divide the body or other structures into top and bottom (Fig. 26),

Sagittal axis: A axis perpendicular to the frontal plane.

Posterior: Refers to something that is more to the back of the body. E.g. the ankle is posterior to the toes.

Anterior: Refers to something that is more to the front of the body. E.g. the toes are anterior to the ankle.

Medial: Refers to something closer to a sagittal plane passing through the center of the body. E.g. the eyes are medial to the ears (closer to the center of the body, or the sagittal plane.).

Lateral: Refers to something further from a sagittal plane passing through the center of the body. E.g. the ears are lateral to the eyes (further from the center of the body, or the sagittal plane.).
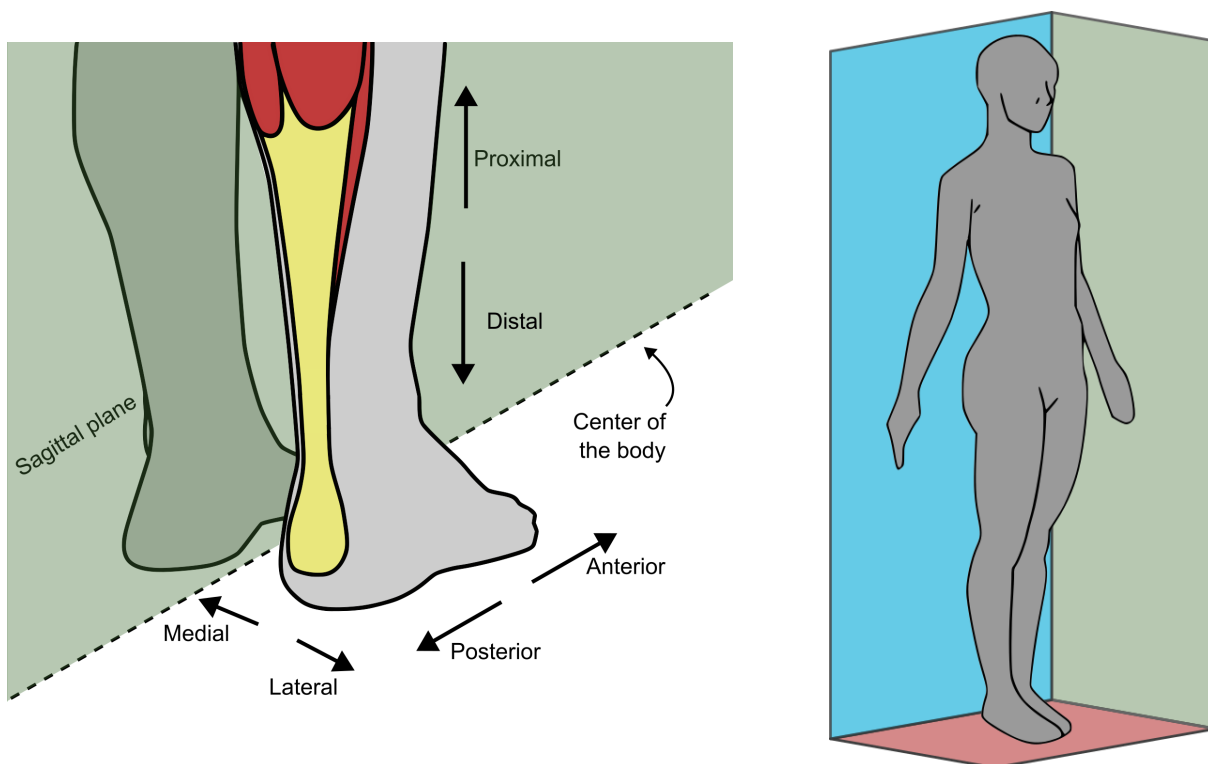

Figure 26 – Diagrams of anatomy location terms. The left image shows the sagittal plane in green. The right image represents the sagittal plane in green, the frontal plane in blue and the transverse plane in red. The planes are usually defined as passing through the center of the body, in this case a more precise description would be: The right image shows planes parallel to the sagittal, frontal and transverse planes.